Aus dem Max-Planck-Institut für Hirnforschung
in Frankfurt am Main

Der Einfluss kortiko-kortikaler Verbindungen auf die Antworteigenschaften von Neuronen im primären visuellen Kortex

Vom Fachbereich Biologie der
Technischen Universität Darmstadt
zur Erlangung des akademischen Grades eines
Doctor rerum naturalium

genehmigte Dissertation von
Dipl. Biol. Thomas Wunderle
aus Seeheim-Jugenheim

1. Referent: Prof. Dr. Ralf A.W. Galuske
2. Referent: PD Dr. Matthias H.J. Munk

Darmstadt, 15.04. 2011
Tag der mündlichen Prüfung: 03.06.2011
D17

Table of Contents

1. Zusammenfassung

In der vorliegenden Arbeit wurde der Einfluss modulatorischer, kortiko-kortikaler Verbindungen auf Neurone im primären visuellen Kortex der Katze untersucht. Visuelle Information wird in der Retina in Form von Aktionspotentialen kodiert und über eine Umschaltstation im Zwischenhirn, dem Corpus Geniculatum Laterale (CGL), der Großhirnrinde (Kortex) zugeführt. Bei der Katze bekommen die Areale 17 und 18, benannt nach der Klassifizierung von Brodmann, direkte Eingänge vom CGL und werden zusammen als primärer visueller Kortex bezeichnet. Erstaunlicherweise machen erregende Eingänge vom Corpus Geniculatum Laterale nur einen geringen Prozentsatz aller exzitatorischen Verbindungen im primären visuellen Kortex aus. Die Mehrzahl der exzitatorischen Synapsen werden daher von kortiko-kortikalen Verbindungen gebildet: Lokale Verbindungen zwischen nahe gelegenen Neuronen ähnlicher Antworteigenschaften, weitreichende (Horizontal-) Verbindungen innerhalb eines Areals, Rückprojektionen („Feedback“) von Arealen höherer Verarbeitungsstufen, sowie Verbindungen zwischen den zerebralen Hemisphären über das Corpus Callosum. Über diese Verbindungen kann ein typisches Neuron tausende synaptischer Eingänge bekommen, über die es integriert, um eine entsprechende Antwort in Form einer Serie von Aktionspotentialen zu generieren. Es ist daher eine zentrale Frage der Neurowissenschaften, wie (modulatorischer) synaptischer Input das Antwortverhalten eines Neurons beeinflusst.

Eine Möglichkeit dies zu untersuchen besteht darin, die Aktivität eines empfangenden Neurons zu messen, und dabei gleichzeitig die Menge an synaptischem Input durch Deaktivierung projizierender Neurone zu kontrollieren. Die Kontrolle interhemisphärischer (kallosaler) Verbindungen bietet sich besonders an, da hierbei das projizierende und das empfangende Neuron auf unterschiedlichen Hemisphären, und damit räumlich voneinander getrennt, liegen. Dies stellt sicher, dass eine Deaktivierung des projizierenden nicht auch einen direkten (experimentellen) Einfluss auf das empfangende Neuron hat. Weiterhin konnte gezeigt werden, dass kallosale Projektionen anatomische und physiologische Gemeinsamkeiten mit den weitreichenden Horizontalverbindungen aufweisen, wie etwa eine präferierte Verbindung zwischen Neuronen gleicher Orientierungspräferenz. Es ist daher zu

vermuten, dass die aus der Untersuchung kallosaler Projektionen gewonnenen Erkenntnisse auch auf andere kortiko-kortikalen Verbindungen übertragen werden können.

In dieser Studie wurde die elektrische Aktivität einzelner kortikaler Neurone in Reaktion auf visuelle Stimulation extrazellulär gemessen. Dazu wurden Mikroelektroden in den Kortex anästhesierter Katzen eingebracht. Gleichzeitig wurden korrespondierende Bereiche auf der kontralateralen Hemisphäre mittels Kühlen reversibel deaktiviert. Ein Vergleich der gemessenen Aktivität vor, während und nach der Deaktivierung ließ daher Rückschlüsse auf die Natur des Einflusses kallosal projizierender Neurone zu.

Wir verwendeten zwei unterschiedliche Stimuli: Zum einen Balkengitter mit hohem Kontrast, die sich rechtwinklig zu ihrer Orientierung bewegten, und zum anderen bewegte Punktwolken zufälliger Anordnung (so genannte „random dot textures“ kurz RDTs). Die beiden Stimuli unterscheiden sich grundlegend in ihren physikalischen Eigenschaften, und damit in der Art und Weise wie sie das kortikale Netzwerk ansprechen. Ein Thema dieser Arbeit war daher, ob die Art der Stimulation einen Einfluss auf die Antwortmodulation über kortiko-kortikale Verbindungen hat.

Zunächst wurde die Antwortstärke der abgeleiteten Neurone quantifiziert, indem die Anzahl der Aktionspotentiale pro Sekunde (die so genannte Rate) berechnet wurde. Es zeigte sich, dass, gemittelt über alle abgeleiteten Neurone, die Rate während der Deaktivierung über die gesamte Stimulationsdauer abnahm. Interessanterweise war die Abnahme der Rate, und damit der Einfluss der kallosalen Projektionen, größer wenn mit RDTs stimuliert wurde anstatt mit Balkengittern. Es wurden Kontrollen durchgeführt die dieses Ergebnis bestätigten. Weiterhin war auffällig, dass die Stimulation mit Balkengittern sowohl zu einer signifikanten Erhöhung als auch Erniedrigung der Rate einzelner Neurone führte, während für die Stimulation mir RDTs nur ein signifikanter Abfall der Rate zu verzeichnen war. Auch konnte eine Erniedrigung der Rate während spontaner Aktivität, d.h. ohne visuelle Stimulation, festgestellt werden.

Im nächsten Schritt untersuchten wir den Einfluss der Deaktivierung auf die Orientierungsselektivität („tuning“) einzelner Neurone. Die Selektivität für bestimmte Reizorientierungen ist eine der hervorstechendsten Eigenschaften der Neurone im primären visuellen Kortex. Durch Beschreibung mit einem mathematischen Modell konnte gezeigt werden, dass der Einfluss kallosaler Projektionen zum größten Teil einer multiplikativen Skalierung der Tuningkurve entspricht. Dies war umso ausgeprägter, je stärker der Abfall oder Anstieg der Rate aufgrund der Deaktivierung war. In Einklang mit diesem Mechanismus konnte gezeigt werden, dass sich Orientierungsselektivität und -spezifität nicht grundlegend

änderten. Für die wenigen Neurone, die über einen additiven Mechanismus beeinflusst wurden, konnte jedoch eine geringfügige Änderung der Orientierungsselektivität festgestellt werden.

Eine weitere Eigenschaft kortikaler Neurone ist die Variabilität ihrer Antwort. Dies bedeutet, dass bei wiederholter Stimulation sowohl die zeitliche Abfolge, als auch die Summe der generierten Aktionspotentiale für jeden Stimulationsdurchgang unterschiedlich sein kann. Um diese Variabilität der Neurone zu quantifizieren, bedienten wir uns einer Reihe von mathematischen Methoden. Es zeigte sich, dass während der Deaktivierung der kallosalen Verbindungen die Antwortvariabilität der Neurone sank. Im Umkehrschluss bedeutet dies, dass im Normalfall kortiko-kortikale Verbindungen zur Antwortvariabilität der Neurone beitragen. Dieser Effekt konnte insbesondere bei Neuronen beobachtet werden, die durch die kortiko-kortikalen Verbindungen eine Verminderung der Rate erfuhren.

Unsere Ergebnisse zeigen, dass kortiko-kortikale Verbindungen über das Corpus Callosum einen reizabhängigen, hauptsächlich exzitatorischen Einfluss auf ihre Zielneurone ausüben, ohne die Stimulusspezifität substanziell zu ändern. Weiterhin konnten wir, durch direkte Manipulation (kausaler Versuchsansatz), in vivo den Modulationsmechanismus dieser Verbindungen und deren Einfluss auf die Antwortvariabilität beschreiben. Unsere Arbeit liefert damit, zum ersten Mal, eine ausführliche (mathematische) Beschreibung des funktionellen Beitrags lateraler Verbindungen zur Verarbeitung visueller Information im Kortex. Dieser Beitrag wurde sowohl qualitativ als auch quantitativ beschrieben. Die experimentell ermittelten Befunde konnten in Modelle übertragen werden, um die Natur der Modulation durch Lateralverbindungen näher zu bestimmen. Dabei wurden sowohl bestehende als auch neue Modelle überprüft bzw. bestätigt.

Obgleich unsere Ergebnisse auf Einzelzellableitungen beruhen, lassen sich Rückschlüsse auf die Funktionalität des kortikalen Netzwerkes ziehen. So konnten wir einen kausalen Zusammenhang zwischen dem Maß an spontaner Aktivität im Netzwerk und dem Vorhandensein von weitreichenden Verbindungen herstellen. Auch ist es entscheidend, wie ein Reiz das kortikale Netzwerk anspricht. Neurone die durch schwächere, weniger optimale Reize stimuliert werden, profitieren mehr von der Integration über das Netzwerk, als dieselben Neurone, die mit einem kontrastreichen, auf ihr Antwortverhalten optimierten Reiz stimuliert werden.

2. Introduction

We all know that our brain is the organ which receives and processes information about the "outside world", the environment we interact with in order to survive. It is exactly this information processing which keeps neuroscientists busy for decades now. But what is "information" and how is it encoded, processed and stored in the brain? Those questions cannot be easily answered, because the concept of information cannot be described with any real world analogue. In the brain, the basic computational unit is the neuron. It is now clear, that single neurons are capable of performing mathematical operations, but groups of neurons or whole networks might be required to perform more complex operations. A single neuron in the cerebral cortex is heavily interconnected with its surrounding neurons, but also with distant targets giving rise to a "small world" architecture. Therefore, every neuron in the brain is connected to any other neuron with only a few synapses in between.

The visual system is maybe the best understood part of the brain. Based on anatomical and physiological studies one can distinguish several steps of hierarchical processing. Connections between each hierarchical level include "bottom up" (feedforward), "top down" (feedback) and lateral connections linking neurons on the same hierarchical level. Inputs from all those sources may converge onto a single neuron determining its response properties, namely the generation of sequences of action potentials. This raises the question of how the different inputs interact in order to create a specific output. More precisely, is the interaction dependent on the external stimulus, driving the whole system? By which mechanism do the individual inputs add up? And, is a certain type of input important for the timing and reliability of the action potentials produced by the neuron? Those are questions which will be addressed in this thesis combining different neurophysiological techniques. We recorded the electrical activity of neurons in the primary visual cortex of cats in response to visual stimulation, while at the same time controlling lateral input coming from the contralateral hemisphere via the corpus callosum. The following sections provide a brief review of the visual system together with an overview of the input and output situation of a neuron in the visual cortex. Finally, previous studies, performed to investigate the interplay between the input and output of such a neuron, are reviewed.

2.1 The visual system of the cat

The following part gives a brief introduction to the visual system of cats. A comprehensive review including references can be found in Payne and Peters: The Cat Primary Visual Cortex (2002).

2.1.1 From the eye to the cortex

In animals, visual perception starts at the retina of the eye, where photoreceptors detect incoming photons. The detection of one or more photons is converted into a hyperpolarization of the photoreceptor's membrane through a cascade of receptor-ligand interactions. The transmission of a biochemical interaction into an electrical signal is an important fact, because this concept is kept throughout the whole nervous system and is highly conserved throughout evolution. The electrical signal is passed through the layers of the retina and leaves the eye via the optic nerve targeting the lateral geniculate nucleus (LGN) of the thalamus. Before reaching the LGN, fibers coming from the nasal hemiretina of the eye cross at the optic chiasm. Conversely, the fibers originating from the temporal hemiretina stay ipsilaterally. Finally, from the LGN, neurons are projecting to the primary visual cortex of the telencephalon.

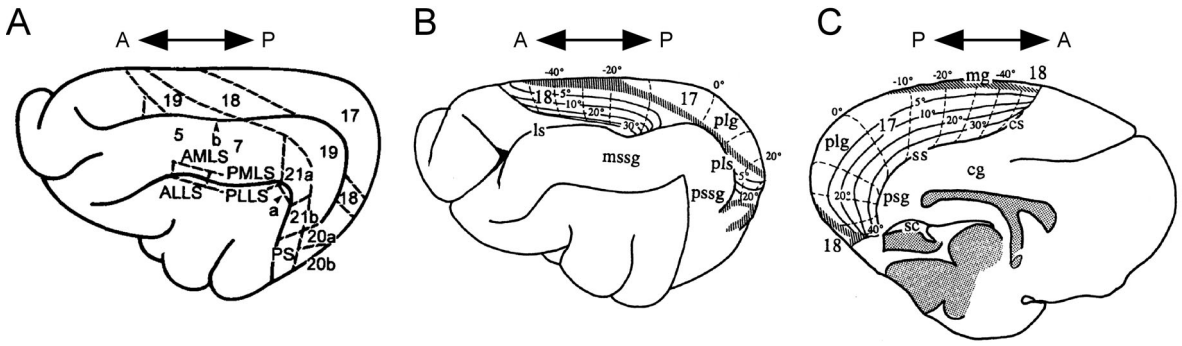

Figure 2-1: Schematic drawings of a cat brain. (A) Outline drawing of lateral view of the left hemisphere. Solid and dashed lines depict the borders of gyri and visual areas, respectively. Classification of the visual areas is indicated by numbers and abbreviations. AMLS: anterior, medial lateral-suprasylvian area; PMLS: posterior, medial lateral-suprasylvian area; ALLS: anterior, lateral lateral-suprasylvian area; PLLS: posterior, lateral lateral-suprasylvian area. (B) lateral view of the cat brain together with a retinotopic map of area 17 and 18. Iso-azimuth lines are drawn solid, iso-elevation lines dashed. The shaded area denotes the 17/18 transition zone (TZ) (C) same as A for medial view. A modified from MacNeil et al., 1996; B and C modified from Payne, 1991.

In the cat, two areas can be termed as "primary" visual areas, because they receive direct geniculocortical input. They are named area 17 and area 18 after the classification of Brodmann (1909; figure 2-1A). Area 17 receives input from the X- and Y-System and sends projections to area 18, whereas area 18 is dominated by input from the Y-System. X- and Y-

System were defined based on anatomical and functional differences of the retinal ganglion cells. According to their different input, area 17 responds to stimuli with high spatial and low temporal frequencies and has small receptive fields (RF), whereas for area 18 the opposite is the case. The border between area 17 and 18 holds a representation of the vertical meridian (VM) of the visual field. Rather than being a strict border, the cytoarchitectonic characteristics of both areas blend into each other, forming a transition zone (TZ) of about 1 mm (Rochefort et al., 2007; 2009).

2.1.2 Structure and connectivity of the cortex

The neocortex is structured into six layers which can be histolocially defined, for example by Nissl stains. This is because the distribution and density of cell types is not uniform throughout the cortical layers. More interesting, connections in the cortex are not random, but respect (to some extent) the borders of the different laminae. For example, the main input from the LGN terminates in layer 4 of area 17 and 18 onto spiny stellate cells. From there, connections are made to other layer 4 cells and to cells in layer 2/3, which distribute the information to other layers / areas. From area 17 and 18, the visual information is send back to subcortical structures as the LGN, superior colliculus or pulvinar, and to feedforward higher visual areas (e.g. Gilbert, 1983). Interestingly, only about 5% of the excitatory synapses formed in layer 4 originate from thalamic afferents (Peters & Payne, 1993; Ahmed et al., 1994). This implies that a neuron in primary visual cortex receives most of its excitatory input from other neurons in the same area, or from feedback projections from higher areas. Therefore, already at the first cortical step, the processing of visual information is not done in a serial way, but involves a highly interconnected system operating in parallel.

2.1.3 Structure and organization of receptive fields

Neurons in the retina and LGN have concentric receptive fields with center/surround antagonism, responding best to spots of light presented in their “on” region. Instead, neurons in the primary visual cortex have receptive fields which respond preferentially to oriented bars (i.e. orientation selectivity). For orientations away from the preferred one, the neuron fires less spikes, and can even be inhibited (firing below spontaneous level) for orientations orthogonal to the preferred one. Receptive fields in the primary visual cortex can be further subdivided into the “simple” and “complex” type (e.g Hubel & Wiesel, 1962). Simple receptive fields exhibit separate “on” and “off” regions and respond to static and moving light

bars of the preferred orientation, whereas complex receptive fields cannot be separated into distinct on and off regions and respond primarily to moving bars. Thereby, some neurons respond to both directions of a given orientation, whereas others are selective for a particular stimulus direction (i.e. direction selectivity).

A prominent feature of the neurons in primary visual cortex is the retinotopic organization of their receptive fields. This means, that neurons which are close by in the cortex also have receptive fields which are close together in visual space. It is therefore possible to map the visual space onto the surface of the cortex (figure 2-1B, C; and Tusa et al., 1978 for example). Because of the smaller surface of area 18 as compared to area 17 (approx. five times smaller), its magnification factor is much larger. That means that a certain distance between two points on the cortex of area 18 corresponds to a much larger distance in the visual field then it would be for the same cortical distance in area 17 (Tusa et al., 1978; Tusa et al., 1979).

While the properties of a receptive field were initially explained by a feedforward model (e.g. Hubel & Wiesel, 1962), a number of studies have shown a contribution of cortico-cortical connections in shaping the response of a stimulus presented in the classical receptive field of a neuron (for review see Allman et al., 1985; Angelucci & Bressloff, 2006). Such connections provide synaptic input from other parts of the same cortical area, other areas or even from the other hemisphere. The latter type of connections, namely the interhemispheric connections were chosen in this study as a model for the influence of cortico-cortical connections on the response properties of their target cells.

2.1.4 Intrinsic horizontal connections

In the somatosensory and visual cortex of cats and monkeys, neurons preferring similar orientations are grouped together into functional orientation columns (Mountcastle, 1957; Hubel & Wiesel, 1962;1968). This was supported by early anatomical studies showing an extensive vertical connectivity across the cortical layers (Lorente de Nó, 1949). Consequently, most synaptic input to a neuron should come from other neurons close by sharing similar orientation preference. In contrast to this view, degeneration studies performed some years later revealed the existence of long range connections extending several millimetres parallel to the cortical surface (Fisken et al., 1975, for review see Schmidt & Löwel, 2002). This was confirmed by intracellular tracer injections showing some axonal arbours extending up to 8 mm (Gilbert & Wiesel, 1979). Recently, the fraction of excitatory long-range projections making synaptic contacts with a certain neuron was found to be surprisingly high; about 92%

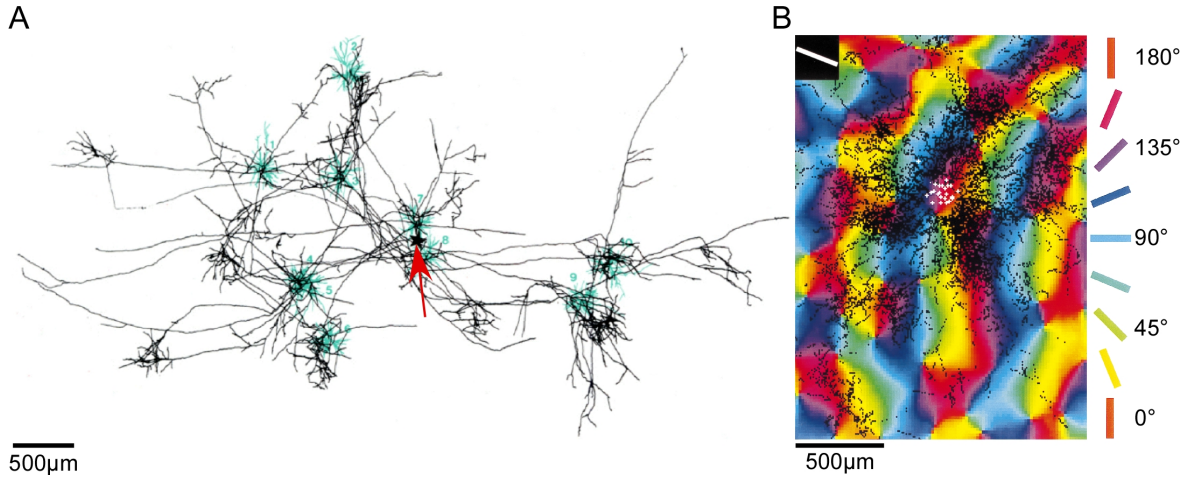

Figure 2-2: (A) Patchy intrinsic horizontal connections. Biocytin injection (marked by red arrow) resulted in the labeling of 10 pyramidal neurons. Axons drawn in black, dendrites in green. Note the patchy organization of axonal terminals with a spacing of about 1 mm. (B) Orientation selectivity of intrinsic horizontal connections. Biocytin injections (white crosses) into an orientation domain preferring oblique orientations around 135° (purple) result in bouton clustering in domains of similar orientation preference. A modified from Kisvarday & Eysel, 1992. B modified from Bosking et al., 1997.

of all synapses formed in a cylinder of 200 µm, corresponding to an orientation column, originate from neurons outside this column (Stepanyants et al., 2009)! The axons of the long-range horizontal connections form patches of about 300 – 500 µm in diameter with a periodicity of 0.5 – 1 mm in several species (figure 2-2A; Rockland & Lund, 1982; Gilbert & Wiesel, 1983; Livingstone & Hubel, 1984; Kisvarday & Eysel, 1992). Thereby, most of the connections originate from pyramidal and spiny stellate cells making excitatory connections on other excitatory neurons. About 5 - 20% of the synaptic boutons target inhibitory cells (Kisvarday et al., 1986; LeVay, 1988; McGuire et al., 1991). The inhibitory network is more restricted in space, only about 3 - 10% of all inhibitory neurons (20% of the total neurons in area 17 and 18 are inhibitory; Gabbott & Somogyi, 1986) give rise to long-range horizontal projections (Fisken et al., 1975; Matsubara & Boyd, 1992; Stepanyants et al., 2009).

Moreover, cross-correlation analysis suggested that neurons with similar orientation preference are preferentially linked together (Ts'o et al., 1986). This was confirmed by combining electrophysiological recordings or imaging techniques with tracer injections (Malach et al., 1993; Bosking et al., 1997; Kisvarday et al., 1997; Schmidt et al., 1997a). Those studies revealed that the patchy organization of the long-range horizontal connections coincides with the orientation domains in primary visual cortex (figure 2-2B). Consequently, in rodents lacking orientation columns, long-range horizontal connections were found not to be organized in a patchy manner (Van Hooser, 2006).

Because of their horizontal spread, the long range intrinsic connections could serve to integrate visual information across space, thereby shaping the responses of the “classical”

receptive field. Contextual modulations like visual "pop-out", perceptual grouping or collinear facilitation could be mediated by the horizontal network, already at early stages of visual processing (Bosking et al. 1997; Schmidt et al. 1997b; for review see Albright & Stoner, 2002; Angelucci & Bressloff, 2006; Roelfsema, 2006).

2.2 The input situation of a neuron in V1

2.2.1 Origin of inputs

In order to evaluate the output (spiking activity) of a neuron one first has to consider its input situation. The input to a particular neuron may originate from different sources, all contributing to a certain extent to the output amplitude of this neuron. Layer 2/3 pyramidal neurons, for example, receive a variety of inputs: (1) They are the predominant targets of layer 4 spiny stellate cells (Mitzdorf & Singer, 1979; Gilbert & Wiesel, 1983; Martin & Whitteridge, 1984a;b). (2) Pyramidal neurons in the infra- and supragranular layers receive feedback from higher visual areas (Gilbert, 1983; Symonds & Rosenquist, 1984; Felleman & Van Essen, 1991). (3) Long-range horizontal connections are mainly formed by layer 2/3 pyramidal cells (Rockland & Lund, 1982; Gilbert & Wiesel, 1983). (4) Most interhemispheric or callosal connections arise from pyramidal cells in supragranular layers (Innocenti, 1980; Segraves & Rosenquist, 1982). In turn, the axon terminals of callosal projections form clusters that span the whole cortical depth (Fisken et al., 1975; Houzel & Milleret, 1999). A simplified sketch of the general connectivity of such a pyramidal neuron is shown in figure 2-3. Three types of inputs are distinguished: Direct or indirect feedforward input from the thalamus (gray), feedback from higher areas (orange) and lateral connections (green) originating from the same area / lamina as the example neuron (red). The latter type of connections contributes most to the total number of synapses formed in visual cortex. A layer 2/3 pyramidal cell receives approx. 7000 synapses (including excitatory and inhibitory ones), 40 – 60 % of them originating from other layer 2/3 pyramidal cells (Binzegger, 2004).

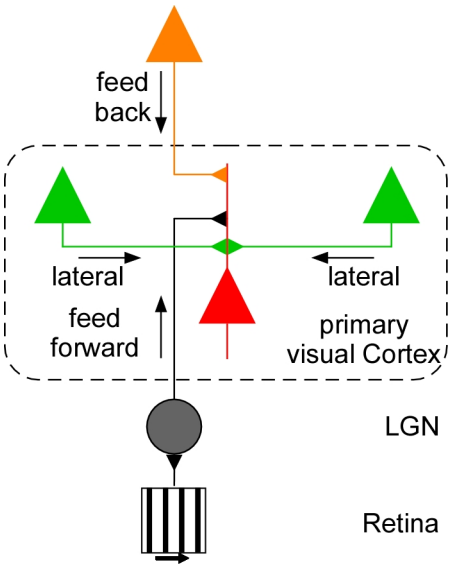

Figure 2-3: Schematic drawing of types of (long- range) input to a principal neuron (red) in primary visual cortex. Inhibitory input is not shown in this sketch, but emerges (primarily) locally.

2.2.2 A balance of excitation and inhibition

From what was laid out above it becomes clear that a single neuron receives strong input from a variety of different sources. In this "high input" regime, the problem of output saturation arises (Shadlen & Newsome, 1994;1998). The reason is that, considering only excitatory synaptic input, only 10 – 400 excitatory inputs arriving within 10 – 20 ms are sufficient to depolarize the postsynaptic membrane from rest (about -75mV) to spike threshold (about -55mV) (Mason et al., 1991; Otmakhov et al., 1993). If only 5% of all excitatory synapses (approx. 5000) are active at a certain time point, with a mean rate of 50 spikes per second (sp/s or Hz), then the output rate of that neuron would be between 30 and 1250 sp/s!

Thus, it is likely that the strong excitation a neuron receives must be balanced by inhibition. About 20% of the neurons in V1 are inhibitory using the neurotransmitter γ-aminobutyric acid (GABA, Gabbott & Somogyi, 1986) and the fraction of inhibitory synapses a typical pyramidal cell receives is in the order of 10 to 20 % (Fisken et al., 1975; Beaulieu et al., 1992; Binzegger, 2004). Despite their lower number, inhibitory neurons can have a strong influence on their target cells. This includes several mechanisms (Shadlen & Newsome, 1994): (1) Inhibitory neurons usually have a higher firing rate then excitatory neurons. (2) Inhibitory conductances are usually larger then excitatory ones (Miles & Wong, 1986). (3) A larger fraction of inhibitory neurons may be active at a time. (4) Inhibitory synapses may be more reliable then excitatory ones. (5) Inhibitory neurons usually make multiple contacts on a target neuron (Somogyi et al., 1983). Indeed, a number of in vitro and in vivo studies suggest that in the cortex excitation is tightly balanced with inhibition, thereby preventing saturation and increasing the dynamic range of a neuron (Sanchez-Vives & McCormick, 2000; Shu et al., 2003; Haider et al., 2006; Okun & Lampl, 2008). During rest, the cortical network is by no means inactive. Instead, persistent background activity maintains the membrane potential of a neuron in a depolarized and highly variable state (Pare et al., 1998; Steriade, 2001; Chen & Fetz, 2005; Crochet & Petersen, 2006).

2.2.3 Dendritic integration

The basic operation of a neuron is to integrate all its excitatory and inhibitory inputs in order to create an output spike. In the simplest case, the neuron performs a linear average across its synaptic inputs (Jagadeesh et al., 1993; Bernander et al., 1994). Further, a variety of nonlinear effects, including active dendritic conductances have been described, which can

make the prediction of the neuron's output very difficult (Branco & Häusser, 2011; for review see Silver, 2010). Such nonlinear effects can enable a single neuron to perform more complex mathematical operations such as multiplication and division.

2.3 The output situation of a neuron in V1

2.3.1 Input-output transformation and gain modulation

As described in the previous section, a particular neuron can get input from many different sources. Those inputs are integrated and translated into an output train of spikes. At the soma, once the membrane potential (input) has crossed a threshold, it can be linearly related to the firing rate (output). Such an input-output (i-o) relationship is called a "threshold-linear function" (Anderson, 2000; Carandini, 2004). In a different model, voltage fluctuations in the membrane potential (V_m) can smooth the i-o relationship around firing threshold. In this case, the i-o function approximates a power law rather then a linear function, amplifying small differences in membrane potential into large differences in spike rate

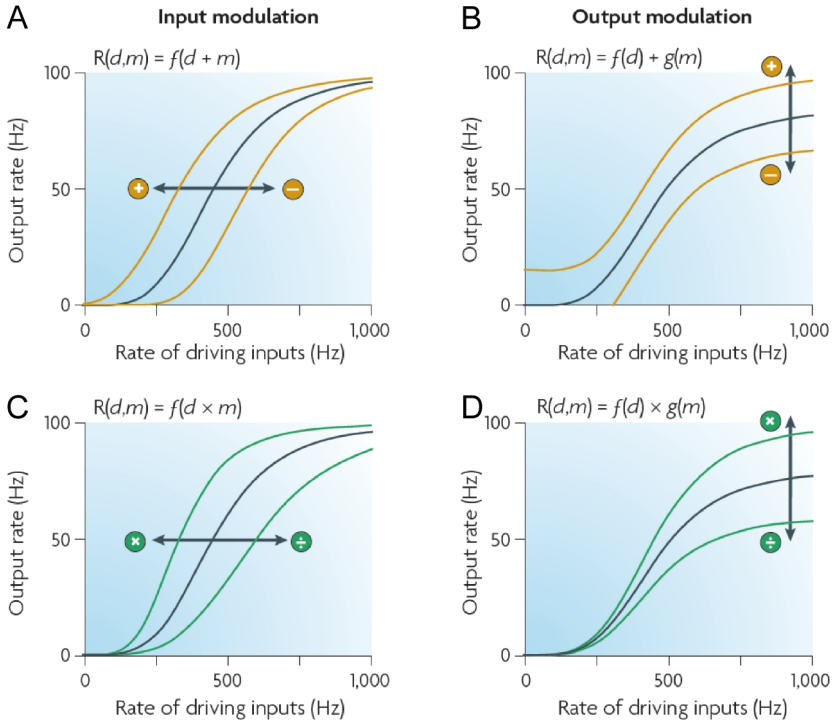

Figure 2-4: Neuronal input-output (i-o) relationships and possible mathematical operations performed by modulatory input (indicated by equations above plots). (A, B) An additive/subtractive modulation shifts the i-o curve along the input axis (for input modulation) or the output axis (for output modulation). The slope of the curve is not changed for both conditions. (C, D) A multiplicative/divisive modulation (gain change) changes the slope of the i-o curve. Note that for output, but not for input modulation, the maximal output firing rate is altered for both the additive and multiplicative scaling. Modified from Silver, 2010.

(Heeger, 1992; Miller & Troyer, 2002). Independently of which model prevails, two modes of input modulation can change the output of a neuron: In the first mode, an additive/subtractive modulation shifts the i-o curve along the input or output axis, without a change in its slope (figure 2-4 A, B). In the case of input modulation, the modulatory input is added to the driving one and the result is passed through the spike generating mechanism. In that case, the minimal and maximal evoked spike rates do not change. Mechanistically, a subtractive shift,for example, can be obtained by a hyperpolarizing conductance or by shunting inhibition (Chance et al., 2002; Ayaz & Chance, 2009). In the second mode, a multiplicative/divisive scaling of the function leads to a change in the slope of the i-o curve (figure 2-4 B, C). Such a change is often termed "gain" modulation, first mentioned by (Andersen & Mountcastle, 1983) to describe the multiplicative interaction of visually evoked responses and eye position in parietal cortex of monkeys. In general, one can define gain modulation "… as a change in the sensitivity of a neuronal response to one set of inputs that depends on the activity of a second set of inputs" (Brozović et al., 2008). A gain modulation on the input level does not alter the maximal firing rate of the neuron.

A number of cellular mechanisms have been shown to affect the gain of a neuron, including changes in the level of background excitation/inhibition (Chance et al., 2002; Shu et al., 2003), noisy synaptic input (Ayaz & Chance, 2009), input correlations (Salinas & Sejnowski, 2000) and a stimulus induced combination of depolarization, voltage fluctuations (noise) and input resistance (shunting) (Cardin et al., 2008). By gain modulation, a neuron can directly combine two inputs in a multiplicative manner, thereby increasing its computational capabilities (for review see Silver, 2010).

2.3.2 Examples of input-output gain modulation in visual cortex

Gain modulation has been shown to play an important role in many cortical functions. A prominent example is the scaling of orientation tuning curves. Gain modulation in that sense means that a modulatory input scales the responses to all stimulus orientations by a constant factor, thereby increasing the tuning amplitude while preserving the tuning selectivity. The orientation tuning width of a neuron, for example, has been shown to be largely invariant to stimulus contrast, a fact which is not explained by a simple linear summation of inputs (feedforward model) (Anderson, 2000; Finn et al., 2007). In the feedforward model, increasing the stimulus contrast would increase the synaptic drive to all orientations, thereby increasing orientation tuning width by raising also inputs to non- preferred orientations above

threshold (the so called “iceberg effect). Instead, by a combination of mechanisms the gain of the neuron is increased preserving orientation selectivity.

Another example for the modulation of tuning curves comes from spatial attention experiments in awake, behaving monkeys. In those experiments, the tuning curve of a neuron for different orientations or contrasts was compared between situations, where the monkey paid attention to a stimulus inside the receptive field of the recorded neuron, and situations where the monkey’s focus of attention was somewhere else in the visual field. It turned out that orientation and direction tuning curves were roughly multiplicatively scaled in area V1 and V4 by spatial attention (McAdams & Maunsell, 1999a; Treue & Martinez Trujillo, 1999), preserving the tuning width despite a change in amplitude. On the contrary, some neurons decreased their tuning width and thus responded more selectively with attention (Spitzer et al., 1988). The cellular mechanisms mediating those effects of attention are largely unknown, but it is very likely that feedback from higher areas provides modulating input which could lead to a gain change by the mechanisms mentioned in section 2.3.1 (Williford & Maunsell, 2006).

2.3.3 Variability in spike output

As discussed in the previous section, a neuron with thousands of inputs receives a bombardment of synaptic inputs, which raises the problem of early response saturation. This comes together with an interesting phenomenon familiar to every neurophysiologist working experimentally in vivo: Repetitive stimulation of a neuron leads to a different pattern and number of spikes for each cycle, although the stimulus continues exactly the same. Many studies have shown high trial-to-trial variability in spike count for anesthetized and awake animals (Heggelund & Albus, 1978; Rose, 1979; Tolhurst et al., 1983; Vogels et al., 1989; Reich et al., 1997). The variance of the spike count across trials in those experiments ranged between one and three times the mean spike count. This type of variability is measured over a long time period of many trials, and one therefore assumes that it reflects non-stationarities in cortical excitability (Tomko & Crapper, 1974; Kelly et al., 2010). As mentioned before, spontaneous fluctuations (Arieli et al., 1996) and background synaptic inputs are high in visual cortex. Interestingly, high response variability emerges in the cortex and is not inherited from the LGN or the retina, where response variability is low (Kara et al., 2000).

Additionally, the timing of subsequent spikes (i.e. the interspike intervals) of a neuron recorded in vivo is highly irregular. This has important implications on the synaptic integration mechanism: If a neuron would simply integrate the randomly arriving EPSPs,

firing would be predicted to be very regular (Softky & Koch, 1993). Indeed, the timing of spikes in response to current injections in vitro is very regular (Stevens & Zador, 1998).

Where does the high variability observed in vivo come from? Two sources are possible: Either it is a result of noise intrinsic to the neuron, or it is determined by the nature of the synaptic input. Intrinsic noise includes stochastic opening of ion channels (White et al., 2000), differences in EPSP amplitude (Mason et al., 1991), synaptic failure (Stevens & Wang, 1995) and a variable spike threshold (Azouz & Gray, 1999). While all of those mechanisms may contribute to output variability, slice recordings in vitro have shown that the spike generating mechanism is highly reliable (Mainen & Sejnowski, 1995). Thus, the high output variability must be the result of the synaptic inputs.

To obtain the high amount of variability observed in vivo, two mechanisms have been proposed. First, balancing excitation with inhibition leads to irregular firing. This is because for the extreme case of a fully balanced input, firing is caused by the input fluctuations only (the mean net synaptic drive is zero). The balance of excitation with inhibition prevents the neuron from early saturation and increases its dynamic range of response, but comes at the cost of an irregular firing (Shadlen & Newsome, 1998). Second, correlations between inputs will also increase spike time variability (Salinas & Sejnowski, 2000). In this regime, synchronously arriving EPSPs have a higher impact on the membrane potential and therefore have a higher probability in eliciting a spike. Correlated noise has an important consequence for the propagation of a signal, because it cannot be averaged out by a population of neurons and will persist in the system. In vitro slice experiments have shown that both mechanisms are necessary to explain the high variability seen in vivo (Stevens & Zador, 1998).

Similar to the response gain, spatial attention has been shown to also influence the response variability of neurons in visual cortex. When a monkey pays attention to a stimulus inside the receptive field of a recorded neuron, response variability decreases. This is accompanied by a decorrelation of neuronal activity (Mitchell et al., 2007; Cohen & Maunsell, 2009). Recently, such a decorrelation of the network has been shown to be induced by visual stimulation (Oram, 2011), which in turn leads to a decrease in trial-to-trial variability (Churchland et al., 2010).

In summary, the nature of the synaptic input determines the output response function of a neuron, and this output is highly variable. If modulatory projections to a particular neuron alter the response amplitude and variability, they should have an impact on the coding capabilities of this neuron for a specific stimulus. This is because both, the rate and timing of spikes can convey information.

It should be noted that some of the considerations above about modulation of output variability and response gain are mainly valid in a "high input regime". In contrast, coding of sensory inputs has been shown to be sparse (e.g. Olshausen & Field, 2004) and in this regime other mechanism may determine the response of a neuron.

2.4 Effects of input modulation

From anatomical studies it is known that synaptic input from many sources converges onto a neuron (see section 2.2). How can one study, experimentally, the impact of each individual source on the firing properties of such a neuron? A straightforward approach is to silence, or deactivate a particular type of input to a neuron and compare its activity to the native condition. Indeed, a lot of studies have been performed revealing the contribution of intrinsic horizontal and feedback projections to the response properties of neurons in visual cortex (for review see Lamme et al., 1998; Angelucci & Bressloff, 2006).

2.4.1 Response modulation through intrinsic horizontal connections

The contribution of intrinsic horizontal connections to the orientation and direction tuning of neurons in primary visual cortex has been studied in detail. In one set of experiments, the inhibitory neurotransmitter GABA was locally applicated into regions with an orientation preference orthogonal to the recorded neuron (Crook & Eysel, 1992; Crook et al., 1998). The result was a broadening of the orientation tuning curve, possibly due to reduced cross-orientation inhibition. Similarly, application of the $GABA_a$ blocker bicuculline led to an increase in orientation tuning width of neurons in cat area 17 and 18 (Sillito, 1979; Eysel et al., 1998; Jirmann et al., 2008). In contrast, another study failed to obtain any change in orientation selectivity by local application of GABA, but a change in the neuron's preferred orientation angle was observed (Girardin & Martin, 2009b).

2.4.2 Response modulation through feedback connections

Several studies have described the contribution of feedback projections to the tuning properties of visual cortical neuron. For example, deactivation studies in the cat visual cortex revealed a primarily excitatory influence of those connections on their target cells, as spontaneous and stimulus driven activity declined upon thermal deactivation of area 21a (Wang et al., 2000; 2007). Furthermore, some cells showed a broadening in their orientation

tuning whereas for other cells the tuning became sharper. Interestingly, despite a change in tuning amplitude, the signal-to-noise ratio of the responses was not affected. Similar results have been obtained in studies inactivating feedback from V2 to V1 in squirrel monkeys (Sandell & Schiller, 1982). Here, upon cooling deactivation most of the tuning curves of neurons recorded in V1 decreased in amplitude without a change in tuning width, albeit for some neurons increases in tuning amplitude occurred.

Another study, using intrinsic signal imaging combined with thermal deactivation of area PMLS in the cat, demonstrated a substantial impact on direction selectivity, whereas the basic structure of orientation maps was largely preserved (Galuske et al., 2002).

In addition to the increase of the response amplitude and the contribution to direction and orientation selectivity, synaptic input from feedback connections seems to play an important role in shaping the "extra classical" receptive field properties of neurons in V1 (for review see Angelucci & Bressloff, 2006). Deactivating parts of V2, for example, led to an increased responsiveness of neurons in V1 to stimulations of their surround regions (Bullier et al., 1996). Moreover, deactivation studies have emphasized a role of feedback connections in improving the discrimination between figure and background in monkey visual areas V1, V2 and V3 (Hupe et al., 1998).

2.5 Callosal projections as a model for intrinsic connectivity

In deactivation studies, one always fights the problem that the deactivation procedure itself may directly influence the recording. This is especially a problem when investigating connections on the same hierarchical level. In contrast to feedback studies, one has to interfere with the same area one records from. An elegant way of avoiding this problem is to take advantage of the separation of the cerebral hemispheres connected via the corpus callosum. Figure 2-5A illustrates this experimental setup. While recording visually evoked activity from one hemisphere, one can control the additional input coming from the corresponding regions on the contralateral side.

2.5.1 Anatomy of visual callosal projections

Virtually all areas on the two hemispheres are densely interconnected by callosal connections (CC) forming about 32 million axons in the cat (Berbel & Innocenti, 1988). Because each half of the visual field is represented on a separate hemisphere, early reports suggested that the CC serve to integrate the visual information along the vertical meridian (VM) in order to create a

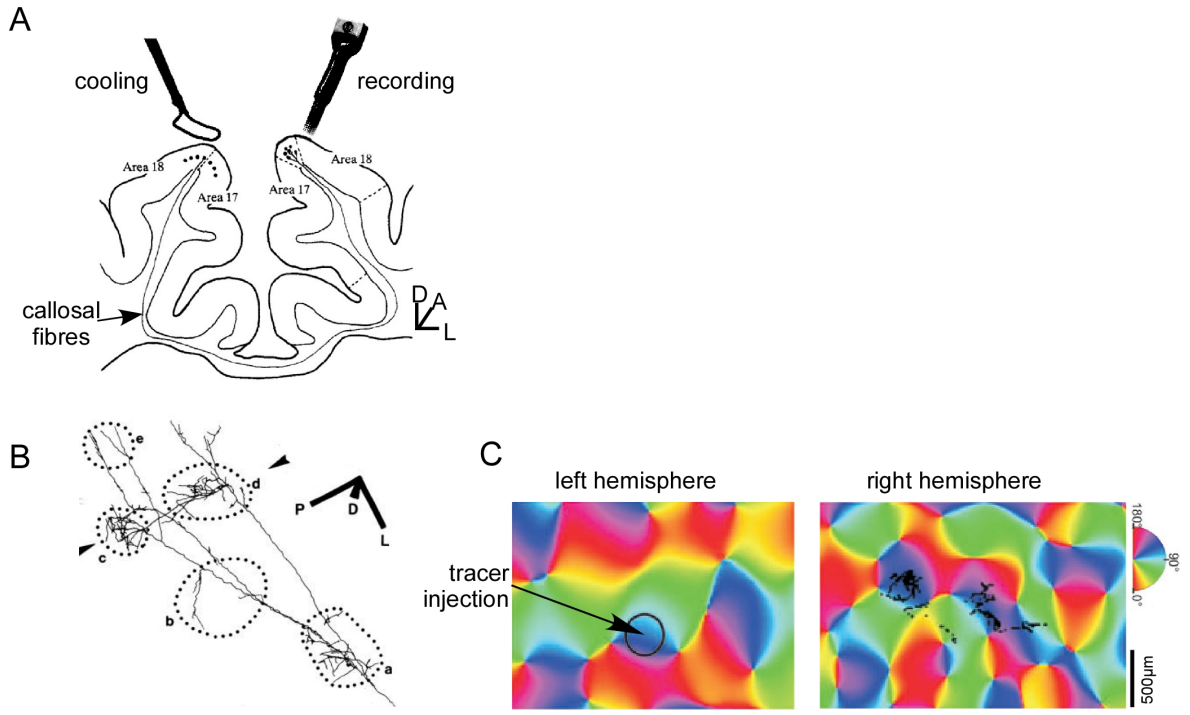

Figure 2-5: (A) Experimental setup. Recordings were performed from one hemisphere around the area 17/18 border, while deactivating corresponding regions on the other hemisphere, linked by callosal connections. Because of the spatial separation one doesn't interfere with the recording during cooling deactivation. (B) Patches of callosal terminals (marked by dashed lines) visualized by biocytin injections in the contralateral hemisphere. (C) Orientation specificity of callosal connections. Tracer injections in an orientation domain preferring oblique (135°, red) stimulus orientations in one hemisphere results in bouton clustering in domains of the same orientation preference on the contralateral hemisphere. A modified from Payne, 1994; B modified from Houzel et al., 1994; C modified from Rochefort et al., 2009.

unified percept (Choudhury et al., 1965; Hubel & Wiesel, 1967).Indeed, the density of callosal connections was found to be greatest at the border between area 17 and 18, holding a representation of the VM (Daniel & Whitteridge, 1961; Hubel & Wiesel, 1967; Houzel et al., 1994). Therefore, in cats, a part of the ipsilateral visual field is represented that extends from 2° up to 20° from the VM, depending on the elevation of the receptive field (Segraves & Rosenquist, 1982; Payne, 1994). Studies in cats, with a section of the optic chiasm, confirmed that indirect input via the corpus callosum matches the direct, ipsilateral responses in terms of their orientation preference and receptive field position (Berlucchi & Rizzolatti, 1968; Lepore & Guillemot, 1982). In contrast, some studies have revealed a non-homotopic pattern of CC (Olavarria, 1996;2001; Alekseenko et al., 2005; Rochefort et al., 2009). Here, neurons in area 17 and 18 project to the 17/18 TZ on the contralateral hemisphere, whereas projections originating from the 17/18 TZ terminate preferentially in area 17 or 18 on the other side. This is supported by the arrangement of callosal terminals in the projection target zone. They usually form 2 - 8 clusters of 100 – 800 µm in diameter with a spacing of 100 – 2000 µm (figure 2-5B; Houzel et al., 1994; Innocenti et al., 1995; Houzel & Milleret, 1999). Those clusters have been shown to coincide with orientation domains, indicating connections of

neurons of similar orientation preference, like for long-range horizontal connections (figure 2-5C; Schmidt et al., 1997a; Rochefort et al., 2009). Despite the large divergence of axon terminals, spikes can arrive synchronously at the target synapses, because axonal conduction velocity compensates for offsets in distance. This is because of the large variety in callosal axon diameter (0.25 – 2.5 µm) corresponding to a conduction velocity between 1.4 – 27 m/s (Houzel & Milleret, 1999). Large parts of the callosal projection fibers have a high conduction velocity which results in a short latency between the two hemispheres of about 2 – 6 ms (Innocenti, 1980).

Most callosal fibres originate from pyramidal and spiny stellate cells in layer III and superficial layer IV as well as layer 6 (Fisken et al., 1975; Innocenti, 1980; Segraves & Rosenquist, 1982; Voigt et al., 1988) and form excitatory synapses on pyramidal cells in layer III and superficial layer IV (Shoumura, 1974; Fisken et al., 1975), albeit a few directly projecting inhibitory neurons have been described (Buhl & Singer, 1989; Fabri & Manzoni, 1996). The target cells of the CC are mainly pyramidal and spiny stellate cells in supra- and infragranular layers (Voigt et al., 1988; Houzel et al., 1994), but some projections onto inhibitory neurons exist, too (Martin et al., 1983).

2.5.2 Functional studies on the callosal system

Taken together, the callosal system has much in common with long range intrinsic connections, regarding the type, morphology and specificity of projections. Therefore, one can assume that the callosal system is just an extension of the intrinsic network across the two cerebral hemispheres (Voigt et al., 1988).

Early studies revealed the contribution of callosal projections in generating a representation of the ipsilateral visual field along the VM, together with binocular convergence on neurons close to the 17/18 border, possibly supporting depth perception (Choudhury et al., 1965; Blakemore et al., 1983). Thus, cooling deactivation of a restricted area along the 17/18 border in one hemisphere led to a shrinkage of the ipsilateral field representation on the other hemisphere (Payne, 1994). On a cellular level, cooling the contralateral hemisphere revealed a mixed picture of spike rate changes. In the superficial layers, about 60% of the modulated units showed a decrease in spike rate in response to a moving bar stimuli, while the spontaneous activity showed the same proportion of in- and decreases (Payne et al., 1991; Payne, 1994; see also Schmidt et al., 2010).

Berardi and co-workers (Berardi et al., 1987; see also Rochefort et al., 2007) took advantage of the split chiasm preparation in cats to study the physiological properties of

visual callosal connections. In both, areas 17 and 18, neurons could be driven through the corpus callosum by visual stimulation. However, the response threshold of the callosal pathway was much higher as compared to direct, geniculocortical excitation, and the contrast gain for grating stimulation was three times smaller. Interestingly, in area 18 only a few cells had lower contrast thresholds for the callosal pathway compared to the direct geniculocortical one. Furthermore, the tuning for temporal and spatial frequencies was comparable between the two pathways.

Moreover, input through the corpus callosum has been shown to be orientation tuned, with an even sharper tuning compared to the thalamic pathway (Lepore & Guillemot, 1982; Rochefort et al., 2007). In agreement, interactions between the two hemispheres have been shown to be stimulus specific, particularly strong for collinear stimulus orientations presented to the two visual fields, in contrast to an orthogonal orientation (Carmeli et al., 2007; Makarov et al., 2007), and stimulation with flashed squares evoked no interactions at all (Nakamura et al., 2008). Moreover, callosal connections have been described in shaping the orientation and direction tuning of neurons in area 17 and 18 of the ferret, especially for vertical contours along the VM (Schmidt et al., 2010).

Given the anatomical and physiological properties of callosal connections, one can conclude that the callosal system is an appropriate model to study the impact of modulating input on cells in primary visual cortex.

2.6 Purpose of the study

As already laid out in the beginning of the introduction, a central question of information processing in the brain is how converging input from different sources are processed in order to produce a certain output. This can happen on the level of whole brain areas, subpopulations of neurons or even single cells. In this thesis, we focused on single neurons and their output modulation by the horizontal network. To this end, we combined reversible thermal deactivation of a restricted cortical area with extensive electrophysiological recordings in primary visual cortex of cats. By focussing on the callosal system, we could reversibly control lateral input to the recorded area in an in vivo system. This is a powerful setting and has several advantages compared to other experimental designs. First, experiments are performed in vivo, so the environment of the recorded neurons is as close as possible to the natural condition, albeit the experiments were performed during anaesthesia. This is important, because a recent study has highlighted the extensive synaptic connectivity over long distances, which is destroyed in in vitro slice preparations (Stepanyants et al., 2009).

Second, one can perform multiple deactivation cycles in one animal, improving statistical power and reducing the need of animal experiments, because the deactivation method is reversible. A successful recovery after rewarming is an important control for the specificity of the cooling effect. Third, one minimizes direct effects of the deactivation method, because the callosal system provides a spatially separated system. Forth, by using multielectrode arrays, one can record from many neurons at the same time and therefore during the same state of the cortex.

Using this experimental setting, we now could ask different questions on how response modulation in visual cortex works:

1. Is response modulation dependent on how the system is driven by a visual stimulus? By using two different stimuli, namely moving gratings and random dot patterns, we could drive the visual system in different ways because of the unique properties of those stimuli. This complements previous work which focused manly on stimulation with moving gratings and bars.
2. Does response modulation differ for different visual areas? Many previous studies on the callosal system have focussed on the integration of the two visual fields along the vertical midline. We tested, if response modulation is also present in portions of area 17 and 18 up to 10° away from the VM.
3. What is the mechanism of the response modulation with respect to the tuning properties of neurons to different stimulus orientations? Can it be described by a gain change, as described for other input manipulations? And if, how can this be explained by the removal of synaptic input?
4. Does synaptic input via the horizontal network alter the response variability of single neurons? If so, is there a relationship between changes in the timing of individual spikes and the count variability across many trials, as predicted by theory?

3. Materials and Methods

Eleven adult cats bred at the Institute's colony were used in this study. All experimental procedures have been performed in accordance with the guidelines of the Society for Neuroscience and the German law for the protection of animals.

3.1 Surgical procedures

Anesthesia was initiated by intramuscular injection of 10 mg/kg ketamine hydrochloride (Ketamin, CP-Pharma) and 1 mg/kg xylazine hydrochlodride (Rompun®, Bayer) supplemented with 0.1 mg/kg atropinesulfat (Atropin, B.Braun). It was maintained after tracheotomy by artificial ventilation with a mixture of 0.6/1.1 % halothane (for recording/surgery respectively) and N_2O/O_2 (70/30 %). After all surgical procedures had been terminated, the animals were paralyzed by continuous intravenous infusion of pancuronium bromide (0.15 mg/kg/h, Pancuronium, DeltaSelect). Depth of anesthesia was controlled by continuously monitoring the electrocardiogram and the CO_2 and anesthesia gas level in the expiration air. The temperature was also monitored and regulated by an automated heating pad.

A craniotomy was performed on both hemispheres in topographical correspondence, leaving a ridge of bone above the superior sagittal sinus intact. For each animal, the position of the craniotomy was chosen to cover a portion of both area 17 or 18 as well as the 17/18 border region (centered around Horsley–Clarke coordinates AP 0 to -2, ML +2). A recording chamber was implanted over one of the craniotomies (in ten out of eleven animal the recording was performed on the left hemisphere), fixed with dental cement (Paladur®, Heraeus) and, after removing the dura, filled with silicon oil (50 cs, Boss Products) for optical imaging. Following the optical recordings, the silicon oil was removed and two microelectrode arrays were inserted for electrophysiological recordings.

A surface cryoloop was placed on the brain on the other hemisphere and covered with a clear agar (agarose type XI, Sigma) to allow visual inspection of the correct position throughout the experiment. At the end of an experiment, the animals were killed with a lethal dosis of pentobarbital (Narcoren®, Merial).

3.2 Determining recording position

The position of the craniotomy roughly determines the recording area. This position was chosen according to stereotactic coordinates described in the literature (e.g. Rochefort et al. 2007). Those coordinates can only give an approximation of the true 17/18 border, because of interindividual differences. We therefore tried to determine the 17/18 border during the experiment using an imaging technique based on intrinsic signals. This technique allows to map the 17/18 border on the cortical surface. Using the blood vessel pattern as a reference, one can subsequently position the recording electrodes at a specific position relative to the 17/18 border.

3.2.1 Optical imaging of intrinsic signals

Optical imaging of intrinsic signals is based on the light absorption characteristics of hemoglobin (Bonhoeffer & Grinvald, 1996). More specifically, deoxygenated hemoglobin absorbs more light at a wavelength of 605 nm then does oxygenated hemoglobin. Neuronal activity is an energy consuming process, which in turn leads to an increase in local oxygen consumption, essential for oxidative phosphorylation. The fine network of capillaries ensures an optimal supply of oxygen to the neurons. The oxygenation state, which can be measured as the light absorption, can therefore serve as a physiological marker for the activity of a local population of neurons.

The functional definition of the 17/18 border with optical imaging is based on different preferred stimulus characteristics of areas 17 and 18 as described in (Bonhoeffer et al., 1995). Area 17 neurons respond preferentially to high spatial and low temporal frequencies, whereas area 18 neurons respond optimally to low spatial and high temporal frequencies. Moreover, the primary visual cortex in cats is organized in functional orientation columns. Stimulation with a grating of a single orientation leads to the activation of only those regions preferring that particular orientation. Such a map is called “single condition map”. For a uniform stimulation of the cortex, we thus showed a set of gratings of four different orientations (0°, 45°, 90° and 135°) moving back and forth. Each set was presented with a spatial and temporal frequency optimized for either area 17 or 18 (details see section 3.4) and repeated 20 - 40 times. The light absorption was measured with a CCD camera positioned above the recording camber. This camera uses a tandem lens system with a high numerical aperture in order to obtain a shallow depth of field (Ratzlaff & Grinvald, 1991).

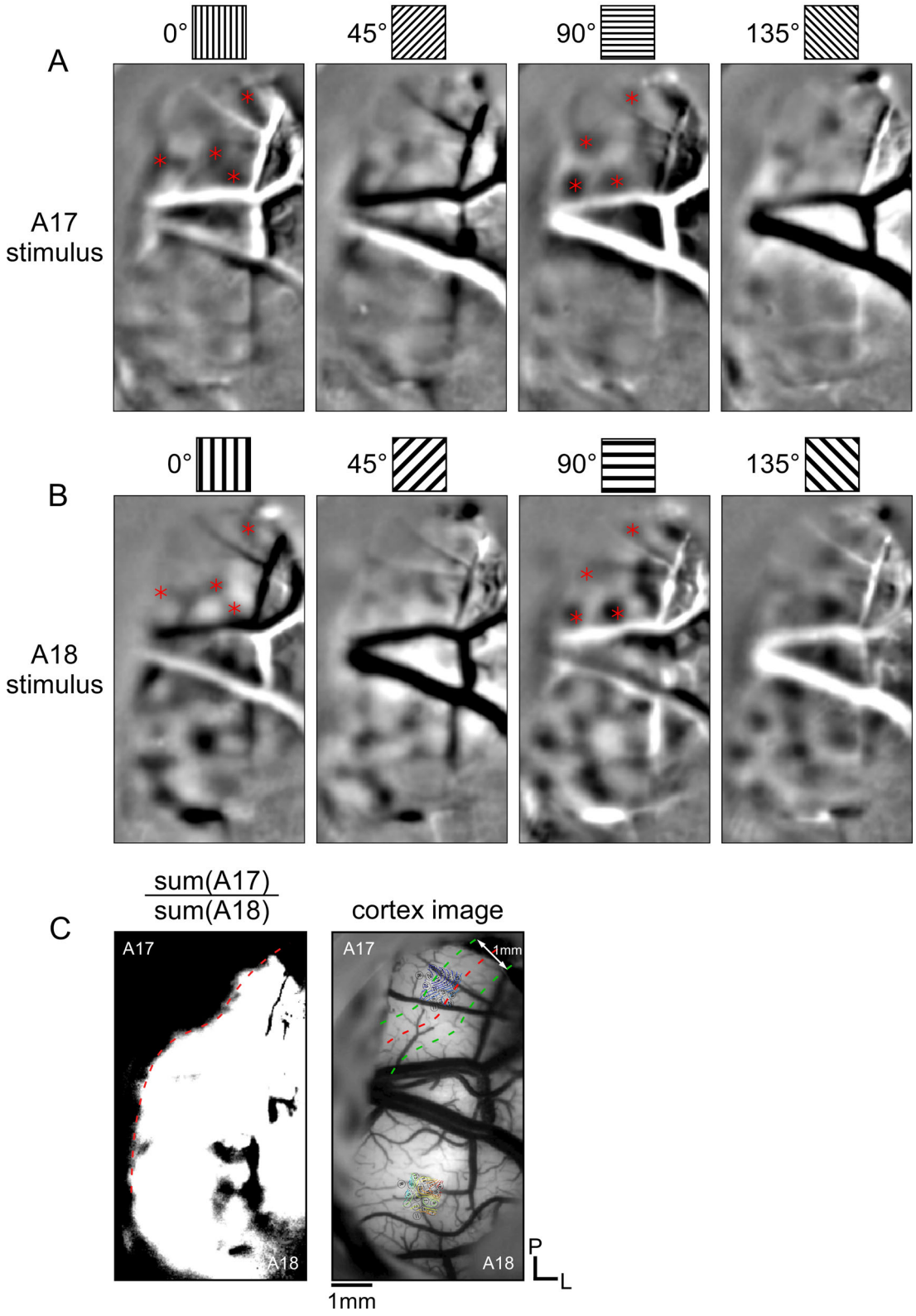

Figure 3-1: (A) Orientation maps for stimulation with gratings optimized for area 17. The corresponding stimulus orientation is depicted above each map. The red stars in the 0° and 90° maps indicate orientation columns. Note the absence of any orientation columns in the lower half of the map. (B) Orientation maps for stimulation with gratings optimized for area 18. Orientation columns are clearly visible throughout the map. For comparison with the area 17 stimulation, the same orientation columns as in (A) are labeled. (C) Thresholded map between area 17 and 18 stimulation. The red dashed line is drawn at the region of equal brightness. (D) Overlay of the 17/18 border on the blood vessel image. The extent of the TZ is assumed to be 1 mm and depicted by the green dashed lines flanking the 17/18 border. Additionally, the positions of the recording matrices are drawn.

This allows to focus under the cortical surface (about 500 – 600 µm), and blurs out the superficial blood vessels, which would give rise to large artifacts. 15 frames of 200 ms duration were captured during one stimulus presentation.

In a first step, frames and trials were averaged for each stimulus separately. Then, single condition maps (0°, 45°, 90° and 135°) obtained by stimulating with a grating of high spatial frequency (figure 3-1A) were summed and divided by the same set of maps obtained by low spatial frequency stimulation (figure 3-1B). The result is a difference image with dark regions representing area 17 and bright regions representing area 18, respectively. The border between the areas was defined as the region of equal brightness (figure 3-1C, left). The right part of figure 3-1C demonstrates the 17/18 border (dashed red line) estimated by that method superimposed on an image of the blood vessels. The width of the 17/18 border was chosen to be 1 mm according to previous work (Rochefort et al., 2007; Rochefort et al., 2009), indicated by the green dashed lines. The position of the recording electrodes is indicated by the circles representing the shanks of the matrix electrode. In this example, the posterior electrode resides in the 17/18 border region, whereas the anterior electrode is positioned in area 18. Using this classification method, all electrode positions were classified as either belonging to area 17, area 18 or the 17/18 transition zone.

3.2.2 Retinotopic representation

In addition to the classification by optical imaging, we characterized the positioning of the electrodes relative to the 17/18 border after the experiments by determining the retinotopic relationship inside one electrode matrix. To this end, for each recorded channel, the center of the receptive fields of the recorded neurons was estimated. The receptive fields were mapped during the experiment with a single bar moving across the stimulation monitor in 16 directions. Knowing the speed of the bar and the size of the mapping area, one can calculate the position on the screen where the neuronal activity was highest (Lima et al., 2010). The x and y coordinates in visual space for each electrode were expressed relative to the smallest value of one matrix pair and averaged over all mapping protocols of one experiment (usually 8-15 per cat). Given the channel layout, those coordinates can be interpolated and overlain as iso-contour lines on a scheme of the recording matrix. An example is shown in figure 3-2 for the same animal as in figure 3-1. For better visibility, iso-elevation and azimuth lines are plotted separately on top of the electrode layout. The numbers indicate the extension in visual space (in units of degrees) for each iso-contour line relative to the smallest value.

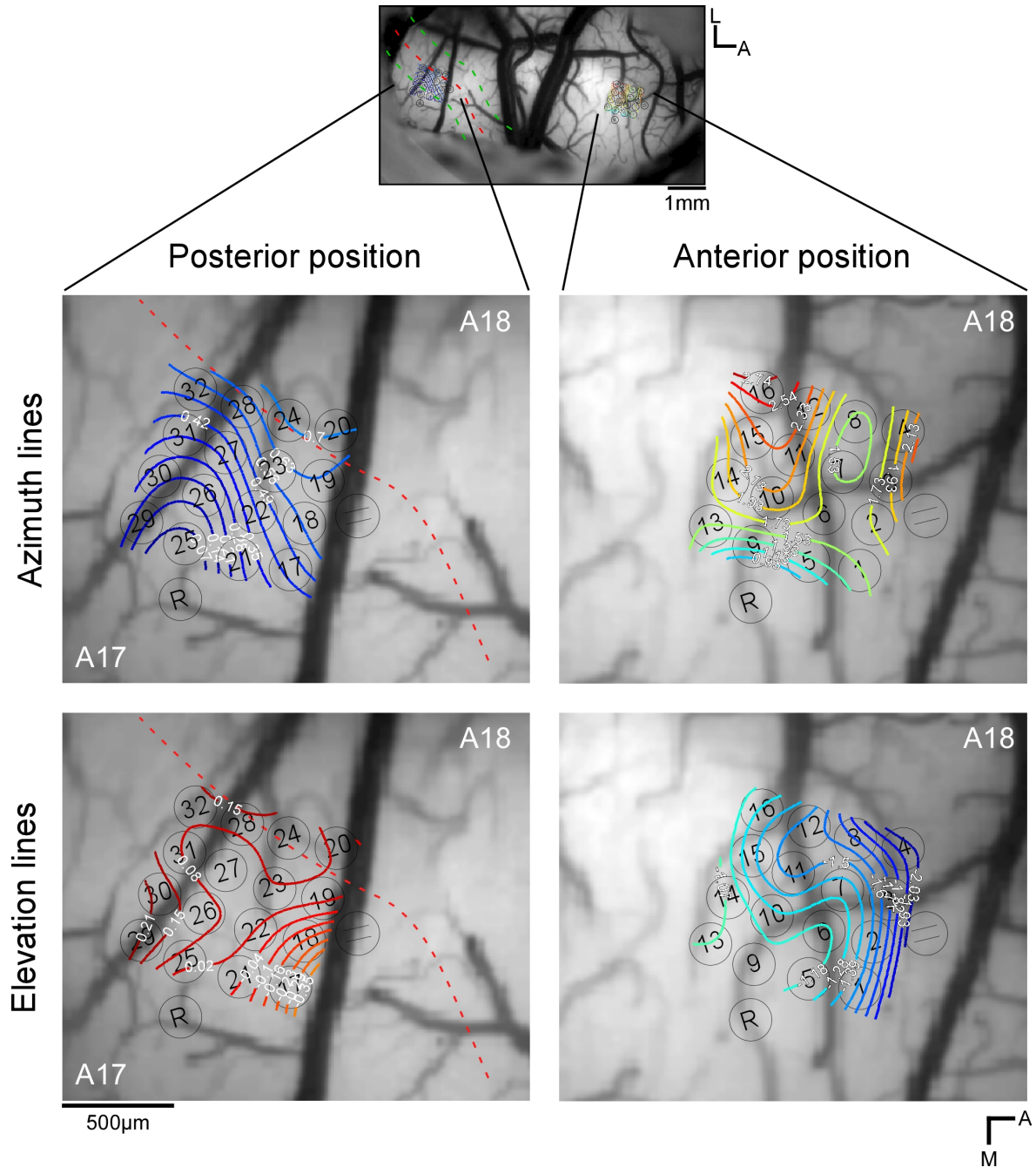

Figure 3-2: Enlarged view of the cortex image from figure 3-1. The retinotopic organization of the recorded portion of cortex is indicated by the iso-contour lines for the anterior and posterior recording position. Note that for the posterior recording position the iso-azimuth lines are running in parallel to the 17/18 border, whereas the iso-elevation lines intersect the border orthogonally. Numbers depict the distance of each iso-contour line to the smallest value in units of degree of visual space.

For azimuth lines, receptive fields move temporally, away from the vertical meridian, when moving away from the 17/18 border. Conversely, the elevation lines roughly intersect the 17/18 border orthogonally, indicating that receptive fields shift up and down in the visual field along the vertical meridian when moving along the 17/18 border. This method is limited by the accuracy with which receptive field centers can be estimated and small fluctuations in

electrode shank spacing. Nevertheless, the method complements the classification done by the optical imaging procedure.

3.3 Cooling deactivation

In order to investigate the impact of cortico-cortical connections on their target neurons, we used reversible cooling deactivation. The following parts give a description of the technical implementation and the physiological basis of the deactivation technique.

3.3.1 Assembly of cooling probes

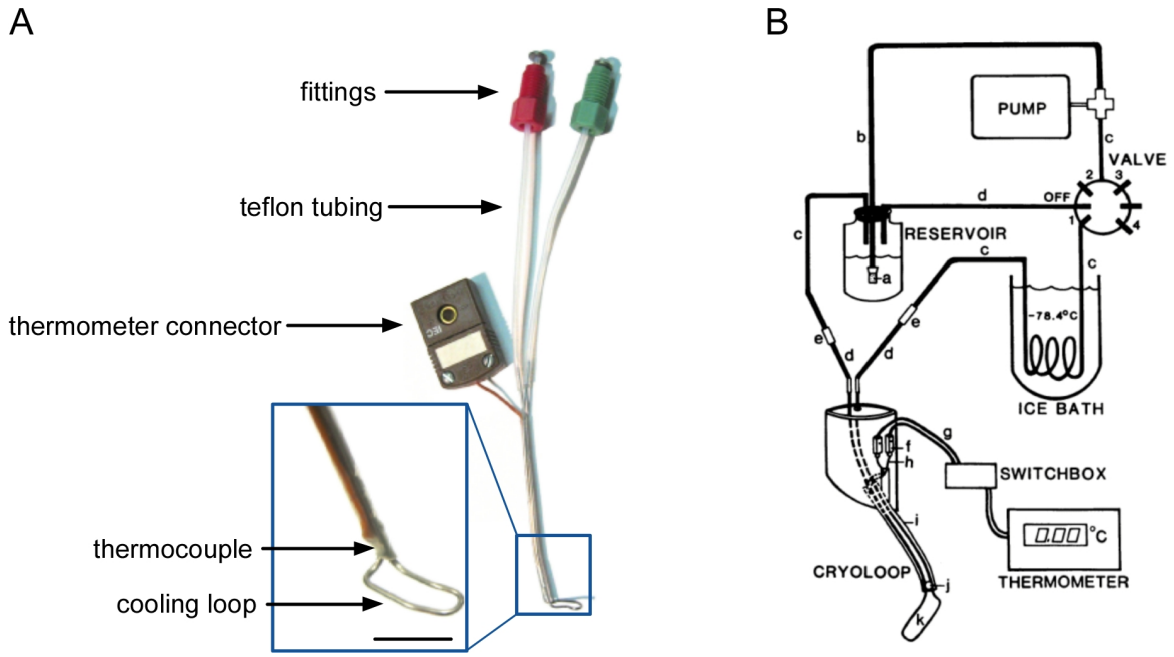

Figure 3-3: Configuration of cooling probes (A) and cooling setup (B). The probe can be connected through the fittings with the cooling setup. The inset shows an enlarged view of the cooling loop (bar = 5 mm). The loop is shaped to fit the surface of the cortex for each experiment individually. A thermocouple is soldered at the union of the metal tubes, which allows monitoring the loop's temperature. Methanol is drawn from a reservoir and pumped through a Teflon tube, coiled to a spool inside an ice bath. The chilled methanol is then flooded through the cooling probe and finally reaches the reservoir again. B modified after Lomber et al., 1999.

In this work, we used custom made cooling probes, according to the cryoloop technique first described by Salsbury & Horel (1983). The cooling probes were made of hypodermic stainless steel tubing (ID: 0.42 mm, OD: 0.64 mm, Varian) shaped to fit the marginal gyrus around the 17/18 border (figure 3-3A). Loop dimensions were around 7 x 3.4 mm (outer diameter). In order to evaluate the temperature at the basis of the cooling probe, a micro-thermocouple was soldered to the union of the loop. The micro-thermocouple was made by twisting together bared copper and constantan wires followed by a careful trimming of the tip.

The remaining ends of the wires were attached to a sub-miniature connector (SMPW-T-F, Omega Engineering), so that a thermometer (HH-25TC, Omega Engineering) could be easily connected. The in- and outlet of the stainless steel tubing were attached to a piece of Teflon tubing (ID: 0.51 mm, OD: 1.6 mm, Varian) and the remaining end was connected to a flanged fitting (1.6mm, Upchurch Scientific). The use of connectors allows for an easy connection of the cooling probe to the rest of the cooling setup. The cooling setup is schematically depicted in figure 3-3B. Methanol is drawn from a reservoir by a synchronously rotating pump (QSY-1CSC, Fluid Metering Inc) and pumped into a long Teflon tube (ID: 0.51 mm, OD: 1.6 mm, Varian), which is coiled in a Dewar vessel filled with methanol. This methanol is chilled down by dry ice pallets to about -70°C. As a result, the methanol flowing through the Teflon tube is also cooled, which in turn cools down the loop of the cooling probe. The desired temperature, after placing the cooling probe on the brain surface, can then be monitored by the thermometer and regulated by the speed of the pump.

3.3.2 Physiological effects of cooling

Cooling the brain tissue affects many structures in multiple ways, depending on the temperature, the type of brain tissue and the cooling technique used (for review see Brooks, 1983). Some studies showed that lowering the temperature only slightly below physiological values, leads to a hyper-responsiveness in spinal cord neurons (Klee et al., 1974) and neurons of the somatosensory system (Siegfried et al., 1962). A more recent study, using brain slices of rat visual cortex, observed also hyperexcitability of neurons at a temperature about 20°C (Volgushev et al., 2000). Those authors measured basic membrane properties as well as evoked postsynaptic potentials (PSPs) in response to electrical stimulation near an intracellular recording electrode. They found that during cooling the membrane resistance, time constant and latency of PSPs increased with decreasing temperature. More important, the resting membrane potential got depolarized while lowering the temperature at a rate of about 1-2.2 mV/°C. This explains the observed hyper-excitability of neurons cooled to about 20°C, because in this case, the resting membrane potential is brought closer to firing threshold, even though the amplitude of evoked PSPs is reduced. Cooling down below 10-20°C abruptly blocks neuronal responses by a complete depolarization block. It is assumed that cooling induced depolarization is mainly due to a decreased potassium conductance and/or inactivation of the Na^+/K^+ ATPase. Sodium conductance is not affected that strongly, so that a larger amplitude and duration of action potentials are observed. Despite those actions, a variety of effects has been assumed to act on pre- and post synapses, affecting synaptic

transmission. This includes increased/decreased probability of transmitter release, kinetics of vesicle replenishment, transmitter re-uptake and receptor binding. Also changes in active conductances by NMDA channels (release of the Mg^{2+} block by cooling induced depolarization) have been discussed (Brooks, 1983).

Cooling down to > 10°C seems to influence only synaptic transmission and spike generation. Cooling below 10°C also affects fibers, with myelinated fibers being more sensitive to cold then non-myelinated fibers (Franz & Iggo, 1968).

In order to deactivate a specific brain area, it is very important to know the critical temperature where neuronal activity ceases. Also, knowledge about the spread of temperature in the brain tissue is essential to estimate the deactivated brain region. Values of the critical temperature are situated between 10 and 20°C depending on the experimental setup (Sherk, 1978; Girard & Bullier, 1989; Michalski et al., 1993). Estimations of the lateral spread of temperature vary between 3 and 15 °C/mm (Kalil & Chase, 1970; Lomber et al., 1999), depending on the probe and its positioning. The spread of temperature in depth was estimated around 5-8°C depending on the absolute temperature of the cooling probe (Michalski et al., 1993; Girardin & Martin, 2009a).

We usually set the temperature to 2±1.5°C by adjusting the pump speed, which should make sure that all cortical layers had been deactivated. It is likely that the brain tissue directly under the probe was slightly warmer because the micro-thermocouple was not touching the brain. Assuming a brain temperature of 5°C directly under the probe and a critical temperature of 20°C gives a temperature window of 15°C for deactivation. Assuming a spread of 10°C/mm a deactivation area of 10x5 mm^2 for a probe dimension of 7x2 mm^2 will be the result. Using an atlas of retinotopic representation (Tusa et al., 1979; Payne & Siwek, 1990), we could estimate the extent of deactivation in visual space. Because of the different magnification factors for area 17 and 18, the extent in the azimuth direction was estimated to be 3° for area 17 and 10° for area 18 extending in one half of the visual field from the midline. For the elevation, the extent was about 30° (similar for both areas).

3.4 Visual stimulation

For visual stimulation, the eyes were fitted with contact lenses and the pupil was dilated with topical application of atropine sulphate (1%, Atropine-POS®, Urspharm) and phenylephrine (5%, Neosynephrin®, Urspharm). Eye alignment was checked throughout the experiment and corrected with a prism if necessary.

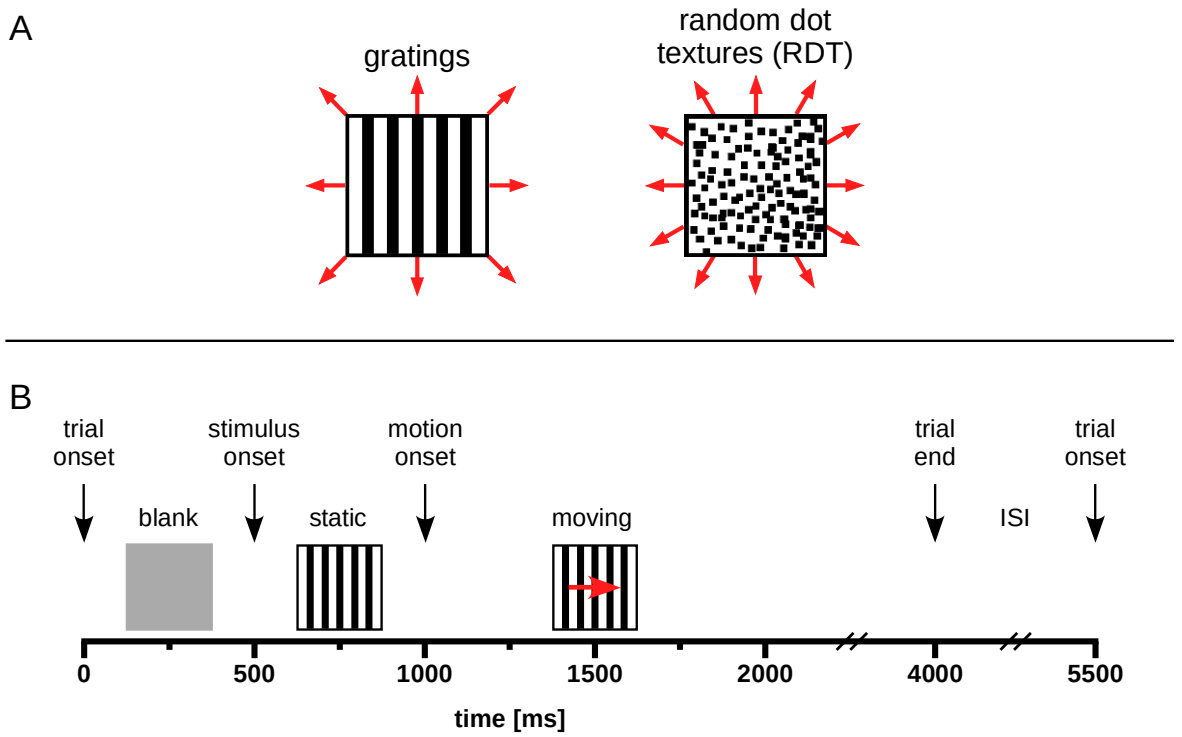

Figure 3-4: (A) Stimuli used in this thesis. Gratings move orthogonal to their orientation in 8 directions. RDTs are composed of randomly scattered squares moving in 12 directions. (B) Timing of stimuli. Stimuli appeared at 500 ms and were held static for another 500 ms. The duration of the moving period varied between 1000 and 3000 ms. A new trial started after an interstimulus interval (ISI) of 1500 ms.

Visual stimuli were presented on a 21" CRT monitor in 57 cm distance to the animal's eyes covering both visual fields. Stimulation was controlled and synchronized with the recording system through a personal computer running custom written stimulation software ("StimPlayer" by Sergio Neuenschwander and "ActiveStim" by Danko Nicolić). Two sets of stimuli were used in the experiments: High contrast (Michelson contrast 1.0) square wave gratings moving in 8 directions (45° steps) orthogonal to their orientation and coherently moving random dot textures (RDTs) moving in 12 directions (30° steps) with reduced contrast (Michelson contrast: 0.8) to prevent motion streaks (figure 3-4A). The Michelson contrast (C) of a stimulus is defined as:

$$C = \frac{L_{Max} - L_{Min}}{L_{Max} + L_{Min}}$$

where L_{Max} and L_{Min} are the maximal and minimal luminance of the stimulus. The mean luminance was 22 cd/m^2 for grating stimuli and 4.2 cd/m^2 for RDTs. Spatial frequency and speed of the gratings as well as the size and speed of the random dots were chosen depending on the cortical area in which the recording was performed. A18: 0.15 cycles/°, 16 °/s for gratings and 0.6°, 20°/s for random dots. A17: 0.5 cycles/°, 4°/s for gratings and 0.4°, 13°/s for random dots. Both stimuli were held stationary for 500 ms (stationary period) after

presentation of a blank screen (spontaneous period) for the same duration and then moved for a period of 1000–3000 ms (dynamic period). Each condition was randomly presented 20-30 times with an interstimulus interval of 1.5 s (figure 3-4B).

As a control, we introduced a third stimulus presented in three cats: moving random bar textures (RBTs). Bars were of the same width as dots, but three times as long. RDTs, RBTs and gratings were presented randomly in 8 directions and repeated 20 times each. Additionally, we adjusted the contrast of the gratings and bars in this new set of stimuli such that the evoked firing rate in response to those stimuli matched that of the RDT stimuli. To this end, we first obtained average contrast response functions by stimulating with gratings/bars of 6 different contrasts (0.03125, 0.0625, 0.125, 0.25, 0.5 and 1.0 Michelson contrast, at optimal orientation for each unit) averaged over a set of selected units. According to this response function we then created grating and bar stimuli choosing a contrast where firing rates matched the firing rate evoked by dots.

3.5 Electrophysiological Recordings

Recording the activity of a neuron means recording its electrical properties over time. Several methods have been developed including intracellular recordings of the membrane potential as well as extracellular measurements of the neuron's electrical field. We used extracellular recordings with microwires usually sampling from a few neurons in the vicinity of the electrode's tip. In an active neuron, current flows in and out of the cell (in the form of ions) creating an electrical dipole. The electrical field of this dipole can be measured with microelectrodes. The measured change of voltage over time is the result of the sum of the capacitive and ionic currents, with the fast influx of sodium ions contributing most to the overall shape. The shape also strongly depends on the position of the electrode relative to the neuron and its morphology. Because the electric field of a dipole decays with the square of the distance from its source (the neuron), neurons close to the electrode tip contribute more to the recorded signal then neurons farther away. Therefore, the size (surface) of the electrode's tip determines how many neurons contribute to the recorded signal. The impedance of an electrode can be used as an approximation of the exposed tip area. The higher the impedance of an electrode is, the smaller is its tip area and the lower is the number of neurons contributing to the recoded signal. A 1 MΩ electrode samples from a radius of about 50 – 100 µm around the tip (Henze et al., 2000). Assuming a neuronal density of 40000 neurons per mm^3 (Cragg, 1967), this electrode would sample from 7 – 50 neurons. Recordings of that type are therefore called "multi unit activity" (MUA) meaning that the recorded spikes originates

from several units, in comparison to "single unit activity" (SUA) which includes only the spikes from one neuron. On the other hand, for high impedance, thermal noise contributes more to the signal and therefore decreases the signal to noise ratio. Because the amplitude of the extracellular recorded signals are only in the range of a few ten to hundred micro volts, the thermal noise will limit the maximal impedance one can use for recording.

3.5.1 Recording setup

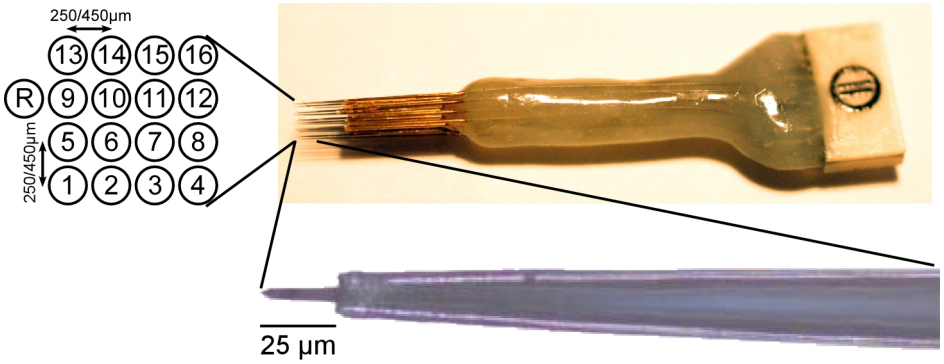

Figure 3-5: Photograph of the matrix electrodes. The channel layout is depicted on the left of the picture, on the bottom one can see an enlarged view of the electrodes tip photographed through a microscope.

Recordings were performed by commercially available microelectrode arrays (Microprobes, Gaithersburg, USA). An array consisted of 16 tungsten electrodes arranged in a 4x4 matrix with a spacing of 450 (used for 6 cats) or 250 µm (used for 5 cats) and an average impedance of 1 MΩ. The electrodes are electrically insulated except for a small tip of 75 µm (see figure 3-5). For each experiment, usually two of those arrays were implanted in either area 17, 18 or in the transition zone (see section 3.1) under microscope control. The electrodes were lowered 200 - 600 µm below the cortical surface, using a micro drive (Narishige), in order to target the superficial layers, and subsequently covered with agar and bone wax to prevent pulsations of the cortex evoked by the ventilation and the heart beat. Signals were amplified (1000 fold) and band pass filtered (0.7 - 6 kHz) by a Plexon preamplifier box (Plexon Inc., Dallas, TX, USA), digitzed, further amplified and thresholded around 4 standard deviations above noise level to obtain spike time stamps by National Instruments IO boards applying custom written Acquisition software ("SPASS" by Sergio Neuenschwander written in LabView®, National Instruments). Spike waveforms were kept for offline sorting. A recording session consisted of a baseline, cooling and recovery period, each with 20 - 30 repetitions per condition. Recording during the cooling period was begun after the cooling

loop reached a stable temperature of 2 ± 1.5° for 5 minutes. The recovery recording started ~20 minutes after cooling was terminated.

3.5.2 Spike sorting

As described above, an extracellular electrode will sample from many cells in the close vicinity of its tip. The separation of individual spikes into different groups called clusters (ideally, a cluster should contain only spikes from one and the same single neuron) is called "spike sorting". We used an automatic sorting algorithm implemented in Matlab® (Mathworks Inc) for offline sorting (Shoham, 2003). The sorting procedure includes the following steps: (1) For a given protocol, all spike waveforms from baseline, cooling and recovery period are merged. This ensures that for the three experimental conditions the same clusters will be been defined. (2) From the merged waveforms, max. 25000 waveforms are picked randomly. This is necessary, because the total number of spikes (= waveforms) may be too large for efficient computation. (3) The original waveform has 38 data points (= time points) which equals 38 dimensions. First, the dimensionality is reduced by taking the first 5 dimensions explaining most of the variance using principle component analysis (PCA). Then, the 5 dimensions are fitted with multivariate t-distributions and decomposed using an expectation-maximization (EM) algorithm. This algorithm is initialized with a large number of components which are reduced in subsequent steps until convergence. The iterative nature of this algorithm can lead to different clustering results each time the algorithm is run. (4) To assign the total of spikes to one of the identified clusters, we used a simple template matching method. First, 100 waveforms are randomly selected from each identified cluster. Then, for the total of spikes, each waveform is tested against the 100 selected waveforms from each cluster to find the closest match by minimizing the residual sum of squares. Some "spikes" cannot be assigned to any cluster because their waveform does not share similarities with other spikes. Those "spikes" are usually artifacts introduced by movement of the electrode or other sources of noise and are therefore sorted out in a "trash" cluster. The result of an example recording is illustrated in figure 3-6. In figure 3-6A, each dot represents one spike in a three dimensional space of the first three principal components. The color coding distinguishes the identified clusters. In figure 3-6B the average waveform for each cluster is depicted with the same color code as above. The black dots in figure 3-6A and the corresponding black average waveform in figure 3-6B represent "trash spikes" which could not be attributed to any cluster and are therefore not considered for further analysis.

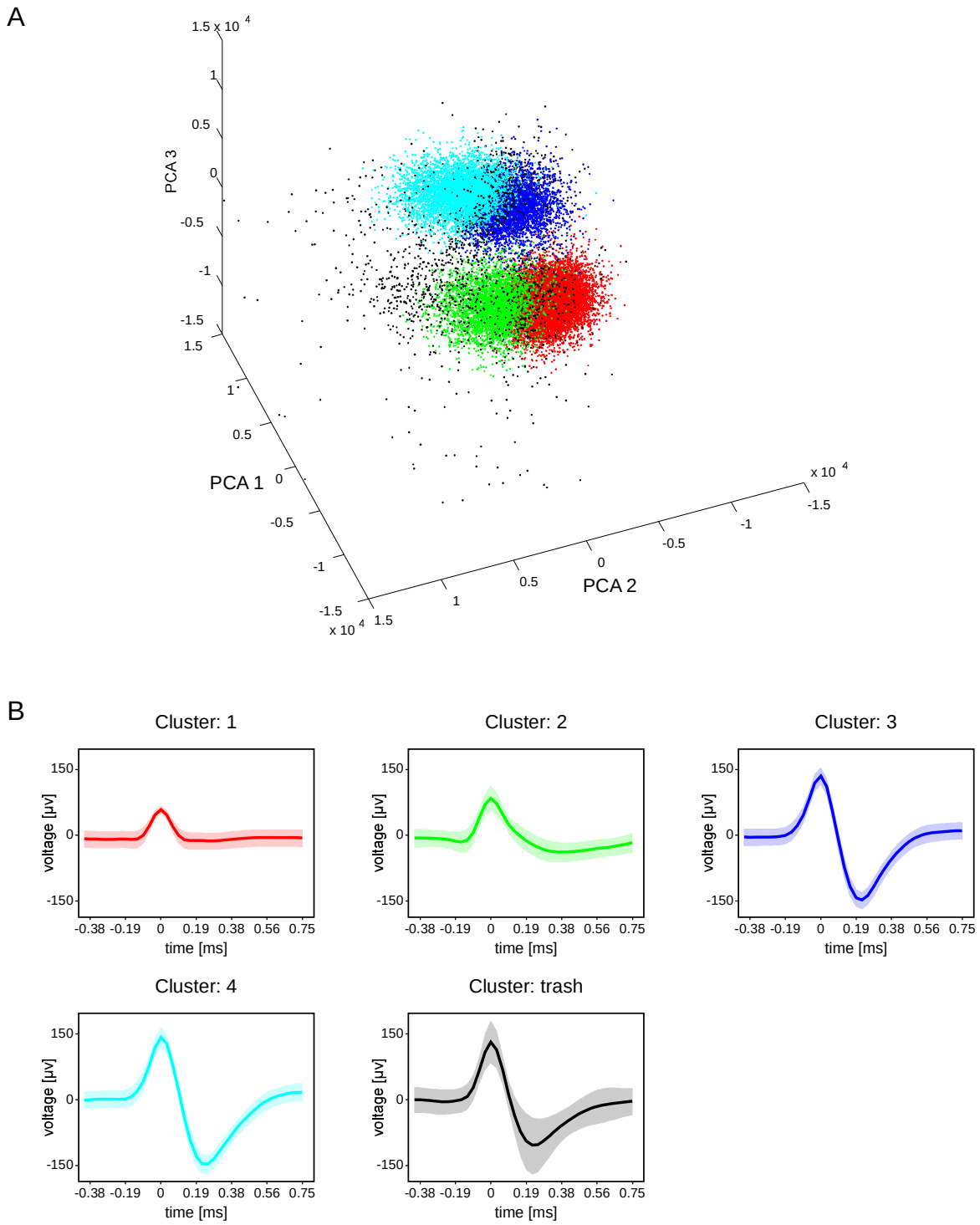

Figure 3-6: Spike sorting of MUA recordings. (A) Plot of the first three principle components of the spike waveforms. Each dot represents one spike waveform. The color codes for the clusters identified by the sorting algorithm. Note the two clearly separated clouds, which are in addition separated into overlapping clusters. Black dots are waveforms which cannot be attributed to any cluster and are sorted out subsequently. (B) Average waveform for each cluster. Color as in A. Shading around the mean denotes ±1 SD. As expected from (A), cluster 1 and 2 as well as cluster 3 and 4 are very similar to each other. The large amplitude of the spike waveforms from cluster 3 and 4 suggest that neurons giving rise to them are closer to the electrode tip then neurons from cluster 1 and 2.

3.6 Data analysis

Offline analysis was done using custom written software in LabView and Matlab. From up to 32 simultaneously recorded channels only those were kept for further analysis exhibiting reliable spiking activity according to the following criteria: I) The response amplitude (measured in spikes/second) to a drifting stimulus should be significantly larger than within the pre-stimulus period (factor 1) and units should be significantly tuned for orientation/direction (factor 2, both $p < 0.05$). This was tested performing a 2-Factor analysis of variance (ANOVA). II) The direction or orientation tuning of the channel should reach a certain threshold. To this end, we computed a direction (DI) and orientation selectivity index (OI) defined as the 1 - CV (circular variance) of the direction or orientation tuning curves, respectively (Ringach et al., 1997):

$$CV = 1 - \frac{\left|\sum R_k \exp(i\theta_k)\right|}{\sum R_k}; \quad CV \in \{0...1\}$$

where R_k is the response to stimulus k, θ_k is the direction of stimulus k and i is $\sqrt{-1}$. DI and OI are 0 for a totally unselective neuron and 1 for a perfectly selective neuron. Only units with a DI or OI larger than 0.2 were included in our sample. This results in a set of 491 units for grating and 348 for RDT stimulation, respectively.

3.6.1 Estimation of tuning width

We fitted vanMises functions to the data using nonlinear optimization and derived the tuning width (full width at half maximum, FWHM) directly from the fitted parameters. The vanMises function is the circular analogue of the Gauss function and defined for orientations between 0 and 180° as follows (Batschelet, 1981):

$$R(\theta) = A\exp\{k[\cos 2(x-\varphi)-1]\}$$

where $R(\theta)$ is the response at the orientation defined by θ, A is the maximum of the function, k is a width parameter, x is the vector of orientations and φ is the center of the function. Before fitting, the offset (minimum across stimulus orientations) was subtracted from all responses. Finally, this offset was then added to the fitted data. The FWHM (in degree) can be calculated from the width parameter k by the following equation:

$$FWHM = \frac{360}{\pi} \times a\cos\left(\frac{\ln 0.5 + k}{k}\right); \quad k > -0.5\ln 0.5$$

Because the tuning width of cells for RDT stimulation can be very broad, we used flat-topped vanMises functions if they fitted the data better (larger R^2 value) than the standard function (Swindale, 1998).

3.6.2 Calculation of PSTHs

We calculated, for each unit and state, a peri-stimulus-time-histogram (PSTH) smoothed with a Gaussian kernel of $\sigma = 10$ ms and normalized it by the maximum response in the dynamic period. The individual PSTHs were then averaged over all animals and units. Statistical significance was assessed by a t-test ($p < 0.05$) corrected for multiple comparisons using the false discovery rate, which controls the proportion of false positives at a specific level (we allowed for 5 % false positives, Benjamini & Hochberg, 1995).

3.6.3 Quantification of spike rate modulation

To quantify neuronal activity, the spike rate was observed in the 500 ms pre stimulus window, and in a 1000 ms window following stimulus motion onset and subsequently averaged over all trials. Additionally, we calculated a modulation index (MI) between cooling/baseline and recovery/baseline for the spike rate (R):

$$MI_{cb,rb} = \frac{R_{c,r} - R_b}{R_{c,r} + R_b}; \qquad MI \in \{-1 \ldots 1\}$$

with MI_{cb} being the modulation ratio between cooling (c) and baseline (b) and MI_{rb} between recovery (r) and baseline (b). This measurement always relates the responses to the baseline, with values < 0 indicating a decrease and values > 0 an increase compared to baseline.

For each unit, a statistical significant difference in spike rate between baseline and cooling was assessed by a nonparametric Mann-Whitney-U test ($\alpha = 5$ %).

3.6.4 Mean matching

Grating stimuli evoke much higher mean spike rates at their preferred direction than RDT stimuli. In order to directly compare the rates, we performed a mean matching procedure on the population of units recorded. This includes the following steps:

(1) A histogram of the rate distribution obtained during the baseline is calculated with a bin width of 1 sp/s for both, grating and RDT stimuli (figure 3-7).

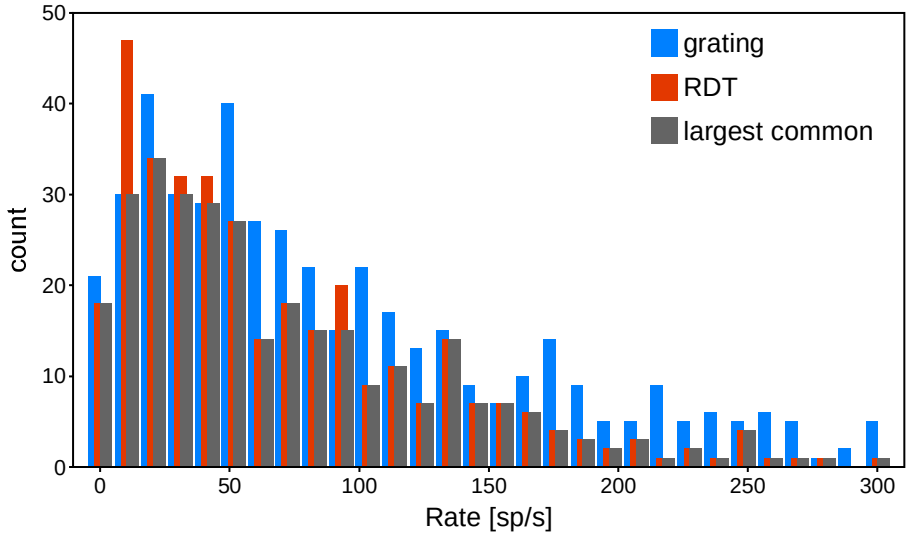

Figure 3-7: Mean matching procedure. The original rate distributions for grating and RDT stimulation are shown in blue and red, respectively. The gray bars denote the largest common distribution for both types of stimuli. For grating stimulation 51 % of the units were kept, whereas for RDT stimulation 67 % survived the histogram matching. For display purposes, a bin width of 10 sp/s was chosen, while for data processing a bin width of 1 sp/s was used.

(2) The largest common distribution (gray in figure 3-7) is obtained, by taking, for each bin, the largest count across the two stimuli for that bin. (3) From the original distributions, for each bin separately, a random subset of units is discarded to make the count of that bin matching the common distribution. (4) For this matched distribution, the mean of the spike rate is calculated for baseline, cooling and recovery period. (5) The last step is repeated 300 times and the resulting 300 values are averaged. Statistical significance between states and stimuli is assessed by an unpaired t-test ($\alpha = 5\%$).

3.7 Gain mechanism analysis

3.7.1 Linear model of tuning curve modulation

To characterize how the removal of callosal input scales neuronal responses, direction tuning curves obtained during baseline and cooling were compared for each recorded unit. First, the directional responses for RDTs and gratings were interpolated to 16 directions using cubic interpolation. Then, the effect of cooling on the tuning curve was expressed by a linear regression model

$$R(\theta)_c = \beta_0 + \beta_1 \cdot R(\theta)_b \quad \text{(full model)}$$

by minimizing the sum of squares between data and model, with $R(\theta)_b$ and $R(\theta)_c$ being the response to direction θ in baseline and cooling, respectively. The parameter β_0 shifts the

whole tuning curve up or down (additive scaling), while the parameter β_1 scales the tuning curve by a constant factor (multiplicative scaling). Only units with an $R^2 > 0.8$ for the linear regression were kept for further analysis. To compare the amount of additive and multiplicative scaling, we also fitted the tuning curves with reduced models:

$R_a(\theta)_c = \beta_0 + R(\theta)_b$ (additive model)

and

$R_m(\theta)_c = \beta_1 \cdot R(\theta)_b$ (multiplicative model)

The ratio between additive and multiplicative scaling was obtained by calculating a reduced-model-index (RMI) of the residual sum of squares (RSS) for the two reduced models

$$RMI = \frac{RSS_m - RSS_a}{RSS_m + RSS_a}; \quad RMI \in \{-1...1\}$$

RSS_m and RSS_a are the residual sum of squares for the multiplicative and additive model, respectively. The RMI is 1 for a perfect multiplicative scaling, -1 for an additive and 0 if both models describe the scaling of the tuning curve equally good. We further tested for each unit, if one or the other model performed significantly better, or if they performed equally well. To this end, we calculated the probability that one or the other model was correct, using Akaike's information criterion (Akaike, 1974). This method, based on information theory, is suitable for comparing non-nested models. The difference in the AIC values for the multiplicative (AIC_m) and additive (AIC_a) model is given by:

$$\Delta AIC = N \cdot \ln\left(\frac{RSS_m}{RSS_a}\right) + 2 \cdot (K_m - K_a)$$

with N being the number of data points (N = 16 directions), RSS_m and RSS_a the residual sum of squares for the multiplicative and additive model, and K the number of parameters plus one (K = 2). The ΔAIC value is then converted to a probability according to

$$p = \frac{e^{-0.5\Delta AIC}}{1 + e^{-0.5\Delta AIC}}$$

A probability of p = 0.5 indicates that both models are equally probable, whereas a probability of $p > 0.5$ indicates that the multiplicative model is more likely than the additive one. Accordingly, a value of $p < 0.5$ indicates that the additive model is superior to the multiplicative. We selected a threshold of $p > 0.95$ to indicate a significant dominance of the multiplicative model and $p < 0.05$ to indicate significance of the additive model, respectively. Units with values between p = 0.05 and 0.95 were classified as being equally good in describing the data.

3.7.2 Model simulations

We performed model simulations to gain a better understanding of the observed effects of multiplicative and additive changes. As a model for orientation tuning curves we used Gaussian functions of the form

$$R(\theta) = A\exp\left(-\frac{(x-\mu)^2}{2\sigma^2}\right) + V_r$$

where R(θ) is the response at angle θ, A is the amplitude of the function, x is the vector of orientations, μ is the center of the function, σ the tuning width and V_r the resting potential (= offset). This function describes the tuning of the membrane potential in response to an oriented stimulus. We choose the following parameters: V_r = -70 mV, A = 50 mV, μ = 0°, σ = 20°. The membrane potential of a neuron is transformed to output spike rate according to a transfer function. Two functions have been described and we tested both functions.

1.) A linear threshold function relates membrane potential V to spike rate r in a linear manner once the membrane potential reaches threshold, T:

$$r(V) = k[V - T]_+$$

where k determines the steepness of the function, T is the threshold for spike generation and $^+$ denotes rectification. We set the parameters k = 3 and T = -50 mV. Even though the relationship is linear once above threshold, the threshold itself makes the whole transformation nonlinear.

2.) Membrane potential V is related to spike rate r as an expansive power law relationship:

$$r(V) = k([V]_+)^n$$

where the constants k and n describe the steepness of the function and $[V]_+ = \max(V_r,0)$ sets the minimum membrane potential to the resting value V_r (Albrecht & Geisler, 1991). The parameter k was set to 0.0005 and n = 3 similar to what was used in previous theoretical work (Murphy & Miller, 2003).

The action of a modulating input was tested in two ways. First, we simply added a constant of m = 10 mV to the "baseline" tuning function and fed this also in the two transformation functions. The parameters for the resulting change of the firing rate tuning curve were then estimated as for real data. Second, instead adding a constant, modulating input was assumed to be tuned itself. We therefore added to the "baseline" tuning curve a fraction of itself. The modulating input was thus defined as

$m(\theta) = R(\theta)*0.3$.

3.8 Variability analysis of spikes

Neuronal discharge variability can be expressed in two different ways: Across-trial variability describes the difference between spike counts of repetitive trials recorded while presenting the same stimulus. This captures the variability on a long time scale of minutes to hours. Within-trial variability, or spiking noise, captures the timing of individual spikes on a relative short time scale of one trial. We quantified both forms of variability for both, spontaneous and dynamic period, and tested if they were affected by cooling deactivation of the contralateral hemisphere.

Rate variability was quantified by means of the Fano factor, FF (Fano, 1947). The Fano factor is defined by the variance of the spike count (N) across trials divided by the mean spike count:

$$FF = \frac{\mathrm{Var}[N]}{\mathrm{E}[N]}$$

For a stationary Poisson process, the FF is equal to one.

Spiking noise was quantified by means of the coefficient of variation (CV) of the interspike interval (ISI) distribution. To this end, we first obtained the sequence X of interspike intervals for a given neuron by calculating the time between successive spikes across all trials. The CV is then calculated as the standard deviation of the interspike intervals divided by their mean:

$$CV = \frac{\mathrm{Std}[X]}{\mathrm{E}[X]}$$

The two measures are not mutually independent: A high variability in the timing of spikes will also result in high count variability and vice versa. For a stationary renewal process in equilibrium it holds that

$$FF = CV^2$$

for long observation windows. Using this equation, one can disentangle changes in spiking noise from true changes in trial-to-trial variability. An increase in the quotient FF/CV^2 indicates an increase in the trial-to-trial variability which exceeds the spiking variability.

The measurement of the CV assumes rate stationarity, which is usually not the case in vivo, because the instantaneous rate is modulated by the stimulus. We therefore applied a time rescaling method introduced by Reich et al. before calculating the FF and CV (Reich et al., 1998; Nawrot et al., 2008, Matlab functions implemented in the Find Toolbox, http://find.bccn.uni-freiburg.de). In summary, for a train of spikes sampled at 1000 Hz, the time axis is rescaled to “operational time” according to a transformation function. This

transformation function is the instantaneous spike rate function, estimated by the average PSTH, smoothed with a Gaussian kernel of σ = 15 ms. Periods of high firing rate are stretched, whereas periods of low rate are compressed to produce a stationary firing rate. The FF and CV are then computed on this time scaled data.

However, there could be changes in spiking statistics due to altered spike rates during cooling (e.g. the impact of the neurons' refractory period). Thus, we also applied the mean-matching method used before to equalize the firing rates evoked by grating and RDT stimuli (3.6.4). This time, we equalized the average firing rate between baseline, cooling and recovery period for each type of stimulus, separately, for the population of sorted units.

3.8.1 Simulation of variability measures

To better understand the effects of a non-stationary rate on the estimation of the FF and CV we simulated spike trains with determined statistics. The procedure is shown in figure 3-8 for a simulated spike train based on the description in Nawrot et. al. (Nawrot et al., 2008). First, a stationary spike train is created by drawing intervals from a Gamma distribution. The Gamma distribution has two parameters: The Gamma order α determines how regular the resulting spikes will occur, with $\alpha = 1$ being equal to a Poisson process. The second parameter ρ determines together with the Gamma order the rate of the process:

$$\lambda = \frac{1}{\mu} = \frac{\rho}{\alpha}$$

where λ is the spike rate (in Hz or spikes/second) and μ is the mean interval (in milliseconds). The Gamma order is related to the coefficient of variation as follows:

$$CV^2 = \frac{1}{\alpha}$$

We simulated a total of 50 trials with a duration of 1000 ms, a bin with of 1 ms and a Gamma order of 2. Then, time was scaled according to a determined rate function in order to create a non-stationary process. As a rate function we used a Gaussian distribution (see section 3.7.2) with the following parameters: R_{min} = 10 sp/s, R_{max} = 150 sp/s, σ = 50 ms, center = 500 ms. This results in an increase in spike rate around 500 ms as can be seen in the raster plot in figure 3-8A. The average spike rate for the whole period of 1000 ms was 51.2 sp/s. The distribution of interspike intervals for this simulation is shown in figure 3-8B. Now, from this data of spike occurrences, the rate function was estimated as for the recorded data by averaging over the trials and smoothing with a Gaussian kernel of σ = 15 ms. In figure 3-8C, the true rate function (red) is shown together with the estimated rate function (blue),

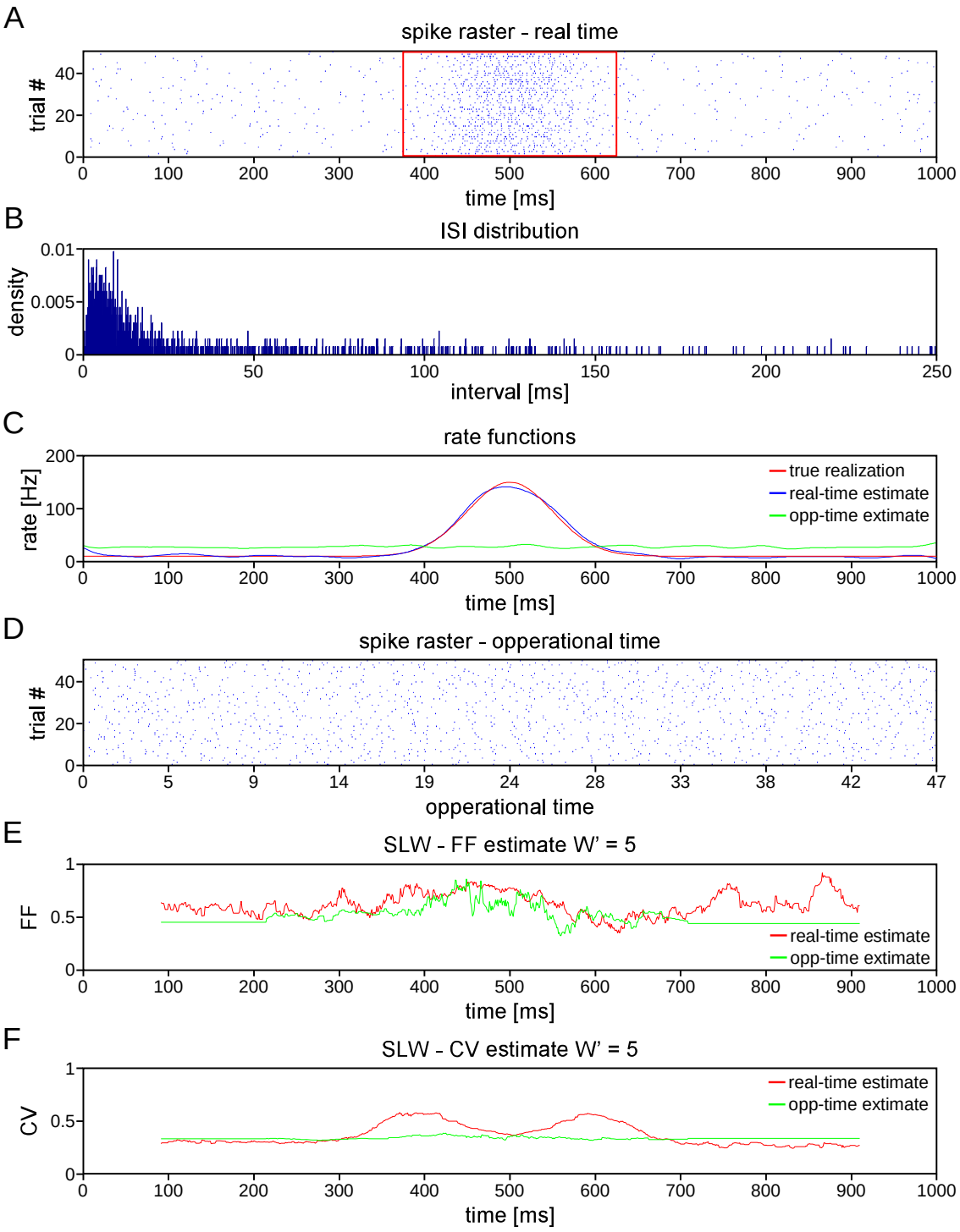

Figure 3-8: Simulation of point processes. (A) A total of 50 trials with a duration of 1000 ms was simulated. The gamma order was set to 2 and the firing rate had a minimum of 10 sp/s and reached a maximum of 150 sp/s at 500 ms. The red frame denotes the analysis window of 250 ms for the estimation of the spiking variability. (B) Interspike interval distribution for the spikes raster shown above. (C) Rate functions of the spike simulations. The red curve denotes the true realization used to create the rate modulation from a stationary process. The estimate of the rate function by calculating the smoothed PSTH is shown in blue. The green curve depicts the rate function for the time demodulated spikes. (D) Time demodulated spike raster according to the estimated rate function shown in (C). Note the uniform distribution of spike events over time. (E) Time resolved sliding window analysis of the FF in real- and operational time. The estimation of the FF in operational time didn't give any values at the beginning and end of the trial. The FF was therefore set to the last valid estimate. This is because time is compressed at the beginning and end of a trial where spike rate is low, so transforming back the data to original time doesn't give a value for those time points. (F) Same as above for the CV. Note the clear increase in the CV when the spike rate changes in real time. Instead, in operational time the CV estimate is constant throughout time.

which closely fits the true realization. According to the estimated rate function, time was now rescaled, or demodulated, to create a stationary process. The result was a homogeneous distribution of the spikes as depicted in figure 3-8D (also expressed in a flat rate function as indicated by the green curve in figure 3-8C). We then estimated the Gamma order by calculating the inverse of the squared coefficient of variation in a 250 ms window, in real and operational time, as indicated by the red frame in figure 3-8B. For real time, α was estimated to 1.43, while for operational time α was 2.06, which is closer to the value of 2.00 initially used to simulate the stationary process.

Additionally, one can take advantage of the time rescaling method in using a sliding window approach to obtain a time resolved estimate of the FF and CV. To this end, we slid a window of W' = 5 in operational time, corresponding to 100 ms in real time, across the trials and calculating for each window position the FF and CV. Then, time is scaled back to real time using the inverse of the rate function used before to demodulate the spike trains. The results for both measures are shown in figures 3-8E and F for real and operational time. It turns out that the impact of a non-stationary rate is strongest on the estimation of the CV. In real time, a strong modulation follows the rate in- and decreases, whereas in operational time the estimate is nearly flat.

3.8.2 Time resolved variability analysis

To test how neuronal variability changes over time throughout the stimulation period, we performed a sliding window analysis on the dataset of sorted units (n = 1475 for grating and n = 1226 for RDT stimulation). To this end, the time rescaling method, as described above, was applied to each sorted unit for a 1200 ms window in the dynamic period. The criteria for selecting a unit from the total of recorded units was the same as for the non-sorted units (see section 1.6). A window of 250 bins was slid across time with a resolution of 1 bin to a maximum of 1000 bins. Because the sliding window analysis was applied on operational time, one bin was not necessarily corresponding to 1 ms, and the real window width varied according to the instantaneous rate. For each window position, the FF and CV were calculated, if the average number of spikes in that window was at least 2.5. Therefore, the number of units entering the analysis changed per time bins. For gratings, the average number of units per time bin was 964, for RDT 739 survived that criterion. Subsequently, the time axis was scaled back to "real time" by applying the inverse transformation as before. Then, the sampling rate was reduced to 100 Hz by averaging together 10 consecutive bins. For the

remaining bins, the FF and CV were averaged across units (using a trimmed mean, discarding the smallest and largest 0.1% of the data).

Statistical significance was assessed by computing a t-test ($p < 0.05$) corrected for multiple comparisons using the false discovery rate, as described in section 1.6.2.

3.8.3 Fixed window variability analysis

A vital aspect in estimating the FF and CV is the total number of spikes in an observation period as well as the length of the observation period itself (Nawrot et al., 2008). If there are to little spikes in the analysis window, the estimation of the FF and CV are biased and may therefore be misleading. We tried different window lengths and selection thresholds for the number of spikes inside a window. Essentially, we choose three window lengths of 250, 500 and 1000 ms placed 50 ms after stimulus motion onset and three thresholds for the minimum average number of spikes, namely 5 sp/s, 10 sp/s and 20 sp/s. For each of the resulting nine combinations we calculated the FF, CV and FF/CV^2 for the raw and mean matched data during the baseline, cooling and recovery separately. We calculated a trimmed mean, discarding the 1% largest and smallest values of the distribution of values before averaging. Trimming renders the mean more resistant against outliers. We then tested, for each combination and measure, the statistical significance between the experimental states baseline versus cooling and baseline versus recovery.

Statistical significance between states was assessed by a non-parametric permutation test. To this end, the data from two states were randomly assigned into two new groups and the measure in question (FF, CV and FF/CV^2) was computed on this shuffled data. Then, the absolute difference between the means of the two groups was taken. This procedure was repeated 10000 times to create the null distribution of no difference between the groups. The percentage of values from this distribution exceeding the true (absolute) difference corresponds to the p-value resulting from a non-paired two-sided test. The p-values were binned into four categories: $p < 0.001$ = ***; $p < 0.01$ = **; $p < 0.05$ = * and $p > 0.05$ = n.s. (not significant). For all measures and combinations, significance levels were listed in a table together with the number of units contributing to each value. The sign of a significant change was indicated by color, with blue standing for significant decrease and red for significant increase of that particular measure.

Neuronal discharge variability was also assessed for spontaneous activity in a 500 ms window preceding stimulus onset of the RDT protocols. A minimum average number of 2 sp/s was chosen because of general low spike count during spontaneous activity.

4. Results

The aim of my thesis was to examine, in vivo, the impact of long-range cortico-cortical connections on their target cells. The recorded cells were driven by two types of visual stimuli: Moving full screen gratings of high contrast and moving random dot textures (RDTs) with lower contrast. We have chosen this type of stimuli, because they exhibit different types of features: Gratings have a single spatial and temporal frequency and a strong orientation component orthogonal to their direction of motion. Random dots, on the other hand, exhibit a broad spatio- temporal frequency spectrum, which results in a continuous stimulation of the receptive fields. We used moderate dot speeds which usually result in a preferred direction similar to stimulation with gratings but a somewhat broader tuning.

4.1 Effects of cooling on response amplitude

4.1.1 Spike rate changes during the trial

Data from 491 units for grating and 348 units for RDT stimulation during baseline, cooling and recovery were selected according to the criteria described in the material and method section. After a blank of 500 ms, stimuli appeared and were held static for 500 ms (static phase) and then started to move for 1000 ms (dynamic phase). Figures 4-1A and B show the average normalized PSTHs for grating and RDT stimulation. The typical response transient can be observed at 500 ms for stimulation onset and at 1000 ms for motion onset, depicted by vertical bars. Firing rate decreased during cooling (blue) in the static and dynamic phase for both stimuli and recovered to baseline level (green) after rewarming (recovery, show in red). Rates decreased significantly during the whole dynamic phase for both types of stimuli, while during the static phase only the initial transient for grating stimulation reached significance (t-test, $p < 0.05$, corrected for multiple comparisons). Interestingly, for RDT stimulation there was also a decrease in firing rate for the period of spontaneous activity prior to stimulus onset for RDT stimulation (see discussion). The firing rate during recovery was not significantly different from baseline for all time bins and stimuli.

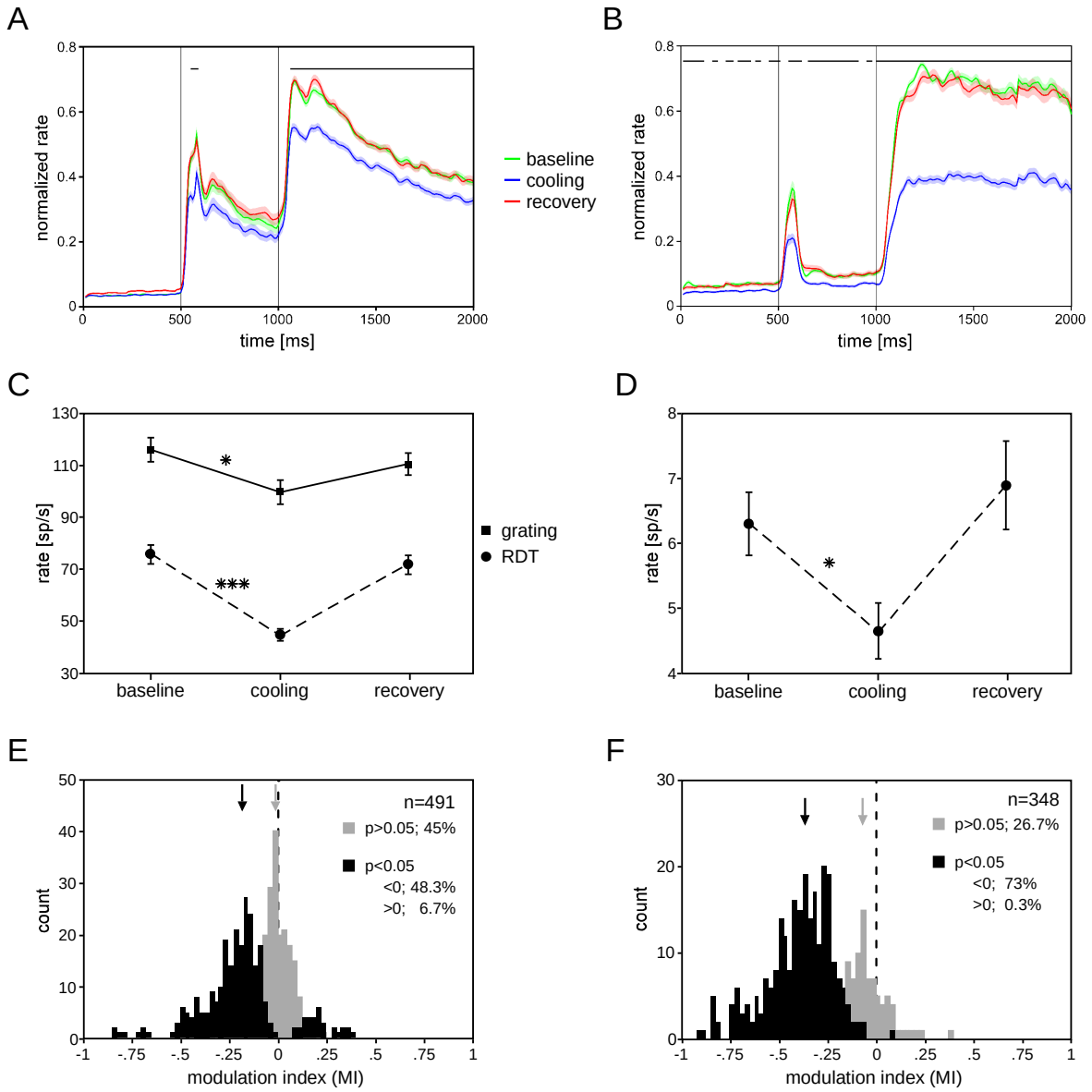

Figure 4-1: Normalized population average of PSTHs for grating (A) and RDT (B) stimulation. Experimental state is indicated by color. The horizontal line denotes statistical significance between baseline and cooling for each time point. Vertical lines indicate stimulus appearance and stimulus motion onset. Shading around the mean ±1 SEM. Note the sustained firing for RDT stimulation, whereas during grating stimulation firing declines over time due to adaptation. (B) Population average of mean spike rate for each experimental state and stimulus. Grating and RDT stimulation are indicated by squares and dots, respectively. Error bars ±1 SEM. *** $p < 0.001$, * $p < 0.05$. (C) Same as B for spontaneous activity during the blank of the RDT stimuli. (E) Distribution of the modulation index (MI) for grating and RDT stimulation (F). Counts significantly modulated by cooling deactivation are shown in black, non-significantly modulated in gray. Arrows indicate the median for each group. The percentage of units in each group is indicated in the plot.

4.1.2 Average spike rate changes

We quantified the effect of cooling deactivation by integrating the firing rate over time in the dynamic phase. The result is shown in figure 4-1C. The average firing rate decreases significantly from 116 sp/s to 99 sp/s for grating (t-test, $p < 0.05$) and from 75 sp/s to 44 sp/s for random dot stimulation (t-test, $p < 0.001$). Although, the average firing rate did not fully

recover (110 and 72 sp/s for grating and dot stimulation), it was not significantly different from baseline (t-test, $p > 0.1$). This demonstrates a robust effect of cooling deactivation on neurons in Area 17 and 18, with a more pronounced rate decrease for RDT than for grating stimulation.

4.1.3 Spontaneous spike rate changes

We also quantified the effects on spontaneous activity by averaging the ongoing activity in the 500 ms before stimulus onset for all RDT protocols. As shown in figure 4-1D, the average firing rate decreased significantly from 6.3 sp/s to 4.6 sp/s during cooling (t-test, $p < 0.05$) and recovered to 6.9 sp/s after rewarming (t-test, $p > 0.1$).

This shows that, even in the absence of a visual stimulus driving the neurons in both hemispheres, cortico-cortical connections exert a tonic, excitatory influence on their target cells.

4.1.4 Individual spike rate changes

We asked whether the effect of cooling deactivation was similar for all units recorded. We therefore calculated for each unit a modulation index (MI) between baseline and cooling (using the average firing rate in the dynamic phase as above), with a negative value indicating a rate decrease and a positive value a rate increase during cooling (see materials and methods 3.6.3). Additionally, each unit was tested for a statistically significant difference between baseline and cooling across trials (Mann-Whitney U, $p < 0.05$). The results are plotted as histograms in figures 4-1E and F. For grating stimulation, 55 % of the units showed a significant modulation by cooling (black area of the histogram, median -0.186) with the total percentage of significant decreases (48.3 %) being more frequent than the increases (6.7 %). In contrast, for RDT stimulation, 73.3 % of the units showed a significant modulation by cooling (median -0.369), with by far most units (73 %) showing a rate decrease, only one unit increased its firing significantly.

Although the major effect of cooling deactivation was a decrease in firing rate, two important differences between grating and RDT stimulation attract attention: First, the number of cells affected by cooling and the strength of the effect was larger for RDT stimulation. Second, rate increases were much more frequent for grating stimulation.

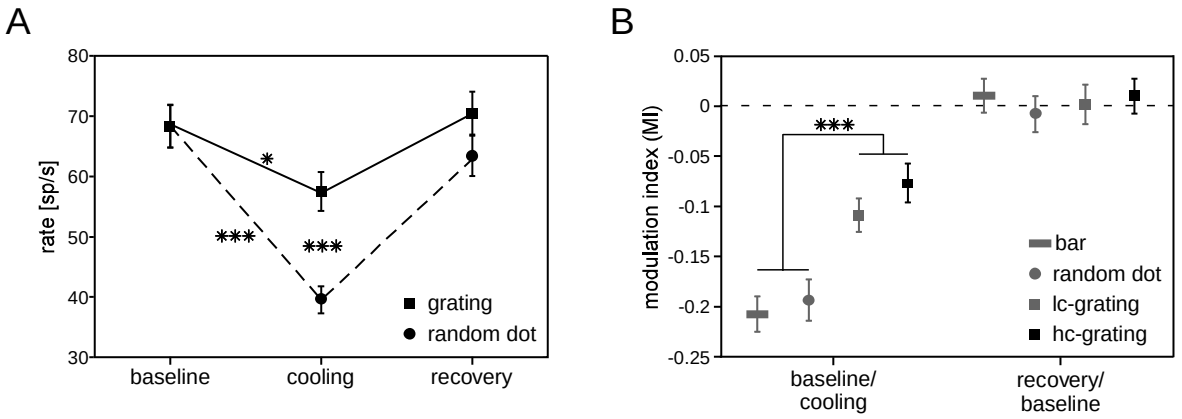

Figure 4-2: Controlling for differences in baseline firing rate between grating and RDT and RBT stimulation. (A) Population average of firing rates after mean matching. Note the identical baseline firing for grating and RDT stimulation. However, the rate decrease for RDT stimulation compared to grating stimulation is much more pronounced. (B) Rate matching through contrast adjustment. Cooling induced changes in spike rate are expressed as a modulation index (MI). Data for contrast adjusted recordings are shown in gray whereas data for high contrast stimulation are black. Note that neurons stimulated with RDTs and RBTs decrease about the same amount, whereas stimulation with high and low contrast gratings also behave similarly, but less pronounced. *** $p < 0.0001$ ANOVA. Other conventions like in figure 4-1.

4.1.5 Controlling for differences in absolute firing rate

We showed that removing callosal input, while stimulating with RDTs, has a bigger impact on the recorded neurons than while stimulating with gratings. Is this difference due to the inherent features of the stimuli used? Or could this difference arise by the fact, that gratings evoke a stronger response in the baseline than RDTs? To answer this question, we performed two controls. First, we applied a mean matching method in order to equalize the baseline rate distributions of gratings and dots. As can be seen in Figure 4-2A, the resulting rates for grating and RDT stimulation in the baseline were identical (68.3 sp/s). As for the non-matched data, the rate decreased significantly for both types of stimuli during cooling deactivation to 57.3 sp/s for grating and 39.3 sp/s for RDT stimulation (t-test, $p < 0.05$). Despite the equalized baseline rates, rate decreases remained much stronger for RDT stimulation than for grating stimulation (t-test, $p < 0.0001$).

The mean matching procedure allows for a direct comparison of the responses for the two stimuli used, but does not control for the amount of driving input to an individual cell. The high contrast grating is likely to drive a neuron to saturation, while the RDTs may not, and the local cortical circuit is therefore operating in a different regime. This could lead to the observed differences during cooling deactivation for the two stimulus conditions. We therefore tried, already during data aquisition, to match the firing rate of a recorded neuron for grating stimulation to that obtained by random dot stimulation. This was done by reducing the

contrast of a moving grating stimulus, until the evoked firing rate matched the rate obtained by RDT stimulation for a set of simultaneously recorded units.

In addition, we introduced a third stimulus, namely random bar textures (RBTs). The idea behind this was to create a stimulus with properties in between grating and random dot textures. The RBTs are similar to the RDTs regarding the broad spatio-temporal frequency spectrum, but show an orientation component orthogonal to the direction of motion, similar to a grating.

In contrast to the previous data, the following controls were done by presenting gratings, RDTs and RBTs together in one protocol. This allowed for a more direct comparison because one and the same cell was tested for all three stimuli in the same session. For these controls, an additional number of 92 units was recorded in three cats. Results are shown in Figure 4-2B. The modulation ratios between cooling and baseline as well as between recovery and baseline are shown for the contrast matched data in gray together with the modulation index for the high contrast grating from the large sample in black. Because the number of units for high contrast grating stimulation was much larger than for low contrast data, we subsampled the high contrast data by drawing randomly 92 units out of the pool. It becomes obvious that RDT and RBT stimulation both resulted in a similar decrease during cooling deactivation (MI_{cb} bar: -0.17, MI_{cb} dot: -0.2), whereas high and low contrast grating stimulation also led to comparable decreases (MI_{cb} hc-grating: -0.08, lc-grating: -0.11). This was confirmed by performing an ANOVA followed by a post hoc test, indicating no significant difference ($p > 0.7$) between dot/bar stimulation on the one and hc-grating/lc-grating on the other hand, but a significant difference between the two groups for all stimulus pairs ($p < 0.05$).

In conclusion, the control experiments indicate a fundamental difference in the way cortico-cortical connections modulate their target cells, whereupon this modulation is dependent on features of the stimulus driving the system.

4.1.6 Difference between recorded areas

Given the topography of callosal connections, i.e. a greater density of connections in the 17/18 transition zone, we asked whether the effect of cooling deactivation was distinct in area 17, 18 or the transition zone. Figure 4-3 shows the average firing rate for the three areas and the two stimuli separately. For all areas and stimuli, the average effect was a rate decrease as reported above. Effects for neurons in area 17 were similar for grating and RDT stimulation, albeit one has to consider the small number of neurons recorded in this area (n =55) compared

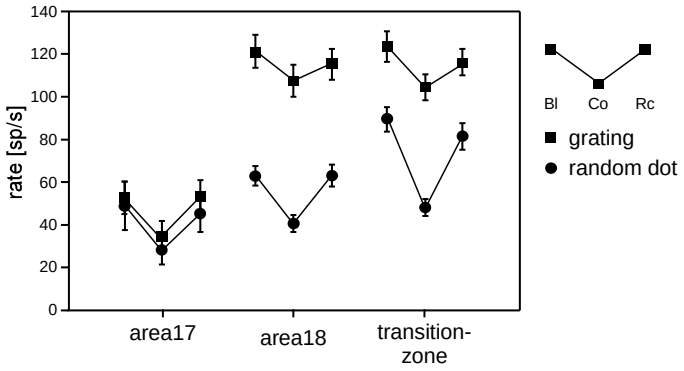

Figure 4-3: Population average of spike rates grouped according to the recording position. For each area, the average firing rates during baseline, cooling and recovery are shown for grating and RDT stimulation. Spike rate decreases are more pronounced for recordings in the transition zone. Same conventions as in figure 4-1.

to area 18 (n = 366) and the transition zone (n = 418). As expected, the rate decrease in the transition zone was more pronounced than in area 18 and 17, especially for RDT stimulation. We calculated a 2-Way RM-ANOVA with factor 1 being the recorded area, and factor 2 the state (baseline/cooling/recovery) as the dependent variables and the firing rate as the independent variable. As expected, the outcome indicates a significant modulation between the areas (factor 1, $p = 0.0001$) and states (factor 2, $p < 0.0001$) as well as a significant interaction (area*state, $p = 0.0008$) confirming the larger rate decrease in the transition zone. This result is in agreement with the anatomy of callosal connections and supports the practicability of our method.

4.2 Linear model of the cooling effect on orientation tuning

4.2.1 Quantification of additive and multiplicative components

In the previous section, we have shown that cortico-cortical connections influence their target cells in a stimulus dependent manner by predominantly enhancing their activity. But what is the mechanism of this modulation? For example, previous studies in the visual cortex of monkeys reported a multiplicative scaling of direction and orientation tuning curves by attention. Such a multiplicative (gain) change scales the response to each orientation proportionally, not affecting tuning width.

We first tested if the impact of cooling deactivation on orientation tuning curves can be described by a linear regression model of the form $R(\theta)_c = \beta_0 + \beta_1 * R(\theta)_b$ (see materials and methods 3.7.1). Figure 4-4 shows the orientation tuning curve for an example cell recorded in the 17/18 transition zone in response to grating stimulation. Cooling deactivation led to a decrease in the tuning curve amplitude as indicated by the blue (cooling) relative to the green

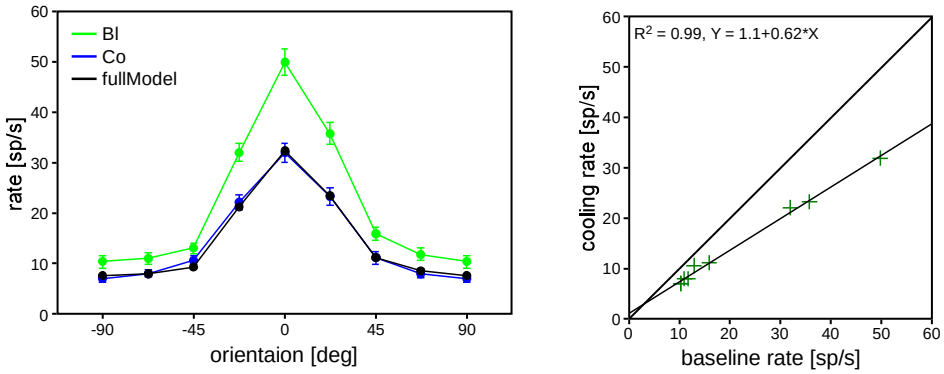

Figure 4-4: Linear model of the cooling induced changes in orientation tuning. Left: Tuning curve for an example neuron recorded during baseline (green) and cooling (blue). Applying the fit coefficients to the baseline tuning curves gives the estimate of the tuning during cooling (black). Note the near perfect match with the real data (blue). Error bars ±1 SEM. Right: Firing rate during baseline against firing rate during cooling. The best fitting linear regression (black thin line) is drawn through the data points.

(baseline) curve. The black curve represents the result of the linear model using the baseline firing rate as the independent and the cooling firing rate as the dependent variable. The model describes the data nearly perfectly, indicated by a R^2 of 0.99 for the linear regression. The right part of figure 4-4 shows the linear regression used to predict the cooling response. The firing rate for the baseline is plotted against the firing rate obtained during cooling together with the best fitted linear regression line. The intercept of the regression line with the ordinate is represented by the parameter β_0 (additive scaling) shifting the regression line up or down along the ordinate. The slope of the regression line is represented by the parameter β_1 (multiplicative scaling). For the example cell, the linear regression gives an additive scaling component of 1.1 sp/s and a multiplicative scaling of the factor 0.62. Note that for better visualization we averaged together opposite stimulus directions to obtain orientation tuning curves centred on the preferred orientation, but the evaluation of the parameters β_0 and β_1 was done on the full 16 directions. The interpolation to 16 directions from 8 grating and 12 RDT directions allowed for a better comparison between both stimuli, although performing the same analysis on the non-interpolated data gave similar results (data not shown). We have chosen a threshold of $R^2 > 0.8$ for the linear regression in order to successfully describe the effect of cooling on the tuning curves. Using this criterion, the effect of cooling was well described by the linear model for 90 % of the units stimulated by gratings (444 / 491 units) and for 77 % of the units stimulated by RDTs (269 / 348 units) . Only those units were considered for further analysis. Figures 4-5A and 4-5B plot the multiplicative component of each unit against the additive one for grating and RDT stimuli, respectively. For all units stimulated with gratings, the median multiplicative component was 0.84, for those stimulated with RDTs 0.56. As the additive component was retrieved in units of sp/s, we normalized each tuning curve by the response to the preferred direction before applying the linear model.

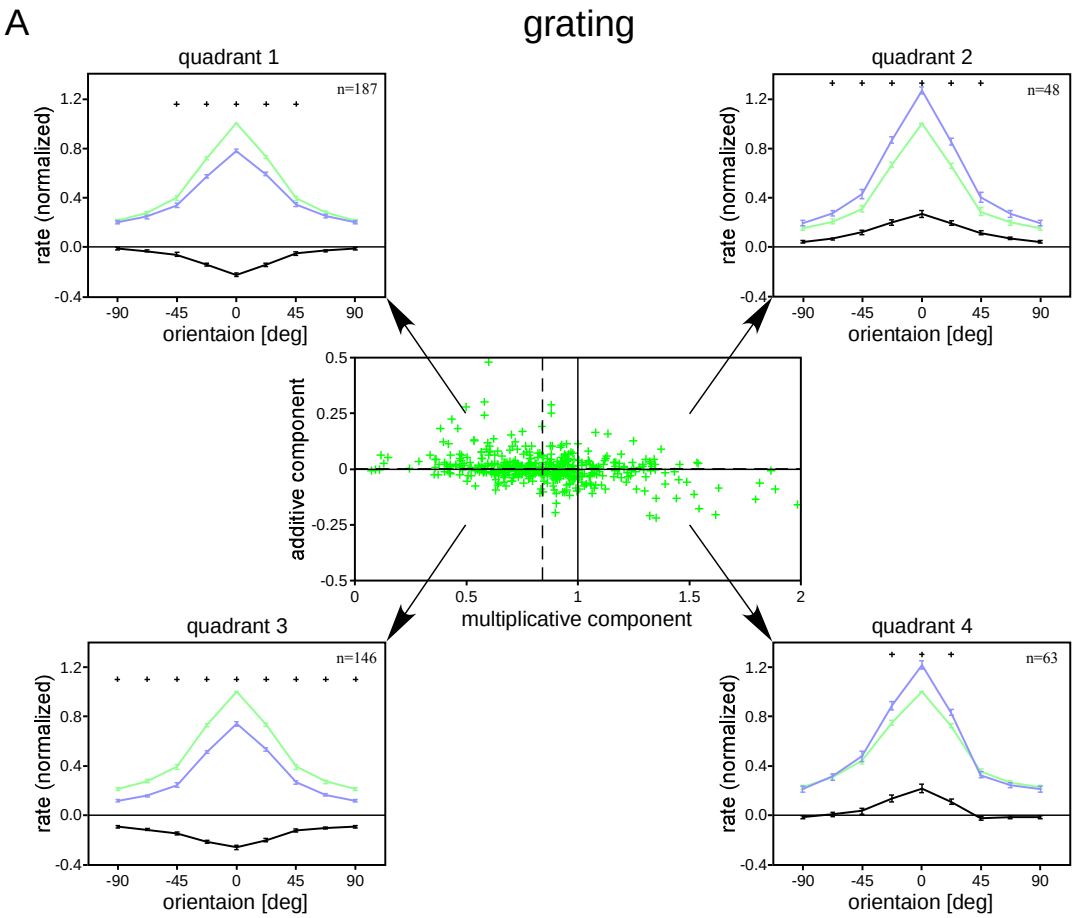
A
grating
quadrant 1
n=187
quadrant 2
n=48
quadrant 3
n=146
quadrant 4
n=63
rate (normalized)
orientaion [deg]
additive component
multiplicative component

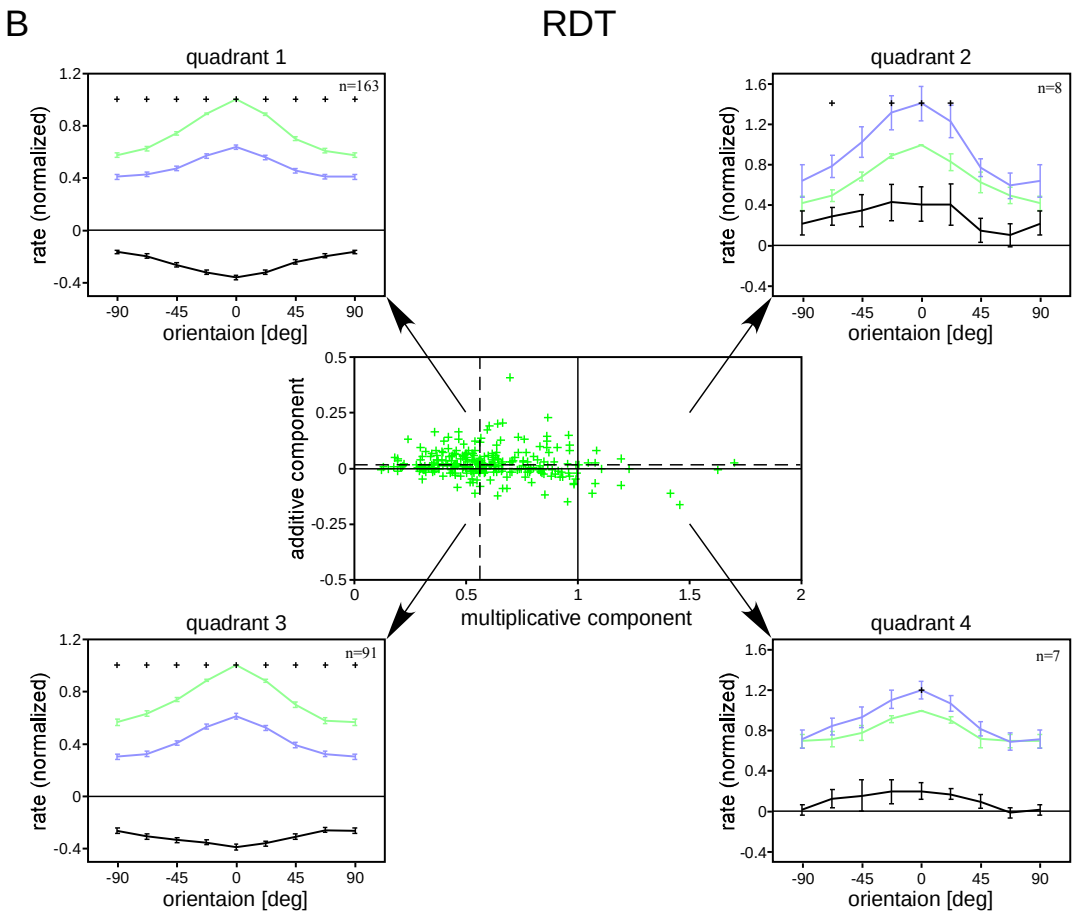
B
RDT
quadrant 1
n=163
quadrant 2
n=8
quadrant 3
n=91
quadrant 4
n=7
rate (normalized)
orientaion [deg]
additive component
multiplicative component

Figure 4-5: Population data of the linear model for grating (A) and RDT stimulation (B). In the center, the multiplicative is plotted against the (normalized) additive component for each recorded neuron. The dashed horizontal (not visible in A) and vertical lines denote the median for the additive and multiplicative component, respectively. For each quadrant, the corresponding tuning curves during baseline (green) and cooling (blue) have been averaged separately. The black curve is the difference between the two tuning curves. The effect of the additive component can be observed best at non- preferred orientations. Crosses above the tuning curves denote significant differences between baseline and cooling (permutation test, $p < 0.05$). Error bars ±1 SEM.

The median normalized additive components for grating or RDT stimulation were 0.006 and 0.02, respectively. To better understand the combinations of additive and multiplicative scaling, we averaged the tuning curves for each combination of additive / multiplicative scaling (additive up – multiplicative down, additive up – multiplicative up, additive down – multiplicative up, additive down – multiplicative down) separately. The black curve depicts the difference between cooling and baseline, the crosses above each orientation represent a significant rate change induced by cooling deactivation (permutation test, $p < 0.05$). The effect of the additive component can be observed best at the non-preferred orientations, either lifting up or pulling down the tails of the tuning curve.

Although the linear model of the cooling effect gives a description of the additive and multiplicative components, one cannot directly judge which of the two components the dominant one is. We therefore constructed two reduced models, expressing the tuning curve in the cooling as either a mere additive or a mere multiplicative scaling of the baseline. We then tested which of the two models fitted better to data obtained during cooling by comparing their residual sum of squares. We computed a reduced-model-index (RMI), similar to that used to compare the firing rates during baseline and cooling. A RMI of -1 indicates a mere additive and of 1 a mere multiplicative scaling, whereas a value of 0 indicates an equally good fit of both models. The procedure is shown in figure 4-6 (left) for the same example cell as before. The additive model (black curve) simply shifts the whole tuning curve (green) down , in order to fit with the tuning curve during cooling (blue). Applying the multiplicative model (gray curve) multiplies the baseline tuning curve with a constant in order to fit with the tuning curve obtained during cooling. The right part of figure 4-6 shows the linear regression for the two reduced models. While the additive model describes a line parallel to the unity line with slope 1 and an intercept of -6.8 sp/s (black dashed line), the multiplicative model describes a line with a slope of 0.66 and an intercept of zero (gray line). For this example cell, the multiplicative model describes the data much better than the additive model. Accordingly, the cell's RMI is 0.94 indicating a nearly complete multiplicative scaling. We applied the two reduced models to all units and averaged the corresponding normalized tuning curves. As shown in figures 4-7A and B for gratings and RDTs, the multiplicative model fits the data much better than the additive model for both types of stimuli.

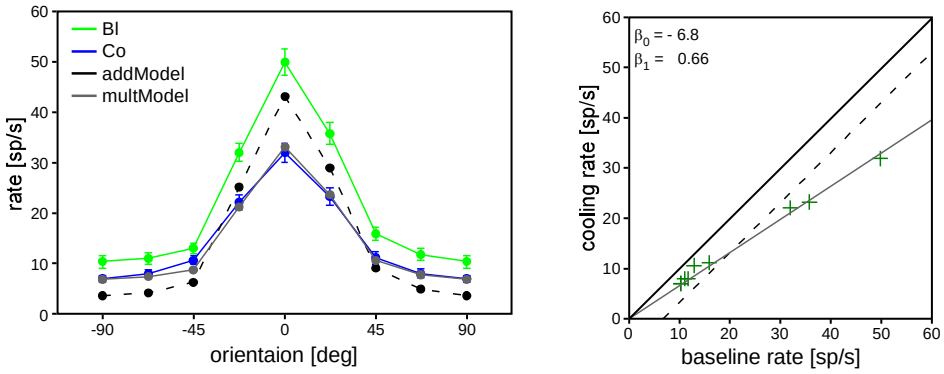

Figure 4-6: (Left) Tuning curve during cooling using reduced models for the same example cell as in figure 4-4 estimated by applying the fit coefficients. The dashed black curve is the result for the additive model whereas the solid gray line gives the multiplicative prediction. Not the much better fit to the real data (blue) for the multiplicative model compared to the additive, also evident from the regression lines shown to the right. (Right): firing rate obtained during baseline and during cooling. The regression line for the best fitting additive model is depicted by the dashed line; the regression line for the best fitting multiplicative model is shown in gray. Error bars ±1 SEM.

Figures 4-7C and D show the distribution of the RMIs for all units during grating and RDT stimulation. The median value for the units recorded during grating stimulation was 0.4, while the median for the units recorded during RDT stimulation was significantly larger (median: 0.78; Mann-Whitney U, $p < 0.0001$). The gray bars in figures 4-7C and D depict the non-significant cases, whereas the black ones represent the significant ones according to the criteria defined in the materials and methods section (3.7.1). For grating stimulation, 31% of the units showed no significant difference between the two models. Most of the units (61%) could be significantly described by the multiplicative model, only 6% were significantly described by the additive model. For RDT stimulation, this trend was even more pronounced, with 83% of the units being significantly described by the multiplicative model. Only 2% were significant for the additive model, and in 15% of the cases the models were not significantly different. How do those results relate to the data described in the previous section? More precisely, is the amount of additive/multiplicative scaling dependent on the overall impact of cooling deactivation? To answer this question we binned the rate change (in sp/s for the preferred direction) and averaged the RMI for each group separately. It turns out, that the stronger the spike rate changes, the more the modulation resembles a multiplicative scaling, independent if the change is a rate increase or decrease.

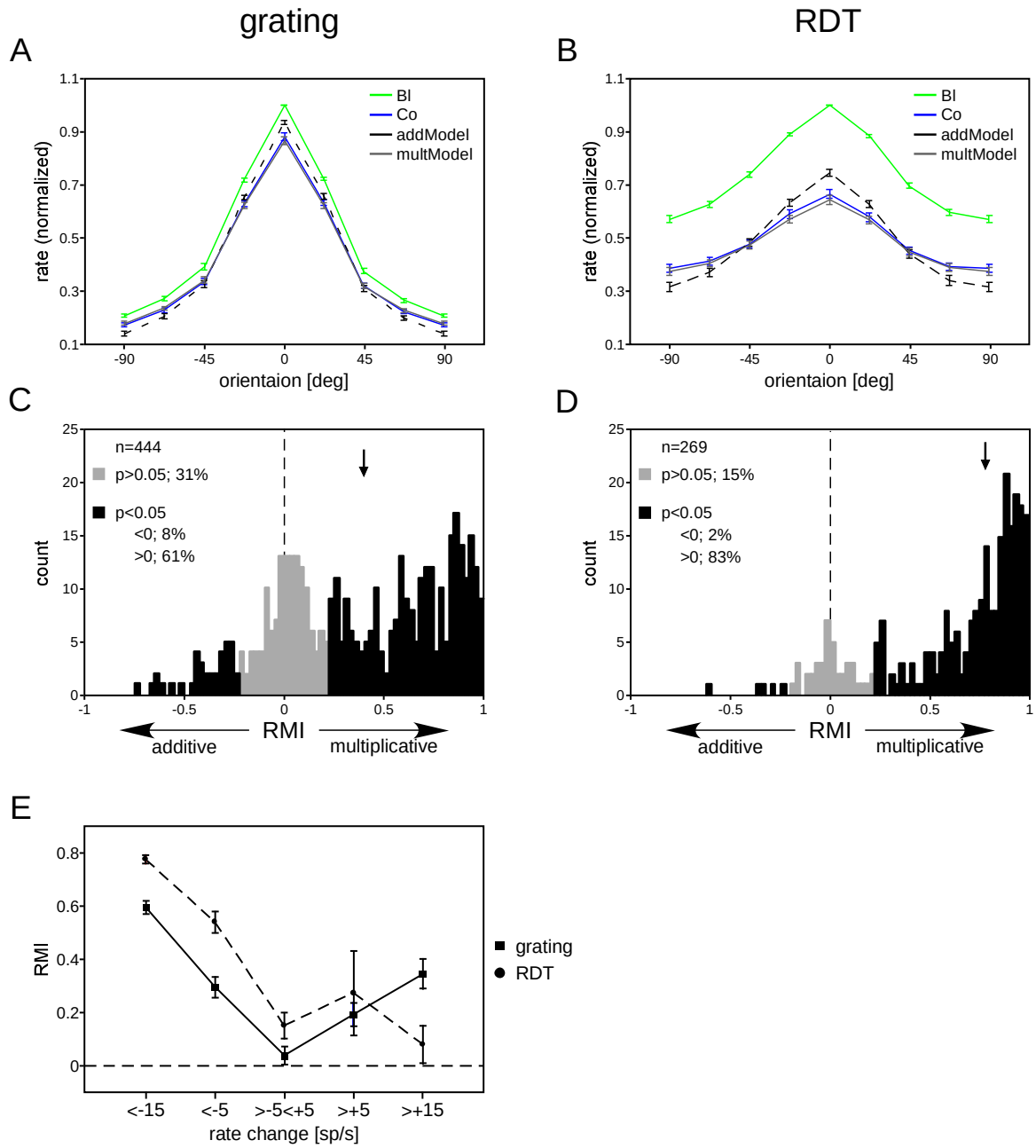

Figure 4-7: (A, B) Population average for the two reduced models for grating (A) and RDT stimulation (B). Again, the multiplicative model provides a better fit to the real data obtained during cooling. Same conventions as in figure 4-6. (C, D) Distribution of the reduced-model-index (RMI) for grating (C) and RDT (D) stimulation. A value smaller than zero indicates additive scaling; a value bigger than zero indicates multiplicative scaling. Unit counts with a significant difference between the two models are shown in black, non- significant units in gray. The percentage of significantly different units is given in the upper left corner. Arrows denote the median for the RMI. (E) Average RMI for different groups of spike rate change between cooling and baseline (negative values indicate rate decrease, positive values rate increase due to cooling deactivation) for grating and RDT stimulation. Note the clear increase in RMI with a more pronounced rate change. Error bars ±1 SEM.

4.2.2 Effects on direction and orientation selectivity

Given the strong impact of callosal projections on their target cells' responsivity, one can ask if the selectivity of those cells is also influenced. One of the main features of cells in primary visual cortex is orientation selectivity. We used direction (DI) and orientation (OI) indices as

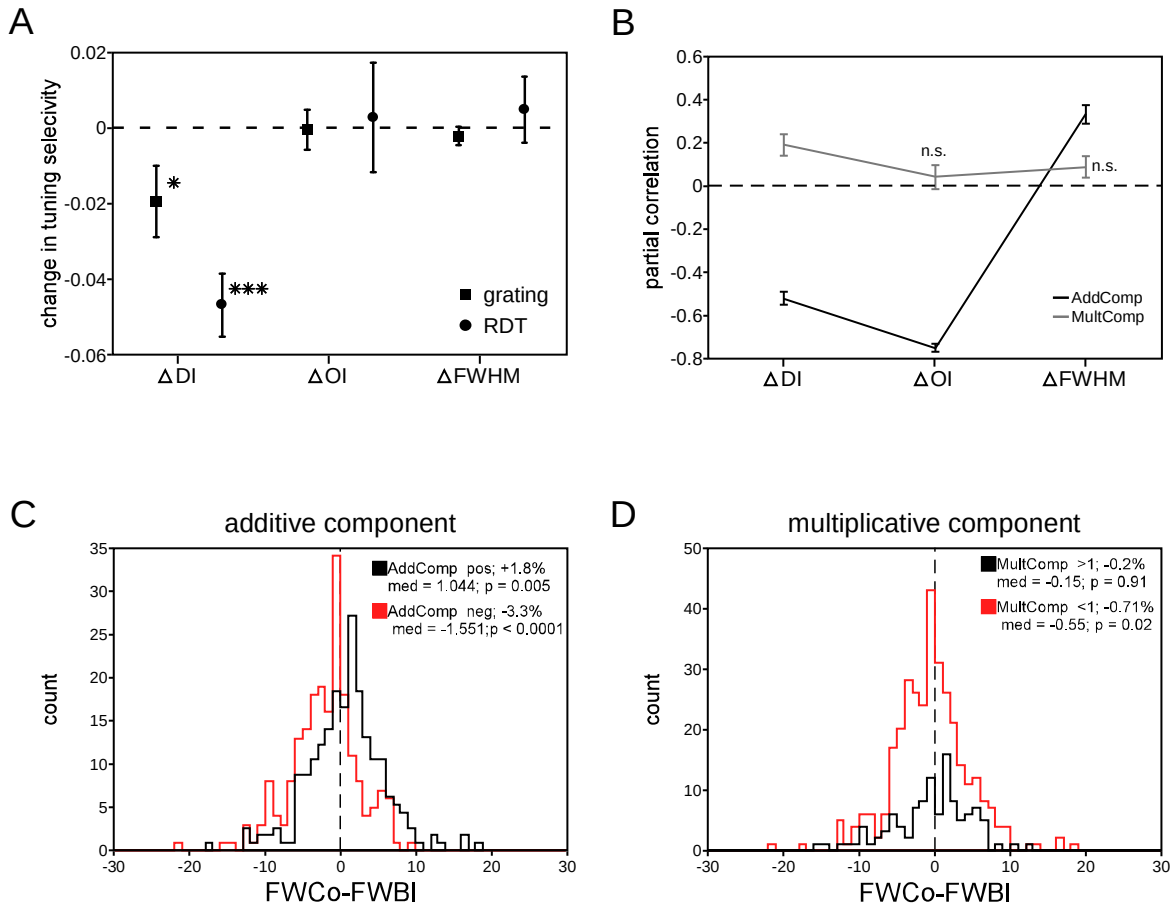

Figure 4-8: (A) Changes in DI, OI and FWHM during cooling compared to baseline for grating and RDT stimulation. Changes are expressed as a modulation index comparable to the MI for rate changes. Same conventions as in previous figures. (B) Relationship between cooling induced additive/multiplicative scaling of tuning curves and direction/orientation selectivity for cells stimulated with gratings. Changes in direction selectivity index (DI), orientation selectivity index (OI) and full width at half maximum (FWHM) are correlated with changes in the additive (black) or multiplicative (gray) component. Note that OI and DI are negatively correlated with the additive component, indicating a decrease in tuning selectivity accompanied with an increase in the additive component. Correlations with changes in FWHM are positive, because increases in FWHM point to a decreased selectivity. n.s. no significant correlation, error bars ±1 SEM. (C, D) Changes in the FWHM between cooling and baseline are shown as histograms for positive and negative additive components (left) and multiplicative components smaller and bigger than one (right), separately. It is evident, that distributions are shifted when splitting the data for additive ($p < 0.0001$ Mann-Whitney U), but not for multiplicative components ($p = 0.317$).

described in the materials and methods section to quantify the amount of direction and orientation selectivity. Furthermore, we fitted model functions to the orientation tuning curves to estimate the tuning width directly by taking the full width at half maximum (FWHM) from the fitted parameters. For all three measures, we calculated a modulation index between the tuning indices during baseline and cooling, similar to MI for spike rate changes.

There was a highly significant decrease in the direction selectivity index (DI, $p < 0.001$) for RDT stimulation, and stimulating with gratings also led to a significant decrease during cooling ($p < 0.05$) (figure 4-8A). Although significant, those changes were very small. The

orientation selectivity index (OI) and the FWHM were not significantly modulated for both stimuli.

Although, there was on average no change in orientation selectivity, we asked if for individual cells there is a relation between orientation selectivity and the additive/multiplicative scaling of tuning curves. To this end, we focused on grating data because they exhibited a broader range of additive/multiplicative effects and a general better orientation tuning then RDTs. It turned out, that the slight changes in DI and OI during cooling showed a strong negative partial correlation with the strength of the additive component (DI: $r = -0.52$, $p < 0.0001$; OI: $r = -0.75$, $p < 0.0001$, controlling for the multiplicative component) shown in figure 4-8B (black lines). The partial correlation with the multiplicative component (controlling for the additive one) was much weaker (DI: $r = -0.18$, $p = 0.004$; OI: $r = -0.04$, $p = 0.41$). The correlation with the FWHM revealed a positive relationship for the additive component ($r = 0.32$; $p < 0.0001$), because per definition a smaller FWHM during cooling indicates increased tuning selectivity. This corresponds to a sharpening of direction and orientation selectivity (increased DI/OI; decreased FWHM) for those neurons which had their tuning curves shifted downwards (negative additive component) and vice versa. In contrast, multiplicative scaling seems to rather preserve the feature selectivity of the recorded neurons.To make this point even clearer, we calculated histograms of the cooling induced changes in the FWHM for the units with a positive and negative additive component separately. The same was done for a multiplicative component smaller or bigger than one. Figure 4-8C shows a small but significant difference in the median of the distributions (Mann-Whitney U, $p < 0.05$). A downwards shift of the tuning curves (negative additive component) was accompanied by a -3.3 % decrease in tuning width and vice versa (1.8 % increase in tuning width). A divisive scaling of the tuning curve resulted only in a small (but significant) decrease in tuning width (- 0.71 %), even though the overall reduction in spike rate could be large. In contrast to the additive components, there was no difference in the median tuning with for units with a divisive/multiplicative effect (figure 4-8D).

4.2.3 Model simulation of observed effects

The presented results give a quantitative and qualitative description of the tuning curve changes induced by cooling deactivation. To better understand, how the synaptic input we removed could have produced these results, we performed simple model simulations. We described the synaptic input to a neuron as a Gaussian function and transformed this input to

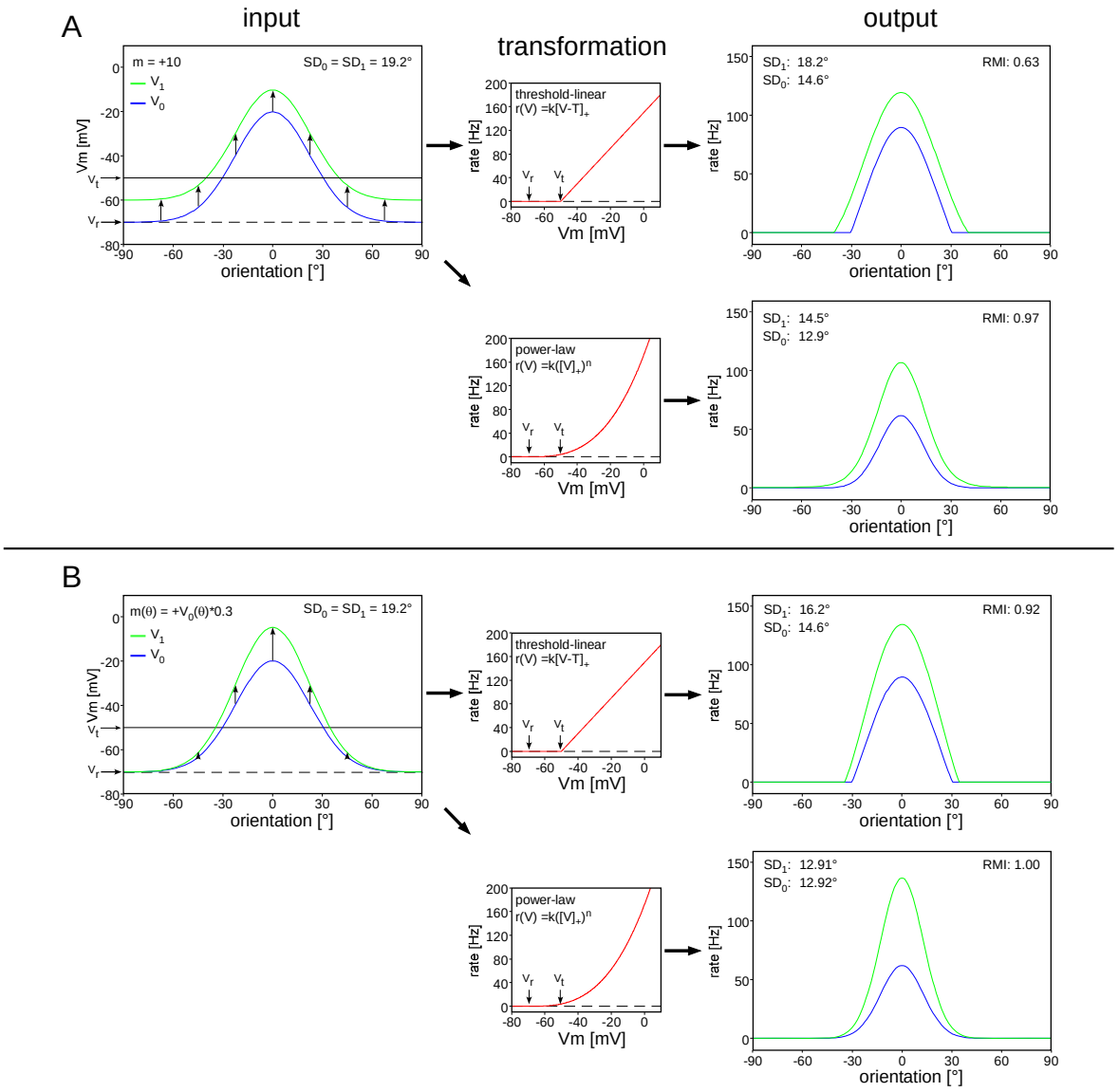

Figure 4-9: Model of tuning curve modulation. (A) Addition of a constant to the membrane potential for all stimulus orientations. Left: Membrane potential of a neuron tuned for stimulus orientation without (V_0, blue) and with an additional 10mV input (V_1, green). The membrane potential for the null orientation is assumed to be at rest V_r and the spike threshold is 20 mV above that at V_t. It is transformed to spike rate by either a linear threshold (upper middle box) or a power law (lower middle box) transformation. Right: Resulting spike output. Note the increase in tuning width by adding the constant to the membrane potential for the linear threshold model. (B) Addition of tuned input to the same model neuron and transformation to spike output as in A. The additional input was set to a fraction of 0.3 of the basic input (V_0). In that case, the result is a near perfect multiplicative scaling of the spike output. SD_0 and SD_1 are the standard deviations of the tuning curves obtained by fitting a gaussian function. RMI: Reduced model index as for real data.

spiking output using either a linear-threshold model or an expansive power-law nonlinearity (see Materials and Methods part 3.7.1). We expressed the action of the modulating callosal fibers in two ways. In one case, we added a constant factor to all orientations resulting in a simple upward shift of the membrane potential (see figure 4-9A). In a second case, the modulating input was itself tuned and expressed as a fraction of the basic synaptic input (figure 4-9B). The results for both modulation types are illustrated in figure 4-9. The transformation function is shown in red in the middle of the figure. Adding a constant

(+10mV) to the basic membrane potential (blue) in the presence of the linear-threshold model led to an upwards shift of the spike rate tuning curve (green). The tuning width increased from 14.6° to 18.1° (SD). This is because adding a constant also raises responses to the non-preferred orientations above threshold ("iceberg" effect). The RMI for this simulated neuron was 0.63, indicating that despite adding a constant, the threshold transformation pointed towards a mechanism resembling more a multiplicative change. This was even more pronounced in the presence of the power-law relationship. Here, the tuning width increased less (SD = 12.9° without and 14.5° with the modulating constant) and the RMI for this simulation was 0.97 indicating a nearly perfect multiplicative scaling.

Figure 4-9B shows the result for the tuned input modulation. This resembles more the anatomical situation as synaptic input through CC is known to be orientation specific (Hubel & Wiesel, 1968; Lepore & Guillemot, 1982; Rochefort et al. 2007). The linear threshold transformation led to a change in tuning width as for the non-tuned input modulation, but the mechanism resembled more a multiplicative change (RMI 0.92 compared to 0.63). Appling the power law transformation to the model neuron resulted in a perfect multiplicative change (RMI = 1) with no change in tuning width.

These results demonstrate that the addition of a modulatory input, regardless of being tuned or untuned, to the membrane potential of a neuron can lead to an approx. multiplicative gain change of its output. A key determinant in this mechanism is the nonlinear transformation of membrane potential into spike rate.

4.3 Effects of cooling on response variability

In the previous two sections we demonstrated that callosal projections influence the response amplitude of their target cells in a stimulus dependent manner. This influence is primarily facilitative, highlighting the predominance of excitatory synaptic contacts formed by callosal fibres. Another way to characterize the impact of modulating (excitatory) input is to describe the statistics of output spike trains. We determined the trial-to-trial variability in the spike rate by calculating the Fano Factor (FF), the ratio of the spike count variance to the mean. The FF measures the variability between trials on a long time scale. Furthermore, we estimated the intra-trial variability (spiking noise) on a relative short timescale by calculating the coefficient of variation (CV) of the inter-spike intervals (ISI). Because those measures relate on single spikes, we used an automatic spike sorting algorithm to obtain single cell responses from the recorded multiunits.

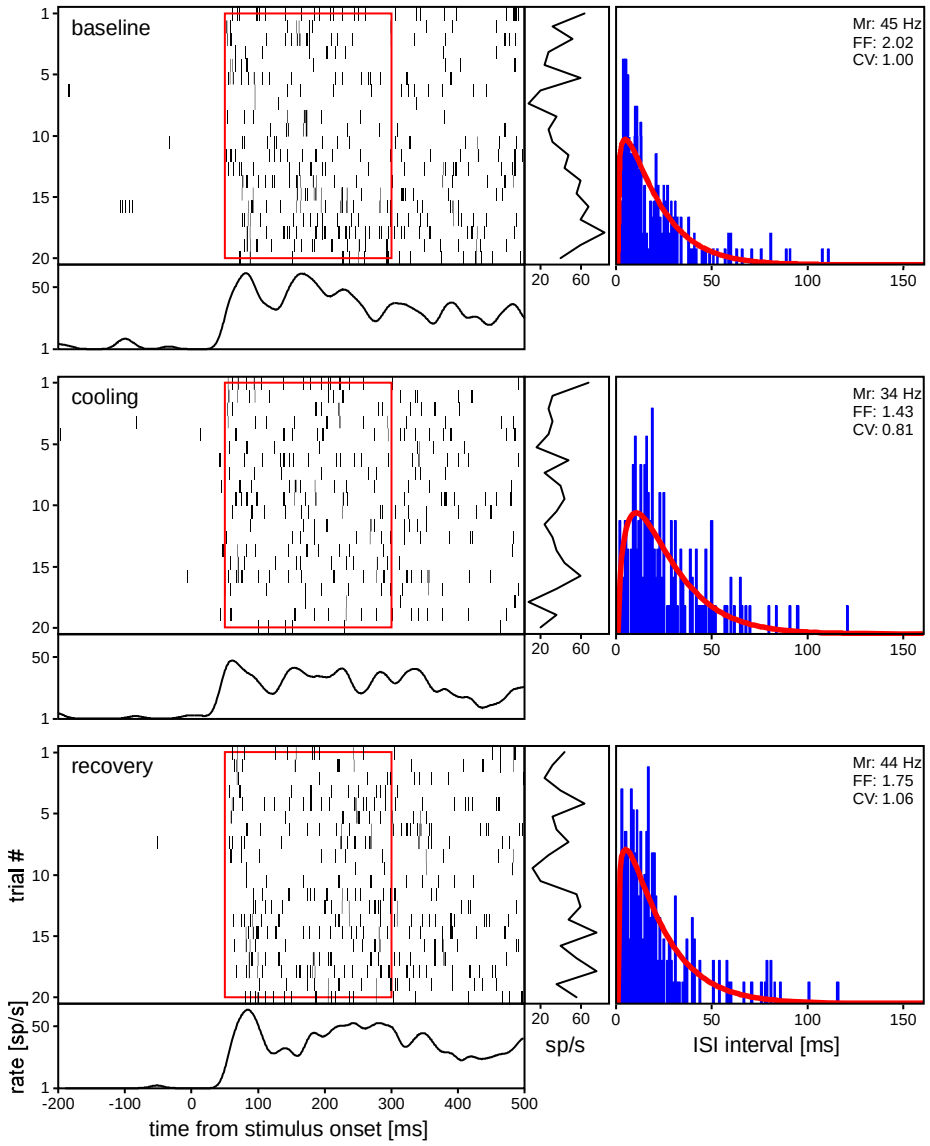

Figure 4-10: Spiking variability for an example neuron. Raster plots of an isolated single unit for grating stimulation during baseline, cooling and recovery. The average spike rate across trials (PSTH) is shown at the bottom of each plot. The middle box of each plot depicts the average rate across time for individual trials. Right column: Interspike interval (ISI) distribution for the corresponding raster plot. The red line is the fit of a gamma function to the ISI distribution. Note the decrease in trial-to-trial variability (FF) and the more regular occurrence of spikes (CV) during cooling deactivation despite a reduction in mean spike rate. Mr: mean spike rate, FF: Fano factor, CV: coefficient of variation. Red frame in the raster plot depicts the analysis window for the variability estimate.

4.3.1 Cooling induced change in spiking variability – single example

Figure 4-10 shows the influence of cooling deactivation on the response variability of an example cell recorded in area 18 while stimulated with a moving grating. Despite a reduction in firing rate during cooling, removing callosal input led to a less variable spike count across trials, expressed in the declining FF. Additionally, firing got more regular, indicated by a smaller CV. The histograms to the right of the raster plots depict the corresponding distribution of the interspike intervals used to calculate the CV. Note the

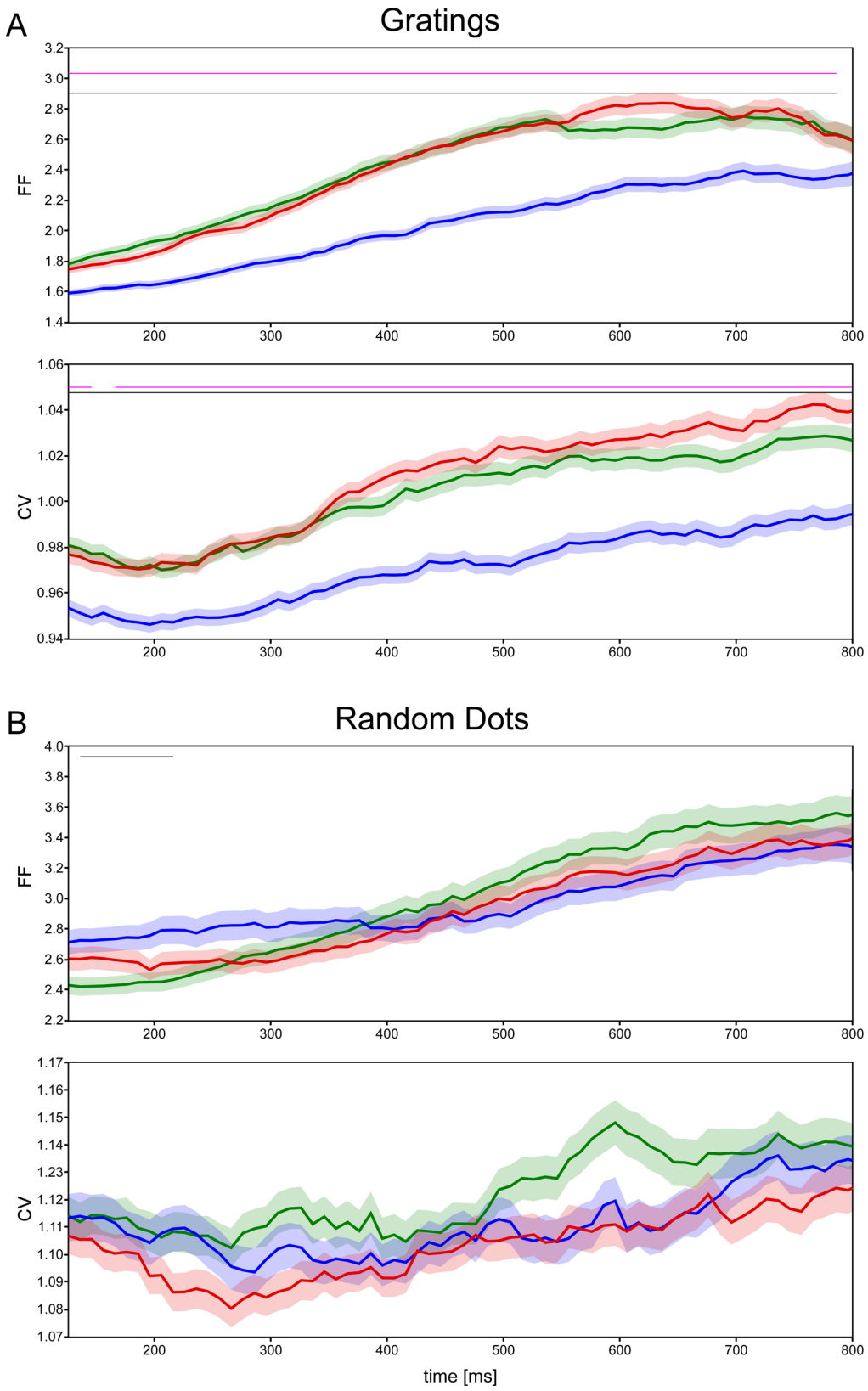

Figure 4-11: Population data for the time resolved analysis of spiking variability for grating (A) and RDT stimulation (B). FF and CV are calculated for each time point using a 250 ms sliding window starting after stimulus motion onset. Green: baseline, blue: cooling, red: recovery. Shading around the mean ±1 SEM. Horizontal lines denote statistically significant differences between baseline/cooling (black) and recovery/cooling (pink). Note the increase in variability over time for both, the FF and CV.

increase in the mean interspike interval during cooling. In the recovery period, all decreases for mean spike rate, the FF and CV reversed.

4.3.2 Cooling induced change in spiking variability – time resolved analysis

Recently, it was shown that spiking variability is modulated throughout the stimulation period of a trial (Churchland et al., 2010). Therefore, we tested for the population of single units, if the cooling induced change in spiking variability differed throughout the stimulation (moving period). This was done by a sliding window analysis with a window length of 250 ms and a time resolution of 10 ms. The measurement of the intra-trial variability (e.g. CV) is only valid if the underlying rate is stationary, which is usually not the case in real neurons. We therefore rescaled, for each unit separately, the time axis according to the trial averaged estimate of the unit's rate function (see materials and methods section 0). This produced a stationary rate in "operational time", and the sliding window analysis (calculation of FF and CV) was applied to this time rescaled data. Before averaging the FF and CV over all units, time was scaled back to "real time".

The results of this analysis are shown in figure 4-11. First, variability increased throughout the stimulus presentation, as expressed by an increase of the FF and CV. This was most prominent for grating stimulation, while the CV during RDT stimulation increased only slightly with time. Second, the cooling induced change in variability differed across time and stimuli. For grating stimulation, both the FF and CV decreased significantly during the stimulation period (black horizontal bar, t-test $p < 0.05$, corrected for multiple comparisons) but the decrease was strongest about 500 ms after stimulus motion onset. Furthermore, this decrease was reversible as indicated by the significant difference between cooling and recovery recordings (pink horizontal bars). For RDT stimulation, FF and CV behaved different. The FF first increased significantly, but then decreased below baseline level at around 400 ms. The CV showed a tendency to decrease during cooling, but this decrease did not reach statistical significance (t-test $p > 0.05$).

4.3.3 Cooling induced change in spiking variability – time average

The observation window length and the average number of spikes per second a unit fires are two important parameters in estimating neuronal discharge variability. We therefore calculated the variability measures for baseline, cooling and recovery period for nine different combinations of the above mentioned parameters and both stimulus types. Those variability

Table 4-1

Gratings

n ges = 1495

RawData n	250ms	500ms	1000ms
5sp/s	n = 1207	n = 1197	n = 1119
10sp/s	n = 1035	n = 996	n = 896
20sp/s	n = 723	n = 671	n = 540

mmData n	250ms	500ms	1000ms
5sp/s	n = 998	n = 938	n = 821
10sp/s	n = 833	n = 773	n = 642
20sp/s	n = 553	n = 462	n = 339

p<0.001 -> ***; p<0.01 -> **; p<0.05 -> *;
n.s > 0.05; Perm test 10000 reps

FF (Co-Bl/Rc-Bl)	250ms	500ms	1000ms
5sp/s	***/-	***/-	***/-
10sp/s	***/-	***/-	***/-
20sp/s	***/-	***/-	***/-

mmFF	250ms	500ms	1000ms
5sp/s	***/-	***/-	***/-
10sp/s;	***/-	***/-	***/-
20sp/s	***/-	***/-	***/-

CV	250ms	500ms	1000ms
5sp/s	***/-	***/-	***/*
10sp/s	***/-	***/-	***/-
20sp/s	***/-	***/-	***/-

mmCV	250ms	500ms	1000ms
5sp/s	***/-	***/*	***/*
10sp/s	***/-	***/-	***/*
20sp/s	***/-	***/-	***/*

FF/CV^2	250ms	500ms	1000ms
5sp/s	***/-	***/-	***/-
10sp/s	***/-	***/-	***/-
20sp/s	***/-	***/-	***/-

$mmFF/CV^2$	250ms	500ms	1000ms
5sp/s	***/-	***/-	**/-
10sp/s	***/-	***/-	-/-
20sp/s	***/-	***/-	-/-

Dots

n ges = 1246

RawData n	250ms	500ms	1000ms
5sp/s	n = 604	n = 643	n = 636
10sp/s	n = 375	n = 408	n = 385
20sp/s	n = 184	n = 204	n = 164

mmData n	250ms	500ms	1000ms
5sp/s	n = 396	n = 417	n = 393
10sp/s	n = 236	n = 232	n = 205
20sp/s	n = 94	n = 105	n = 59

p<0.001 -> ***; p<0.01 -> **; p<0.05 -> *;
n.s > 0.05;Perm test 10000 reps

FF (Co-Bl/Rc-Bl)	250ms	500ms	1000ms
5sp/s	*/-	-/-	-/-
10sp/s	*/-	-/-	-/-
20sp/s	*/-	*/-	-/-

mmFF	250ms	500ms	1000ms
5sp/s	*/-	-/-	-/-
10sp/s	*/-	-/-	-/-
20sp/s	*/-	-/-	-/-

CV	250ms	500ms	1000ms
5sp/s	-/*	-/*	-/*
10sp/s	-/-	-/-	-/*
20sp/s	-/-	*/-	-/-

mmCV	250ms	500ms	1000ms
5sp/s	-/-	-/-	-/-
10sp/s	-/-	-/-	-/-
20sp/s	-/-	-/-	-/-

FF/CV^2	250ms	500ms	1000ms
5sp/s	***/*	-/-	-/-
10sp/s	**/*	-/-	-/-
20sp/s	*/-	-/-	-/-

$mmFF/CV^2$	250ms	500ms	1000ms
5sp/s	*/-	-/-	*/-
10sp/s	-/-	-/-	*/-
20sp/s	-/-	-/-	-/-

Table 3-1: Upper part: Number of sorted units contributing to each combination of analysis criteria for grating and RDT stimulation. mm = mean matched. Lower Part: Summary of cooling induced changes in spiking variability for different combinations of analysis window length and threshold number of spikes. For each combination, blue stars indicate a significant decrease and red stars a significant increase of the corresponding variability measure as compared to baseline. Significance level as indicated.

measures include the FF, CV and FF/CV^2. In addition to a putative change in variability removing callosal input produces significant changes in mean firing rate as described in the first section of the results. This could, in principle, influence the measurement of variability. Therefore we tried to match the mean rate during baseline, cooling and recovery. Time was rescaled to operational time before estimating the FF and CV in the analysis window.

Table 4-1 gives the number of sorted units contributing to the variability measurement for each combination. For each combination and variability measure, we tested for statistical significant changes between baseline/cooling and recovery/baseline (see Materials and Methods 3.8.3). Results are summarized in the lower part of table 4-1, with stars indicating the significance level and colors the sign of a significant change (blue = decrease, red = increase). For grating stimulation, results are very consistent, with a significant decrease for nearly all measures and combinations of parameters. Moreover, for most of the combinations, cooling induced changes in variability were reversible, as indicated by a non-significant difference between recovery and baseline. Only for the CV using long observation windows the value did not fully recover. As described before, effects for RDT stimulation were mixed. First, if there was a significant effect, it was not as strong as for grating stimulation, indicated by a smaller p-value. In addition, the results were more dependent on window length. For the 250 ms window, there was an increase in FF and FF/CV^2 (both raw and mean matched) and a decrease in CV, at least for the 5 sp/s criterion. A longer window abolished this modulation in variability for nearly all combinations of parameters. Also, for some combinations the effects did not recover completely, or changed even more compared to the cooling condition. In general, a reason could be because of the much number of sorted units contributing to each measure for RDT than for grating stimulation.

In figure 4-12A the results for a representative example from the nine combinations of parameters are illustrated. We have chosen a window length of 250 ms and a minimum average spike rate of 10 sp/s. In general, stimulating with random dots resulted in much higher response variability than stimulating with gratings. During cooling deactivation both the across trial variability (FF) and the spiking noise (CV) decreased significantly for grating stimulation. This was true for both raw and mean matched data which gave very similar results, ruling out the possibility that the observed effects were due to mean rate changes induced by cooling. Interestingly, the FF/CV^2 also decreased significantly. This indicates a

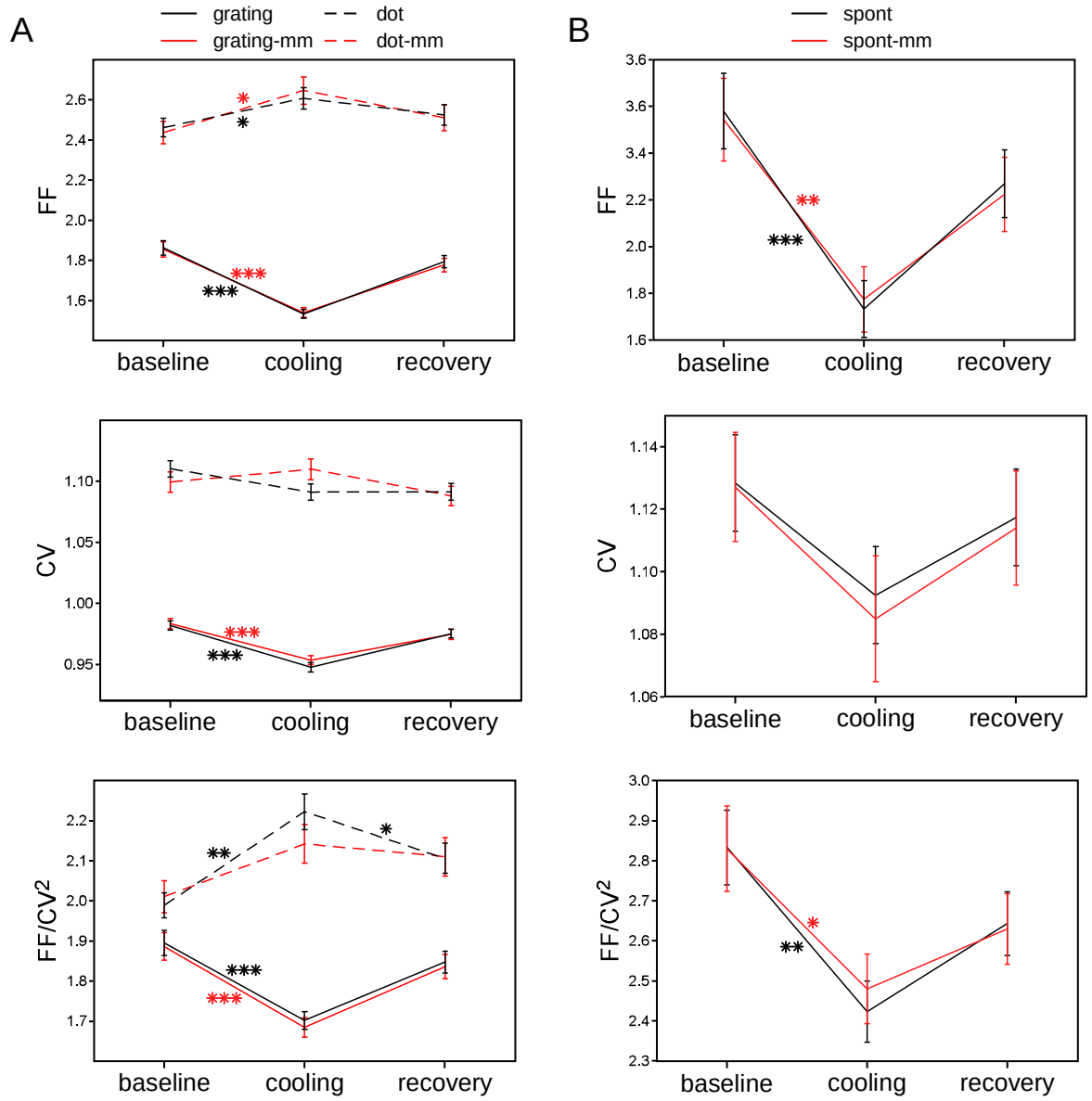

Figure 4-12: Population data of cooling induced changes in variability. (A) Data for stimulus driven activity. As a selection criterion an analysis window of 250 ms and a threshold of at least 10 sp/s were chosen. For each variability measure, raw and mean matched data are presented for grating and RDT stimulation. (B) Same as in A for spontaneous activity recorded in a 500 ms window with a threshold of at least 1 sp/s. Error bars ±1 SEM. *** $p < 0.001$, ** $p < 0.01$, * $p < 0.05$, permutation test. mm = mean matched.

"true" change in trial-by-trial variability and not only a change in (private) spiking noise, which was very small. All effects were reversible after rewarming the cortex. For random dot stimulation, the FF as well as the mean-matched FF increased slightly but significantly (both $p < 0.05$). The CV showed no significant change, while FF/CV^2 was only significantly affected for the raw data and did not reach baseline levels during recovery. Apparently, removing callosal input has only a minor impact on the recorded neurons compared to grating stimulation. Additionally, a significant effect of cooling deactivation could only bee seen for short analysis windows. This is interesting insofar, that for RDT stimulation the effect of cooling on the rate change was stronger and more consistent than for grating stimulation. On

the other hand, one has to consider the smaller sample size of the RDT (raw n = 375, mean matched n = 236) compared to grating stimulation (raw n = 1035, mean matched n = 833). The smaller sample size clearly suffers from limited statistical power. Nevertheless, the effect of cooling deactivation on response variability for RDT stimulation was small as compared to the strong decrease for grating stimulation.

4.3.4 Cooling induced change in spiking variability – spontaneous activity

We tested if spiking variability was also affected during spontaneous activity, measured during the blank period (usually 500 ms) before presentation of the random dots. Only units with a minimum average firing rate of 1 sp/s were included in the analysis. This is less then was accepted for stimulus driven data, but spike rates during the spontaneous period were generally low, so this criterion was needed to get a sufficient number of units (n = 206 for raw and n = 166 for mean-matched data). As for grating presentation, the main effect was a decline in neuronal variability (figure 4-12B). The decline in the FF was significant for both, the raw and the mean-matched data. The CV showed a tendency to decrease during cooling, bud did not reach significance. As for the data obtained during stimulation, the FF/CV^2 also decreased significantly, indicating a true change in trial-to-trial variability. All effects were reversible - although not completely - as indicated by a non-significant difference between baseline and recovery.

4.3.5 Cooling induced changes in spiking variability – influence of rate change

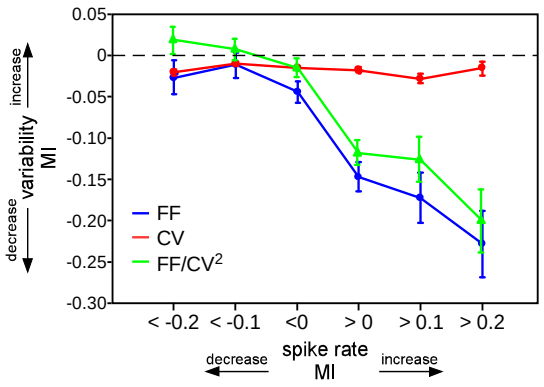

Figure 4-13: Average variability change for different groups of spike rate changes between cooling and baseline for grating and RDT stimulation. Change in variability was expressed as a modulation index (MI) comparable to the MI for rate changes. A decrease in trial-to-trial variability is most pronounced for cooling induced increases in spike rate. Bin width = 0.1. Error bars ±1 SEM.

Observing the pronounced changes in spiking variability for grating stimulation, we asked whether there is a relationship between the change in variability and the change in spike rate. We expressed the change in variability (FF, CV and FF/CV^2) as a modulation index comparable to the change in spike rate described in section (3.6.3). We binned this modulation index into six bins of spike rate changes (also expressed as a modulation index, bin width = 0.1). As is depicted in figure 4-13, the FF and FF/CV^2 changes clearly depended on spike rate changes: FF and FF/CV^2 decreased most strongly when the rate increased, while the (most prevalent) rate decreases were accompanied by only a weak change in variability. A correlation analysis between spike rate and variability change confirmed this observation (Spearman rank correlation, FF: $\rho = -0.23$ $p < 0.0001$; FF/CV^2: $\rho = -0.27$ $p < 0.0001$). The CV, on the other hand, was independent of a change in spike rate ($\rho = -0.028$ $p = 0.39$).

5. Discussion

5.1 Methodological considerations

In this section, the methods applied in this thesis will be discussed in the light of their putative influence on the obtained results. In scientific research, it is of particular importance to critically review the methods used in order to answer a specific question. In systems neuroscience, working experimentally, this includes the acquisition, as well as the subsequent treatment and interpretation of the data. To acquire the necessary knowledge, about the planning and accomplishment of an in vivo experiment in a higher mammal, including its technical realization was therefore a major part of this thesis.

5.1.1 Evaluation of the recording position

Determining the recording position was the first step during the acute experiment. As a first approximation, we used stereotactic coordinates to guide the craniotomy. To determine the recording position more precisely, we identified the 17/18 border for most of the animals using optical imaging of intrinsic signals. This technique has the advantage that - in contrast to microelectrode penetrations which enable a more accurate characterisation of the 17/18 border - it is not invasive, i.e. that the cortex is not penetrated or otherwise damaged. A potential disadvantage of the imaging technique is the fact that it relies on an indirect signal (the hemodynamic response) and a good signal-to noise ratio is thus critical in order to get a satisfying estimate of the 17/18 border. In addition, the determination of the retinotopic relationship between the single electrodes of a matrix electrode after the experiment complements the mapping of the 17/18 border by the optical imaging method. Taken together the intrinsic imaging maps before and the reconstructed receptive field distribution at the end of the experiment, one can be relatively confident about the recording position with respect to the vertical meridian representation. Rather than forming a strict border, the anatomical (and physiological) properties of area 17 and 18 blend into each other smoothly (Otsuka & Hassler, 1962; Orban et al., 1980). Further, we used always full-field stimuli and observed pronounced effects also at recording positions several millimetres away from the estimated border. Thus,

for the results presented here, the exact localization of the 17/18 border and positioning of the monitor on the VM was not necessary.

5.1.2 Cooling deactivation

It is likely that the most critical variable in our experiments was the deactivation technique. The use of local, reversible brain cooling was developed by the German physiologist William Trendelenburg (e.g. Trendelenburg, 1910). He implanted cooling chambers on the skull of dogs, cats and monkeys and observed a variety of behavioral effects, depending on the chamber position. Since then, a lot of studies have been performed using different cooling techniques, such as cooling needles or plates (reviewed by Brooks, 1983).

The cryoloop technique, used in this study, has several advantages over other older deactivation techniques. An important advantage is that the technique is reversible. In contrast to lesion studies, multiple deactivation cycles during one acute experiment are possible, which increase statistical power and reduce the number of animals needed for a particular study. Of further advantage is that shape and dimension of the cooling loop can be flexibly adjusted to the cortical gyrus or sulcus to be deactivated. One can even make slight modifications during an experiment to ensure a good contact with the cortex and therefore a good conductance of temperature.

Of course there are some disadvantages. Lowering the temperature below the physiological level introduces different physiological effects at the same time. These effects range from hyperexcitability of neurons at a specific temperature to complete silencing of synapses and thus depolarization block. Accordingly, the tissue directly under the cooling probe will probably be completely silenced due to the depolarization block. As the cortical tissue warms gradually up with distance from the cooling loop, a region of cortex will be in the temperature range of hyperexcitability, thereby increasing the activity of the neurons in those regions. Therefore, cooling one hemisphere could paradoxically provide excitation onto the contralateral side via callosal connections. Theoretically, even a direct influence of cooling on the recording hemisphere cannot be completely ruled out, because even lowering the temperature a few degrees has been shown to have an impact on neuronal activity (Brooks, 1983). However, we consider a spread of cooling to the recording site unlikely, because in our preparation we leave the bone bridge above the sinus sagittalis and thus the adhesion of the dura duplication – carrying the sinus – to the bone intact, providing an efficient barrier for a direct spread of temperature to the other hemisphere.

Also, the precise position of the cooling probe may have an impact on the observed effects. However, in any case, the deactivated region should have been large enough to cover the area recorded on the other hemisphere. An indirect effect of cooling could be the local counter regulation of the vessels to the cold with probably vasoconstriction. It is possible that the temperature related vessel reaction mediates and thus spreads effects of the deactivation farther away from the cooling probe than the immediate neuronal effects.

A general problem of deactivation studies is based on the state dependence of cortical activity, probably due to anesthesia (Franks, 2008). The start of a cooling cycle may coincide with a state of low or high responsiveness, so a change in spiking activity may not be the result of the cooling deactivation per se. This has also an implication for recovery periods. Because the latter were recorded up to two hours after starting the baseline period, the spike rate might not have reached the initial level because of a state change. In addition, the visual cortex may have adapted to the new input situation during long cooling periods. Therefore, on the one hand, we tried to keep cooling periods as short as possible by decreasing recording time per stimulus and the number of different stimulus conditions, in order to bring the recordings as close as possible together in time. On the other hand, we aimed to average sufficient stimulus repetitions in order to overcome any state related changes in firing behavior.

5.1.3 Recording multi- and single unit activity

In the experiments performed for this thesis, we used commercially available multielectrode arrays for recording of neural activity. The use of such multielectrode arrays has several advantages. One can record from a large number of neurons during one cooling cycle, therefore increasing statistical power. Furthermore, once in the cortical tissue, the recordings turned out to be very stable, so we could record from a specific site for some days.

A disadvantage of those electrodes emerges from the bended surface of the brain's gyri. This means, that when lowering the electrodes in the cortical tissue, individual electrodes will not end up at the same cortical depth. In the worst case, one may not get a signal on every electrode at the same time because one cannot adjust the positioning for each channel separately. From the 16 channels per matrix electrode, usually 50 to 80 % had a clear multiunit signal.

We set a number of criteria a recorded channel had to fulfil in order to be included in our sample. This included a significant difference to spontaneous activity, as well as a certain degree of orientation / direction selectivity. Orientation selectivity is the major feature of

neurons in primary visual cortex, so this criterion is a good estimator for a reliably responding unit. The threshold of 0.2 for the direction and orientation index was chosen rather arbitrary, but Monte Carlo simulations of tuning curves with realistic amplitudes revealed that a DI or OI of 0.2 was only reached by chance in less then 1 % of the cases (data not shown).

Putative single unit responses were obtained by offline spike sorting. Single unit responses were needed for the variability analysis because those measures rely on spiking statistics of individual neurons. We used an automatic sorting algorithm to obtain trains of single unit spikes from the MUA signal. This usually results in two to five clusters per MUA recording. We did not further control the separation of the clusters. This may lead to separation of spikes in two clusters, which in fact stem from the same neuron. However, fully automated sorting does not introduce any bias in the selection of the clusters, which may be an advantage over a user assisted sorting procedure. We made sure that the same clusters were defined for baseline, cooling and recovery period by pooling them together before sorting. This further decreases the impact of any systematic error introduced by automated clustering.

5.1.4 Visual stimulation

Visual stimulation was performed with gratings and random dot textures. We chose those types of visual stimuli for certain reasons: First, they have been used for a long time in visual neuroscience, so the results obtained with these stimuli can be compared to other studies. Second, especially gratings are suited for studies of primary visual cortex because of its capacity in detecting moving edges. The difference between the two stimuli lies in their physical properties, which in turn determine the way in which the cortical network is driven. Grating stimuli contain a single spatial and temporal frequency and a strong orientation component orthogonal to the direction of movement. This leads to a selective but strong activation of a population of neurons. Moreover, stimulating with high contrast gratings will result in more intracortical (cross-orientation) inhibition, known to rise with a stronger recruitment of the horizontal network (Hirsch & Gilbert, 1991; Crook & Eysel, 1992).

Random dot patterns, in contrast to gratings, contain a broad range of spatio-temporal frequencies, which leads to a weak, but broad activation of a population of neurons. Indeed, models of receptive fields in primary visual cortex predict an ambiguous response to stimulation with moving dots at a certain direction (Skottun et al., 1994). The tuning of a neuron, stimulated with RDTs, depends on the size and speed of the dots, as well as on the orientation of its receptive field (Wörgötter & Eysel, 1989; Geisler et al., 2001). This ambiguous response gives rise to a broad tuning curve with its summation vector often

pointing towards the direction of the neurons preferred orientation obtained with a grating stimulus.

Spatial and temporal frequency of the gratings and the speed and size of the dots were chosen to fit the majority of neurons recorded in area 17 or 18. This also means that individual neurons may not be optimally stimulated. Especially, the steps between the stimulation orientations / directions were relatively course. A finer sampling of the orientations would be desirable, but comes at the cost of longer recording periods.

Although, we called them random "dot" textures, the single elements of those stimuli actually consisted of small squares. This was a consequence of the stimulation system we used. As a result, a square passing through the receptive field of a neuron might have eventually evoked a response not corresponding to the exact direction of motion, dependent on orientation preference and size of the receptive field.

5.1.5 Generalization of findings

Can our findings be generalized to other cortico-cortical connections? On the one hand, there is good anatomical evidence that the callosal system can be described as an extension of the horizontal network across the two cerebral hemispheres (Houzel & Milleret, 1999; Rochefort et al., 2009). On the other hand, there is one notable difference between callosal and long-range horizontal connections: The callosal projections can directly drive their target cells (Choudhury et al., 1965; Berlucchi & Rizzolatti, 1968), whereas the latter ones are believed to be only modulatory (Hirsch & Gilbert, 1991). Our finding, that cooling deactivation also affects spontaneous activity, indeed supports a rather driving than modulatory role. However, changes in spontaneous rate have also been observed for different attentional states (Maunsell & Treue, 2006), as well as in feedback deactivation studies (Wang et al., 2007). Both influences are usually believed to be only modulatory but one can imagine that the border between driving and modulatory is not a sharp qualitative one but rather a quantitative.

5.2 Effects of cooling deactivation on response amplitude

Previous work on the functional role of callosal connections using thermal deactivation revealed a mixed picture of spike rate changes, with rate decreases being most frequent (Payne, 1994). This is in agreement with the anatomy of the callosal connections.

Our results are therefore in agreement with previous work and the anatomical connectivity. In addition, we can show that the fine tuning of the modulations is dependent on the properties of the visual stimulus: The way in which the stimulus drives the cortical network also influences the modulation through cortico-cortical connections. Examination of the population PSTHs revealed a significant reduction of spike rate for the spontaneous, static and dynamic period of the stimulus presentation. Although we did not analyze with fine temporal resolution, the apparent effect for the initial transient suggests that the modulation through the callosal system operates on a fast timescale. One maybe would have assumed that the initial transient response, due to stimulus onset, is entirely driven by thalamo-cortical input, and therefore not susceptible to the cooling deactivation. However, transcallosal time delays are quite short, ranging from 4 to 6 ms (Innocenti, 1980). In accordance, firing rate modulations through feedback connections have also been shown to originate within the first 10 ms after stimulus onset (Hupe et al., 2001).

An apparent discrepancy emerges between grating and RDT simulation regarding the cases of spike rate increases. Significant rate increases could be observed only while stimulating with gratings, not with random dots. This stimulus specificity strongly supports the view that the observed effects are due to the action of callosal fibers crossing the hemispheres, and not to a hyperexcitability of recorded neurons induced by a direct influence from the cooled hemisphere. An increase in firing rate could be the result of a direct removal of inhibition through callosally projecting inhibitory neurons, but those neurons a rarely found (Buhl & Singer, 1989; Fabri & Manzoni, 1996).

Another possible explanation for rate increases with grating stimulation could be the recruitment of cortical inhibition evoked by high-contrast gratings. In the visual cortex, excitatory synaptic input is closely balanced with inhibition both in spontaneous and stimulus driven activity (Sanchez-Vives & McCormick, 2000; Shu et al., 2003; Haider et al., 2006; Okun & Lampl, 2008). Additionally, inhibitory interneurons have a higher firing threshold and gain than excitatory pyramidal neurons (e.g. Fricker et al., 1999; Porter et al., 2001). Therefore, one can assume that a visual stimulus alone may not evoke much inhibition, but together with a modulating input make the inhibitory neurons fire. Considering the high gain and firing rate of most inhibitory neurons, the net effect of an excitatory modulating input can be an overall inhibitory one (Lund et al., 1995). In such a configuration, removing excitatory input by cooling deactivation would lead to disinhibition, explaining the (significant) rate increases for grating stimulation but not for RDTs. These mechanisms can explain the rate

increases for grating stimulation, but not why the decreases are less pronounced in amplitude compared to RDT stimulation.

A simple explanation would be a response saturation for high contrast gratings, expressed in the sigmoid relationship between driving input (current) and output rate (figure 2-4). The removal of additional input in such a low gain regime would have only a minor effect on output firing rate. However, we controlled for differences in mean firing rate between gratings and RDTs by lowering the contrast of the gratings. In these control experiments, the stronger rate decrease for stimulation with RDTs compared to gratings was preserved. This held true even though lowering the contrast of gratings resulted in slightly stronger proportional rate decreases during cooling compared to high contrast gratings (data not shown). In addition, bar stimuli including properties of both stimuli used before (e.g. an orientation component, orthogonal to the direction of movement) did not evoke many rate increases and larger decreases than gratings thus emphasizing the unique nature of the latter in driving the cortico-cortical network.

What is then the difference between grating and RDT stimulation with respect to the weaker decrease for gratings? An explanation may be given by studies of spontaneously occurring state transitions in cortical tissue during a wide range of circumstances. More specifically, a single neuron or a group of neurons can slowly (< 1 Hz) alter their responsiveness form a highly responsive, depolarized “up” state to a non- or weakly responsive, hyperpolarized “down” state (Ho & Destexhe, 2000; Shu et al., 2003; Haider et al., 2007). Such changes are mediated by barrages of synaptic input that alter the biophysical properties of a neuron (such as membrane potential, conductance and variance) together with the level of background excitation/inhibition. Interestingly, two studies in the lab of David McCormick have shown that during an “up” state, small inputs are amplified more than medium or large inputs (Shu et al., 2003; Haider et al., 2007). If callosal input changes the neuronal gain by a similar mechanism, stimulation with RDTs, which provides a weaker driving input than grating stimulation, should also be more sensitive to the callosal input, and thus cooling deactivation. Considering the wide spread of callosal terminals, a global change in the level of background balanced excitation/inhibition seems reasonable.

It is worth mentioning, that the observed effects (although strongest at the 17/18 border) could be observed in regions of area 17 and 18 several millimetres away from the 17/18 border (corresponding to >10° away from the VM). This is consistent with the wide spread of callosal terminals and indicates a more general role of callosal connections like the widely discussed merging of the two visual hemifields along the VM (Hubel & Wiesel, 1967;

Schmidt et al., 2010; for review see Houzel et al., 2002). Finally, we could observe a significant reduction of spontaneously occurring firing rates. This is in accordance with the dominant excitatory nature of callosal fibers. Moreover, it is consistent with feedback studies where a similar decrease in spontaneous activity could be observed while cooling area 21a and recording form area 17 in the cat (Wang et al., 2007). Additionally, in studies of attention in awake, behaving monkeys, a reduction of spontaneous activity has been described in the non-attentive state, supporting an excitatory influence of modulatory projections on ongoing activity in visual cortex (Reynolds et al., 2000; Williford & Maunsell, 2006).

5.3 Effects of cooling deactivation on orientation tuning curves

Albeit the orientation selectivity of neurons in primary visual cortex has been largely explained by a feed forward model (e.g. Ferster & Miller, 2000), some studies have shown the contribution of cortico-cortical connections in shaping their tuning curves (Eysel et al., 1990; Crook & Eysel, 1992; Galuske, 2002; Wang et al., 2007; Schmidt et al., 2010). Additionally, recordings in awake monkeys have demonstrated that spatial attention can scale the tuning of neurons in visual areas V1 and V4 (McAdams & Maunsell, 1999a; Treue & Martinez Trujillo, 1999). Indeed, our results demonstrate a predominantly multiplicative scaling with only minor changes in tuning width, as described before for attentional modulation. However, some units showed a pronounced additive shift, especially with grating stimulation for both rate increases and decreases.

Even without changing the tuning width, a multiplicative downscaling of an orientation tuning curve would have an influence on the performance of orientation discrimination, as observed in psychophysical experiments (Li et al., 2000). This is because such a scaling would decrease the maximal slope of the tuning curve, thereby decreasing the sensitivity to orientation differences. Therefore, we conclude that the callosal system, albeit having only minor influences on tuning width, supports orientation discrimination in central primary visual areas.

A number of models have been proposed to explain the impact of modulating synaptic input on the firing of a neuron, enabling the neuron to perform mathematical operations like addition and multiplication (for review see Silver, 2010). Specifically, intracellular recordings showed that synaptic input can modulate the gain of a neuron, its sensitivity to one set of inputs that depends on the activity of a second set of inputs (Brozović et al., 2008). Biophysically, a gain modulation can be achieved by the release of neuromodulators (McCormick, 1992), alterations of synaptic conductances (Sanchez-Vives & McCormick,

2000) or by barrages of synaptic input (Ho & Destexhe, 2000; Chance et al., 2002; Shu et al., 2003; Haider et al., 2007). In the last model, the total level of synaptic input (balanced excitation/inhibition) sets the gain of a neuron, and can be modulated independently from the excitatory drive (main information conduit). A recent study performing intracellular recordings in vivo indeed observed a combination of depolarization, voltage fluctuations and conductance changes giving rise to a gain change (Cardin et al., 2008). Interestingly, those changes were stimulus dependent: A broadband stimulus with a variable spatio-temporal frequency evoked different responses than a sinusoidal grating, dependent on stimulus contrast. This is in agreement with our findings that gratings and random dot textures produce different patterns of rate modulation.

Murphy (Murphy & Miller, 2003) proposed a model termed “nonlinear additive”, in which the addition of an (constant) excitatory or inhibitory input can lead to a roughly multiplicative scaling. In their model, a constant is added to the (nonlinear) tuned input in the presence of an expansive nonlinearity between membrane potential input and spike rate output, expressed as a power law.

To make this point clearer, we constructed a simple model consisting of a tuned synaptic input. It turned out, that the addition of a constant in the presence of a nonlinear transformation between membrane potential and spike rate output was sufficient to get a roughly multiplicative scaling of the spike rate tuning curve. But, especially for the threshold linear model, this scaling was not perfectly multiplicative, thus tuning width increased with the additional input. This is exactly what we saw in our data. Those neurons, for which the tuning curve change had a positive additive component induced by cooling, indeed increased their tuning width while those with a negative additive component decreased their selectivity. This correlation was not found for the multiplicative scaling, for which one would also not predict a change in tuning width.

The fact that a constant input can result in a multiplicative gain change has also been described in studies on the contrast dependence of orientation tuning (Anderson, 2000; Finn et al., 2007). Here, increasing the stimulus contrast increased the overall stimulus drive, and according to the feedforward model proposed by Hubel & Wiesel (Hubel & Wiesel, 1962) one would have predicted a broadening of the orientation tuning curve. This is because (like in our model) introducing a fixed amount of excitation will bring responses to non- optimal orientations above firing threshold, thereby increasing tuning width. Instead, it was found that orientation tuning was largely invariant with contrast. The cellular and biophysical mechanisms mediating this phenomenon include contrast saturation, combined LGN and

cortical input (from other neurons nearby) and, most importantly, a nonlinear i-o relationship caused by membrane potential variance. It is therefore likely that those mechanisms are a general feature of the cerebral cortex and mediate also the observed multiplicative scaling for modulations of callosal input, as seen in our studies. However, in our experiments we can only observe spike output. Finally, we cannot rule out the contribution of other synaptic mechanisms known to modulate output rate (Salinas & Sejnowski, 2000; Chance et al., 2002; Haider et al., 2007).

A multiplicative scaling can be produced also by a rather simple mechanism: If the modulating input is itself tuned, the addition of this input to the driving input would resemble a scaling by a constant factor (assuming the tuning width of the driving and modulatory input being equal). The broader the tuning of the modulatory input becomes, the more it will resemble a constant input, and the more the output will be an additive scaling. In contrast to most theoretical studies, we tested the behaviour of our model if the modulating input itself was tuned for orientation. This gave, for both the threshold linear and the power law transformation, a nearly perfect multiplicative scaling, as would be expected from adding a fraction of a tuning curve to itself. Indeed, there is good evidence that the input from callosal fibres is orientation tuned (Hubel & Wiesel, 1968; Lepore & Guillemot, 1982; Rochefort et al. 2007), as it is for long range horizontal connections (Stettler et al., 2002). Thus, it can be assumed that the observed multiplicative scaling is (at least partially) the result of tuned callosal input.

In the light of the above discussion, it seems to be very difficult to not get a multiplicative scaling. So how does one explain the additive shifts in our data, which correlate with changes in tuning width? Our model would produce an additive shift if the membrane potential for all orientations were above, or close to firing threshold. The threshold linear model would then be reduced to the linear part, and the addition of a constant to the membrane potential would correspond to the addition of a constant to the spike rate tuning curve. Such a situation could occur in a general state of high excitability. In that state, a high contrast grating of the null orientation may depolarize a neuron close to firing threshold. Indeed, for the population of neurons recorded, stimulation with a grating produced additive changes with a higher probability than random dot stimulation.

5.4 Effects of cooling deactivation on response variability

Neurons in sensory cortices usually display a high degree of spike count variability, and the timing of successive spikes is highly irregular (Tomko & Crapper, 1974; Heggelund &

Albus, 1978; Rose, 1979; Tolhurst et al., 1983; Vogels et al., 1989; Reich et al., 1997). We quantified the trial-to-trial variability in spike count by calculating the Fano factor as well as the spike time irregularity by calculating the coefficient of variation of the interspike intervals. However, care has to be taken in interpreting those measures of variability, because a variety of factors can affect them. We therefore applied different controls aimed to correct for the putative distortions (see materials and methods 3.8).

In agreement with recent work performed in monkeys (Churchland et al., 2010; Hussar & Pasternak, 2010) we found a decrease of spiking variability with stimulus onset. Throughout the stimulus period, variability then increased continuously until saturation about 600 ms after stimulus motion onset.

During cooling deactivation, we could observe a pronounced decrease in spiking variability for grating stimulation, both for the FF and CV throughout the stimulation period. This decrease seemed to be strongest about 500 ms after stimulus motion onset, maybe pointing to a stronger role of callosal connections during sustained processing of the stimulus as compared to the initial transient. In contrast, RDT stimulation seemed to initially increase the FF, followed by a later decrease, although the effects were very small. In this case, deactivation could diminish the stimulus dependent modulation of firing variability as observed before.

Following this initial findings, we made a more detailed analysis of firing variability in a fixed window. In addition to the FF and CV, we also calculated the quotient FF/CV^2. Changes in this measure indicated a violation of the renewal assumption ($FF = CV^2$) and therefore a (true) change in trial-to-trial variability. Recordings in the motor cortex of behaving monkeys indeed showed that normally the FF is 2-3 times larger than the CV^2, whereas for in vitro slice recordings the predicted equality was fulfilled (Nawrot, 2003). Using a simple additive model of ongoing activity and stimulus induced spiking, Nawrot could demonstrate that slow state changes boost trial-to-trial variability whereas spike irregularity was only slightly changed. Indeed, a series of studies have shown slow, coherent fluctuations of spontaneous activity that propagate throughout sensory cortex (Arieli et al., 1996; Kenet et al., 2003). Those authors claim that a linear combination of ongoing activity and stimulus induced response account for the observed across trial variability. Then, the different spike count for each trial would not be the result of a stochastic, but of a deterministic (constant) process reflecting a change in the rate of the spike generating mechanism. The non-identity of FF and CV^2 could then be seen as a quantitative measure of across trial non-stationarities.

Indeed, we found that FF/CV^2 was high in the baseline, consistent with previous recordings in monkeys. Moreover, FF/CV^2 decreased significantly during cooling, meaning that the decrease in trial-to-trial variability exceeded the decrease in spiking noise. How can one explain those results? As described in section 5.2, the cortex traverses slowly through "up" and "down" states changing the responsiveness of a neuron. If those changes are not phase-locked to the stimulus, the cortex responds with a different number of spikes for each stimulus presentation depending on the phase of the state. If the removal of callosal input would somehow stabilize one state and decrease the number of transitions, and thus the non-stationarity, the FF would be expected to also decline as we observe in our data. As a cellular mechanism, the stabilization of the spike threshold has been discussed (Azouz & Gray, 1999). Such stabilization could occur due to increased gamma oscillations, which have been shown to go along with reduced spike variability (Rodriguez et al., 2010).

We additionally calculated FF, CV and FF/CV^2 for different groups of rate in- and decreases. It turned out, that the strong decrease in FF and FF/CV^2 was largely due to the rate increases observed for some units with grating stimulation. Spike timing (CV), on the other hand, was more or less independent of the rate change.

Which mechanism could explain the strong decrease in trial-to-trial variability for neurons whose firing rate was enhanced during cooling deactivation? If a neuron fires close to saturation, the refractory period starts to regularize spike timing. Therefore, in such a regime, CV should decrease together with FF. Because CV was only slightly decreased with increasing rates, it is unlikely that the refractory period can explain our results. Different changes of variability for rate in- or decreases have also been shown after iontophoretic application of the neuromodulator acetylcholine (ACh) (Zinke et al., 2006). Here, the count variability during the sustained stimulation period was only reduced for cells with increased firing rate due to ACh application. Although, it is unlikely that callosal connections act similar to cholinergic projections, the experiment emphasizes the general possibility of rate change dependent changes in variability.

Other possible mechanisms introducing variability changes were discussed in studies of attention modulation in awake, behaving monkeys. When a monkey paid attention to a stimulus inside the receptive field of a neuron recorded in V4, the FF was smaller than in the attended away condition (Mitchell et al., 2007). However, another study failed to observe a change of variability in dependence on the state of attention (McAdams & Maunsell, 1999b). In the attentive condition, the firing rate of the recorded neurons usually slightly increased (McAdams & Maunsell, 1999a; Treue & Martinez Trujillo, 1999; Mitchell et al., 2007; Thiele

et al., 2009), which fits to our findings of decreased FF with increased firing rate during cooling. More recently, an attention dependent decrease in variability was attributed to decorrelation of neuronal responses with attention (Cohen & Maunsell, 2009; Mitchell et al., 2009). Input correlations have a strong impact on the firing of individual neurons and the coding capacity of populations of neurons. The reason is that correlated noise cannot be averaged out by simply pooling across a large population of neurons (Shadlen & Newsome, 1998). In model neurons, rather, input correlations increase the gain and spike timing variability (Salinas & Sejnowski, 2000). Callosal connections may provide direct input correlations by making multiple synaptic contacts with their target cells. Indeed, callosal axons form dense clusters of boutons possibly providing correlated input to a population of neurons (Houzel & Milleret, 1999). In that case, removing callosal input would remove input correlations and thus reduce spike timing variability (Salinas & Sejnowski, 2000).

In general, a shift in the balance of excitation and inhibition towards one of both can make a cell fire more regularly (Stevens & Zador, 1998). Such changes could superimpose with changes of correlated input and slow state transitions to give rise to the observed effects during deactivation of lateral input.

Stimulation with RDTs, in comparison to gratings, led to higher response variability in baseline recordings for all three variability measures. This may be the result of the random nature of the stimulus elements, event though the same pattern was repeated in successive trials. The changes in variability for RDT stimulation were small relative to grating stimulation and reached significance only for the FF and FF/CV^2 in short observation windows. This is understandable when considering the time course of the FF change. As the FF initially increased above baseline, and then decreased at about 400ms after stimulus motion onset, the effects cancelled out for large analysis windows. Interestingly, the significant changes in variability for short analysis windows with RDT stimulation were all increases, whereas for grating stimulation, there were only significant decreases in variability. This could be a result of the difference in spike rate change induced by cooling deactivation. For grating stimulation, the pronounced variability decreases were observed for rate increases, which were absent in the case of RDT stimulation. As mentioned above, for RDT stimulation the FF initially increased under cooling deactivation, followed by a slight reduction later in the trial. This diminished the aforementioned reduction in trial-to-trial variability induced by the stimulus onset. Obviously, the removal of input through callosal fibers interferes with a stable encoding of the RDT stimulus. That this happened for RDT stimulation, but not for high contrast gratings, is in line with previous work, showing that weaker, low contrast

stimuli benefit more from the lateral network then stronger, high contrast stimuli (Nauhaus et al., 2008).

An increase in trial-to-trial variability could be the result of the strong reduction in spike rate, which reduced the impact of the stimulus drive, so that ongoing fluctuations dominated over the stimulus induced activity. Overall, because RDTs drive the system less strongly, many units didn't pass the selection criteria. The number of units in the sample was therefore much smaller then for grating stimulation, reducing statistical power.

Furthermore, we saw a significant reduction of trial-to-trial variability for spontaneous activity, but not for spike timing variability, which did not reach significance. The reduction in FF for spontaneous firing supports the hypothesis that cooling induced removal of callosal input acts on ongoing fluctuations of cortical activity. Those fluctuations seem to be bigger with intact cortico-cortical input from the other hemisphere. Indeed, recent studies in humans have shown correlations in resting state fluctuations between the cerebral hemispheres in fMRI and MEG experiments (Fox & Raichle, 2007; Liu et al., 2010). Disturbing interhemispheric communication restricts those ongoing fluctuations to one hemisphere, thereby possibly decreasing their amplitude.

6. Summary and Conclusion

In this study, we investigated the functional impact of interhemispheric projections on neurons in their target zones. Electrophysiological recordings were performed in primary visual areas 17 and 18 of the anesthetized cat. We combined the electrophysiological recordings with reversible cooling deactivation. Our results demonstrate a stimulus specific modulation of firing rates in the callosal recipient zone, with a predominant excitatory influence. The effects could be observed for static and moving stimuli and persisted throughout the stimulation period. Additionally, spontaneous activity was affected in a similar way.

We also characterized the mechanism of those modulations, revealing a multiplicative scaling, especially for those cells which show a strong change in spike rate at their preferred direction. Tuning width was only faintly influenced by the callosal fibers, but a correlation existed between the additive component of amplitude scaling and a small change in tuning width. According to previous experimental and theoretical work, we created a simple model of response modulation of tuning curves. Those simulations indicated that a multiplicative scaling of tuning curves can be obtained by the addition of cortico-cortical synaptic input to the membrane potential, in the presence of a nonlinear input-output transformation or by tuned synaptic input.

Furthermore, we estimated neuronal discharge variability, including trial-to-trial variability measured by the Fano factor and within trial variability, or spiking noise, measured by the coefficient of variation. We found a stimulus-dependent change for both measures, with a more pronounced decrease in trial-to-trial variability compared to spiking noise. A strong decrease in trial-to-trial variability was mainly present in neurons which increased their spike rate during cooling deactivation. The profound effects of cooling on trial-to-trial variability point towards a modulation of ongoing fluctuations by callosal or lateral connections. These fluctuations are added to the stimulus induced responses.

Our results complete the view of how cortico-cortical connections in the brain shape responses to external stimuli and are in line with previous work on the physiological role of feedback projections and callosal connections. They provide, for the first time, an extensive evaluation and mathematical description of the contributions of long-range projections to the

response properties of cortical neurons. Furthermore, they demonstrate that what we usually call “noise”, and try to get rid of by extensive averaging, is indeed part of the system and might be dynamically regulated. Therefore, in understanding more complex features of visual processing, like center-surround interactions or scene segmentation, it might be important to consider the variability of neuronal actions and interactions. Indeed, over the last view years it became clear that neuronal variability in a variety of cortical areas plays a critical role in conscious perception and motor actions. Finally, our results have implications for neuronal coding, showing that cortico-cortical connections can alter the rate and timing of spikes.

7. Bibliography

Ahmed, B., Anderson, J.C., Douglas, R.J., Martin, K.A. & Nelson, J.C. (1994) Polyneuronal innervation of spiny stellate neurons in cat visual cortex. *J Comp Neurol*, **341**, 39-49.

Akaike, H. (1974) A new look at the statistical model identification. *Automatic Control, IEEE Transactions on*, **19**, 716-723.

Albrecht, D.G. & Geisler, W.S. (1991) Motion selectivity and the contrast-response function of simple cells in the visual cortex. *Vis Neurosci*, **7**, 531-546.

Albright, T.D. & Stoner, G.R. (2002) Contextualinfluences Onvisualprocessing. *Annual Review of Neuroscience*, **25**, 339-379.

Alekseenko, S.V., Toporova, S.N. & Makarov, F.N. (2005) Neuronal connection of the cortex and reconstruction of the visual space. *Neurosci Behav Physiol*, **35**, 435-442.

Allman, J., Miezin, F. & McGuinness, E. (1985) Stimulus specific responses from beyond the classical receptive field: neurophysiological mechanisms for local-global comparisons in visual neurons. *Annu Rev Neurosci*, **8**, 407-430.

Andersen, R.A. & Mountcastle, V.B. (1983) The influence of the angle of gaze upon the excitability of the light-sensitive neurons of the posterior parietal cortex. *J Neurosci*, **3**, 532-548.

Anderson, J.S. (2000) The Contribution of Noise to Contrast Invariance of Orientation Tuning in Cat Visual Cortex. *Science*, **290**, 1968-1972.

Angelucci, A. & Bressloff, P.C. (2006) Contribution of feedforward, lateral and feedback connections to the classical receptive field center and extra-classical receptive field surround of primate V1 neurons. *Prog Brain Res*, **154**, 93-120.

Arieli, A., Sterkin, A., Grinvald, A. & Aertsen, A. (1996) Dynamics of ongoing activity: explanation of the large variability in evoked cortical responses. *Science*, **273**, 1868-1871.

Ayaz, A. & Chance, F.S. (2009) Gain Modulation of Neuronal Responses by Subtractive and Divisive Mechanisms of Inhibition. *Journal of Neurophysiology*, **101**, 958-968.

Azouz, R. & Gray, C.M. (1999) Cellular mechanisms contributing to response variability of cortical neurons in vivo. *J Neurosci*, **19**, 2209-2223.

Batschelet, E. (1981) Circular Statistics in Biology. Academic Press.

Beaulieu, C., Kisvarday, Z., Somogyi, P., Cynader, M. & Cowey, A. (1992) Quantitative distribution of GABA-immunopositive and -immunonegative neurons and synapses in the monkey striate cortex (area 17). *Cereb Cortex*, **2**, 295-309.

Benjamini, Y. & Hochberg, Y. (1995) Controlling the False Discovery Rate: A Practical and Powerful Approach to Multiple Testing. *Journal of the Royal Statistical Society. Series B (Methodological)*, **57**, 289-300.

Berardi, N., Bisti, S. & Maffei, L. (1987) The transfer of visual information across the corpus callosum: spatial and temporal properties in the cat. *J Physiol*, **384**, 619-632.

Berbel, P. & Innocenti, G.M. (1988) The development of the corpus callosum in cats: a light- and electron-microscopic study. *J Comp Neurol*, **276**, 132-156.

Berlucchi, G. & Rizzolatti, G. (1968) Binocularly driven neurons in visual cortex of split-chiasm cats. *Science*, **159**, 308-310.

Bernander, O., Koch, C. & Douglas, R.J. (1994) Amplification and linearization of distal synaptic input to cortical pyramidal cells. *J Neurophysiol*, **72**, 2743-2753.

Binzegger, T. (2004) A Quantitative Map of the Circuit of Cat Primary Visual Cortex. *Journal of Neuroscience*, **24**, 8441-8453.

Blakemore, C., Diao, Y.C., Pu, M.L., Wang, Y.K. & Xiao, Y.M. (1983) Possible functions of the interhemispheric connexions between visual cortical areas in the cat. *J Physiol*, **337**, 331-349.

Bonhoeffer, T. & Grinvald, A. (1996) Optical Imaging Based on Intrinsic Signals: The methodology. *A. Toga, and J. C. Mazziotta, eds., San Diego, C A: Brain Mapping: The Methods, Academic Press 1996, pp. 55–97.*

Bonhoeffer, T., Kim, D.S., Malonek, D., Shoham, D. & Grinvald, A. (1995) Optical imaging of the layout of functional domains in area 17 and across the area 17/18 border in cat visual cortex. *Eur J Neurosci*, **7**, 1973-1988.

Bosking, W.H., Zhang, Y., Schofield, B. & Fitzpatrick, D. (1997) Orientation selectivity and the arrangement of horizontal connections in tree shrew striate cortex. *J Neurosci*, **17**, 2112-2127.

Branco, T. & Häusser, M. (2011) Synaptic Integration Gradients in Single Cortical Pyramidal Cell Dendrites. *Neuron*, **69**, 885-892.

Brodmann, K. (1909) Vergleichende Lokalisierungslehre der Grosshirnrinde: in ihre Prinzipien dargestellt auf Grund des Zellenbaus. *Leipzig: Johann Ambrosius Barth Verlag*.

Brooks, V.B. (1983) Study of brain function by local, reversible cooling *Reviews of Physiology, Biochemistry and Pharmacology, Volume 95*. Springer Berlin Heidelberg, pp. 1-109.

Brozović, M., Abbott, L.F. & Andersen, R.A. (2008) Mechanism of gain modulation at single neuron and network levels. *Journal of Computational Neuroscience*, **25**, 158-168.

Buhl, E.H. & Singer, W. (1989) The callosal projection in cat visual cortex as revealed by a combination of retrograde tracing and intracellular injection. *Exp Brain Res*, **75**, 470-476.

Bullier, J., Hupe, J.M., James, A. & Girard, P. (1996) Functional interactions between areas V1 and V2 in the monkey. *J Physiol Paris*, **90**, 217-220.

Carandini, M. (2004) Amplification of trial-to-trial response variability by neurons in visual cortex. *PLoS Biol*, **2**, E264.

Cardin, J.A., Palmer, L.A. & Contreras, D. (2008) Cellular Mechanisms Underlying Stimulus-Dependent Gain Modulation in Primary Visual Cortex Neurons In Vivo. *Neuron*, **59**, 150-160.

Carmeli, C., Lopez-Aguado, L., Schmidt, K.E., De Feo, O. & Innocenti, G.M. (2007) A novel interhemispheric interaction: modulation of neuronal cooperativity in the visual areas. *PLoS One*, **2**, e1287.

Chance, F.S., Abbott, L.F. & Reyes, A.D. (2002) Gain modulation from background synaptic input. *Neuron*, **35**, 773-782.

Chen, D. & Fetz, E.E. (2005) Characteristic membrane potential trajectories in primate sensorimotor cortex neurons recorded in vivo. *J Neurophysiol*, **94**, 2713-2725.

Choudhury, B.P., Whitteridge, D. & Wilson, M.E. (1965) The Function of the Callosal Connections of the Visual Cortex. *Q J Exp Physiol Cogn Med Sci*, **50**, 214-219.

Churchland, M.M., Yu, B.M., Cunningham, J.P., Sugrue, L.P., Cohen, M.R., Corrado, G.S., Newsome, W.T., Clark, A.M., Hosseini, P., Scott, B.B., Bradley, D.C., Smith, M.A., Kohn, A., Movshon, J.A., Armstrong, K.M., Moore, T., Chang, S.W., Snyder, L.H., Lisberger, S.G., Priebe, N.J., Finn, I.M., Ferster, D., Ryu, S.I., Santhanam, G., Sahani, M. & Shenoy, K.V. (2010) Stimulus onset quenches neural variability: a widespread cortical phenomenon. *Nature Neuroscience*, **13**, 369-378.

Cohen, M.R. & Maunsell, J.H.R. (2009) Attention improves performance primarily by reducing interneuronal correlations. *Nature Neuroscience*, **12**, 1594-1600.

Cragg, B.G. (1967) The density of synapses and neurones in the motor and visual areas of the cerebral cortex. *J Anat*, **101**, 639-654.

Crochet, S. & Petersen, C.C. (2006) Correlating whisker behavior with membrane potential in barrel cortex of awake mice. *Nat Neurosci*, **9**, 608-610.

Crook, J.M. & Eysel, U.T. (1992) GABA-induced inactivation of functionally characterized sites in cat visual cortex (area 18): effects on orientation tuning. *J Neurosci*, **12**, 1816-1825.

Crook, J.M., Kisvarday, Z.F. & Eysel, U.T. (1998) Evidence for a contribution of lateral inhibition to orientation tuning and direction selectivity in cat visual cortex: reversible inactivation of functionally characterized sites combined with neuroanatomical tracing techniques. *Eur J Neurosci*, **10**, 2056-2075.

Daniel, P.M. & Whitteridge, D. (1961) The representation of the visual field on the cerebral cortex in monkeys. *J Physiol*, **159**, 203-221.

de Nó, L. (1949) Cerebral cortex: architecture, intracortical connections, motor projections. In: Physiology of the nervous system, 3rd edn (Fulton JF, ed.), chap. 15, pp. 288–330. Oxford: Oxford University Press., .

Eysel, U.T., Crook, J.M. & Machemer, H.F. (1990) GABA-induced remote inactivation reveals cross-orientation inhibition in the cat striate cortex. *Exp Brain Res*, **80**, 626-630.

Eysel, U.T., Shevelev, I.A., Lazareva, N.A. & Sharaev, G.A. (1998) Orientation tuning and receptive field structure in cat striate neurons during local blockade of intracortical inhibition. *Neuroscience*, **84**, 25-36.

Fabri, M. & Manzoni, T. (1996) Glutamate decarboxylase immunoreactivity in corticocortical projecting neurons of rat somatic sensory cortex. *Neuroscience*, **72**, 435-448.

Fano, U. (1947) Note on the Theory of Radiation-induced Lethals in Drosophila. *Science*, **106**, 87-88.

Felleman, D.J. & Van Essen, D.C. (1991) Distributed hierarchical processing in the primate cerebral cortex. *Cereb Cortex*, **1**, 1-47.

Ferster, D. & Miller, K.D. (2000) Neural mechanisms of orientation selectivity in the visual cortex. *Annu Rev Neurosci*, **23**, 441-471.

Finn, I.M., Priebe, N.J. & Ferster, D. (2007b) The Emergence of Contrast-Invariant Orientation Tuning in Simple Cells of Cat Visual Cortex. *Neuron*, **54**, 137-152.

Fisken, R.A., Garey, L.J. & Powell, T.P. (1975) The intrinsic, association and commissural connections of area 17 on the visual cortex. *Philos Trans R Soc Lond B Biol Sci*, **272**, 487-536.

Fox, M.D. & Raichle, M.E. (2007) Spontaneous fluctuations in brain activity observed with functional magnetic resonance imaging. *Nature Reviews Neuroscience*, **8**, 700-711.

Franks, N.P. (2008) General anaesthesia: from molecular targets to neuronal pathways of sleep and arousal. *Nature Reviews Neuroscience*, **9**, 370-386.

Franz, D.N. & Iggo, A. (1968) Conduction failure in myelinated and non-myelinated axons at low temperatures. *J Physiol*, **199**, 319-345.

Fricker, D., Verheugen, J.A. & Miles, R. (1999) Cell-attached measurements of the firing threshold of rat hippocampal neurones. *J Physiol*, **517 (Pt 3)**, 791-804.

Gabbott, P.L. & Somogyi, P. (1986) Quantitative distribution of GABA-immunoreactive neurons in the visual cortex (area 17) of the cat. *Exp Brain Res*, **61**, 323-331.

Galuske, R.A., Schmidt, K.E., Goebel, R., Lomber, S.G. & Payne, B.R. (2002) The role of feedback in shaping neural representations in cat visual cortex. *Proc Natl Acad Sci U S A*, **99**, 17083-17088.

Geisler, W.S., Albrecht, D.G., Crane, A.M. & Stern, L. (2001) Motion direction signals in the primary visual cortex of cat and monkey. *Vis Neurosci*, **18**, 501-516.

Gilbert, C.D. (1983) Microcircuitry of the visual cortex. *Annu Rev Neurosci*, **6**, 217-247.

Gilbert, C.D. & Wiesel, T.N. (1979) Morphology and intracortical projections of functionally characterised neurones in the cat visual cortex. *Nature*, **280**, 120-125.

Gilbert, C.D. & Wiesel, T.N. (1983) Clustered intrinsic connections in cat visual cortex. *J Neurosci*, **3**, 1116-1133.

Girard, P. & Bullier, J. (1989) Visual activity in area V2 during reversible inactivation of area 17 in the macaque monkey. *J Neurophysiol*, **62**, 1287-1302.

Girardin, C.C. & Martin, K.A.C. (2009a) Cooling in cat visual cortex: stability of orientation selectivity despite changes in responsiveness and spike width. *Neuroscience*, **164**, 777-787.

Girardin, C.C. & Martin, K.A.C. (2009b) Inactivation of lateral connections in cat area 17. *European Journal of Neuroscience*, **29**, 2092-2102.

Haider, B., Duque, A., Hasenstaub, A.R. & McCormick, D.A. (2006) Neocortical network activity in vivo is generated through a dynamic balance of excitation and inhibition. *J Neurosci*, **26**, 4535-4545.

Haider, B., Duque, A., Hasenstaub, A.R., Yu, Y. & McCormick, D.A. (2007) Enhancement of Visual Responsiveness by Spontaneous Local Network Activity In Vivo. *Journal of Neurophysiology*, **97**, 4186-4202.

Heeger, D.J. (1992) Normalization of cell responses in cat striate cortex. *Vis Neurosci*, **9**, 181-197.

Heggelund, P. & Albus, K. (1978) Response variability and orientation discrimination of single cells in striate cortex of cat. *Exp Brain Res*, **32**, 197-211.

Henze, D.A., Borhegyi, Z., Csicsvari, J., Mamiya, A., Harris, K.D. & Buzsaki, G. (2000) Intracellular features predicted by extracellular recordings in the hippocampus in vivo. *J Neurophysiol*, **84**, 390-400.

Hirsch, J.A. & Gilbert, C.D. (1991) Synaptic physiology of horizontal connections in the cat's visual cortex. *J Neurosci*, **11**, 1800-1809.

Ho, N. & Destexhe, A. (2000) Synaptic background activity enhances the responsiveness of neocortical pyramidal neurons. *J Neurophysiol*, **84**, 1488-1496.

Houzel, J.C., Carvalho, M.L. & Lent, R. (2002) Interhemispheric connections between primary visual areas: beyond the midline rule. *Braz J Med Biol Res*, **35**, 1441-1453.

Houzel, J.C. & Milleret, C. (1999) Visual inter-hemispheric processing: constraints and potentialities set by axonal morphology. *J Physiol Paris*, **93**, 271-284.

Houzel, J.C., Milleret, C. & Innocenti, G. (1994) Morphology of callosal axons interconnecting areas 17 and 18 of the cat. *Eur J Neurosci*, **6**, 898-917.

Hubel, D.H. & Wiesel, T.N. (1962) Receptive fields, binocular interaction and functional architecture in the cat's visual cortex. *J Physiol*, **160**, 106-154.

Hubel, D.H. & Wiesel, T.N. (1967) Cortical and callosal connections concerned with the vertical meridian of visual fields in the cat. *J Neurophysiol*, **30**, 1561-1573.

Hubel, D.H. & Wiesel, T.N. (1968) Receptive fields and functional architecture of monkey striate cortex. *J Physiol*, **195**, 215-243.

Hupe, J.M., James, A.C., Girard, P., Lomber, S.G., Payne, B.R. & Bullier, J. (2001) Feedback connections act on the early part of the responses in monkey visual cortex. *J Neurophysiol*, **85**, 134-145.

Hupe, J.M., James, A.C., Payne, B.R., Lomber, S.G., Girard, P. & Bullier, J. (1998) Cortical feedback improves discrimination between figure and background by V1, V2 and V3 neurons. *Nature*, **394**, 784-787.

Hussar, C. & Pasternak, T. (2010) Trial-to-trial variability of the prefrontal neurons reveals the nature of their engagement in a motion discrimination task. *Proc Natl Acad Sci U S A*, **107**, 21842-21847.

Innocenti, G.M. (1980) The primary visual pathway through the corpus callosum: morphological and functional aspects in the cat. *Arch Ital Biol*, **118**, 124-188.

Innocenti, G.M., Aggoun-Zouaoui, D. & Lehmann, P. (1995) Cellular aspects of callosal connections and their development. *Neuropsychologia*, **33**, 961-987.

Jagadeesh, B., Wheat, H.S. & Ferster, D. (1993) Linearity of summation of synaptic potentials underlying direction selectivity in simple cells of the cat visual cortex. *Science*, **262**, 1901-1904.

Jirmann, K.-U., Pernberg, J. & Eysel, U.T. (2008) Region-specificity of $GABA_a$ receptor mediated effects on orientation and direction selectivity in cat visual cortical area 18. *Experimental Brain Research*, **192**, 369-378.

Kalil, R.E. & Chase, R. (1970) Corticofugal influence on activity of lateral geniculate neurons in the cat. *J Neurophysiol*, **33**, 459-474.

Kara, P., Reinagel, P. & Reid, R.C. (2000) Low response variability in simultaneously recorded retinal, thalamic, and cortical neurons. *Neuron*, **27**, 635-646.

Kelly, R.C., Smith, M.A., Kass, R.E. & Lee, T.S. (2010) Local field potentials indicate network state and account for neuronal response variability. *Journal of Computational Neuroscience*, **29**, 567-579.

Kenet, T., Bibitchkov, D., Tsodyks, M., Grinvald, A. & Arieli, A. (2003) Spontaneously emerging cortical representations of visual attributes. *Nature*, **425**, 954-1056.

Kisvarday, Z.F., Cowey, A. & Somogyi, P. (1986) Synaptic relationships of a type of GABA-immunoreactive neuron (clutch cell), spiny stellate cells and lateral geniculate nucleus afferents in layer IVC of the monkey striate cortex. *Neuroscience*, **19**, 741-761.

Kisvarday, Z.F. & Eysel, U.T. (1992) Cellular organization of reciprocal patchy networks in layer III of cat visual cortex (area 17). *Neuroscience*, **46**, 275-286.

Kisvarday, Z.F., Toth, E., Rausch, M. & Eysel, U.T. (1997) Orientation-specific relationship between populations of excitatory and inhibitory lateral connections in the visual cortex of the cat. *Cereb Cortex*, **7**, 605-618.

Klee, M.R., Pierau, F.K. & Faber, D.S. (1974) Temperature effects on resting potential and spike parameters of cat motoneurons. *Exp Brain Res*, **19**, 478-492.

Lamme, V.A., Super, H. & Spekreijse, H. (1998) Feedforward, horizontal, and feedback processing in the visual cortex. *Curr Opin Neurobiol*, **8**, 529-535.

Lepore, F. & Guillemot, J.P. (1982) Visual receptive field properties of cells innervated through the corpus callosum in the cat. *Exp Brain Res*, **46**, 413-424.

LeVay, S. (1988) Patchy intrinsic projections in visual cortex, area 18, of the cat: morphological and immunocytochemical evidence for an excitatory function. *J Comp Neurol*, **269**, 265-274.

Li, W., Thier, P. & Wehrhahn, C. (2000) Contextual influence on orientation discrimination of humans and responses of neurons in V1 of alert monkeys. *J Neurophysiol*, **83**, 941-954.

Lima, B., Singer, W., Chen, N.H. & Neuenschwander, S. (2010) Synchronization dynamics in response to plaid stimuli in monkey V1. *Cereb Cortex*, **20**, 1556-1573.

Liu, Z., Fukunaga, M., de Zwart, J.A. & Duyn, J.H. (2010) Large-scale spontaneous fluctuations and correlations in brain electrical activity observed with magnetoencephalography. *NeuroImage*, **51**, 102-111.

Livingstone, M.S. & Hubel, D.H. (1984) Specificity of intrinsic connections in primate primary visual cortex. *J Neurosci*, **4**, 2830-2835.

Lomber, S.G., Payne, B.R. & Horel, J.A. (1999) The cryoloop: an adaptable reversible cooling deactivation method for behavioral or electrophysiological assessment of neural function. *J Neurosci Methods*, **86**, 179-194.

Lund, J.S., Wu, Q., Hadingham, P.T. & Levitt, J.B. (1995) Cells and circuits contributing to functional properties in area V1 of macaque monkey cerebral cortex: bases for neuroanatomically realistic models. *J Anat*, **187 (Pt 3)**, 563-581.

MacNeil, M.A., Lomber, S.G. & Payne, B.R. (1996) Rewiring of transcortical projections to middle suprasylvian cortex following early removal of cat areas 17 and 18. *Cereb Cortex*, **6**, 362-376.

Mainen, Z.F. & Sejnowski, T.J. (1995) Reliability of spike timing in neocortical neurons. *Science*, **268**, 1503-1506.

Makarov, V.A., Schmidt, K.E., Castellanos, N.P., Lopez-Aguado, L. & Innocenti, G.M. (2007) Stimulus-Dependent Interaction between the Visual Areas 17 and 18 of the 2 Hemispheres of the Ferret (Mustela putorius). *Cerebral Cortex*, **18**, 1951-1960.

Malach, R., Amir, Y., Harel, M. & Grinvald, A. (1993) Relationship between intrinsic connections and functional architecture revealed by optical imaging and in vivo targeted biocytin injections in primate striate cortex. *Proc Natl Acad Sci U S A*, **90**, 10469-10473.

Martin, K.A., Somogyi, P. & Whitteridge, D. (1983) Physiological and morphological properties of identified basket cells in the cat's visual cortex. *Exp Brain Res*, **50**, 193-200.

Martin, K.A. & Whitteridge, D. (1984a) Form, function and intracortical projections of spiny neurones in the striate visual cortex of the cat. *J Physiol*, **353**, 463-504.

Martin, K.A. & Whitteridge, D. (1984b) The relationship of receptive field properties to the dendritic shape of neurones in the cat striate cortex. *J Physiol*, **356**, 291-302.

Mason, A., Nicoll, A. & Stratford, K. (1991) Synaptic transmission between individual pyramidal neurons of the rat visual cortex in vitro. *J Neurosci*, **11**, 72-84.

Matsubara, J.A. & Boyd, J.D. (1992) Presence of GABA-immunoreactive neurons within intracortical patches in area 18 of the cat. *Brain Res*, **583**, 161-170.

Maunsell, J.H. & Treue, S. (2006) Feature-based attention in visual cortex. *Trends Neurosci*, **29**, 317-322.

McAdams, C.J. & Maunsell, J.H. (1999a) Effects of attention on orientation-tuning functions of single neurons in macaque cortical area V4. *J Neurosci*, **19**, 431-441.

McAdams, C.J. & Maunsell, J.H. (1999b) Effects of attention on the reliability of individual neurons in monkey visual cortex. *Neuron*, **23**, 765-773.

McCormick, D.A. (1992) Neurotransmitter actions in the thalamus and cerebral cortex and their role in neuromodulation of thalamocortical activity. *Prog Neurobiol*, **39**, 337-388.

McGuire, B.A., Gilbert, C.D., Rivlin, P.K. & Wiesel, T.N. (1991) Targets of horizontal connections in macaque primary visual cortex. *J Comp Neurol*, **305**, 370-392.

Michalski, A., Wimborne, B.M. & Henry, G.H. (1993) The effect of reversible cooling of cat's primary visual cortex on the responses of area 21a neurons. *J Physiol*, **466**, 133-156.

Miles, R. & Wong, R.K. (1986) Excitatory synaptic interactions between CA3 neurones in the guinea-pig hippocampus. *J Physiol*, **373**, 397-418.

Miller, K.D. & Troyer, T.W. (2002) Neural noise can explain expansive, power-law nonlinearities in neural response functions. *J Neurophysiol*, **87**, 653-659.

Mitchell, J.F., Sundberg, K.A. & Reynolds, J.H. (2007) Differential Attention-Dependent Response Modulation across Cell Classes in Macaque Visual Area V4. *Neuron*, **55**, 131-141.

Mitchell, J.F., Sundberg, K.A. & Reynolds, J.H. (2009) Spatial Attention Decorrelates Intrinsic Activity Fluctuations in Macaque Area V4. *Neuron*, **63**, 879-888.

Mitzdorf, U. & Singer, W. (1979) Excitatory synaptic ensemble properties in the visual cortex of the macaque monkey: a current source density analysis of electrically evoked potentials. *J Comp Neurol*, **187**, 71-83.

Mountcastle, V.B. (1957) Modality and topographic properties of single neurons of cat's somatic sensory cortex. *J Neurophysiol*, **20**, 408-434.

Murphy, B.K. & Miller, K.D. (2003) Multiplicative gain changes are induced by excitation or inhibition alone. *J Neurosci*, **23**, 10040-10051.

Nakamura, H., Chaumon, M., Klijn, F. & Innocenti, G.M. (2008) Dynamic properties of the representation of the visual field midline in the visual areas 17 and 18 of the ferret (Mustela putorius). *Cereb Cortex*, **18**, 1941-1950.

Nauhaus, I., Busse, L., Carandini, M. & Ringach, D.L. (2008) Stimulus contrast modulates functional connectivity in visual cortex. *Nature Neuroscience*, **12**, 70-76.

Nawrot, M. (2003) Ongoing activity in cortical networks: noise, variability and context. PhD thesis. Faculty of Biology, Albert-Ludwigs-University Freiburg, Germany.

Nawrot, M., Boucsein, C., Rodriguezmolina, V., Riehle, A., Aertsen, A. & Rotter, S. (2008) Measurement of variability dynamics in cortical spike trains. *Journal of Neuroscience Methods*, **169**, 374-390.

Okun, M. & Lampl, I. (2008) Instantaneous correlation of excitation and inhibition during ongoing and sensory-evoked activities. *Nature Neuroscience*, **11**, 535-537.

Olavarria, J.F. (1996) Non-mirror-symmetric patterns of callosal linkages in areas 17 and 18 in cat visual cortex. *J Comp Neurol*, **366**, 643-655.

Olavarria, J.F. (2001) Callosal connections correlate preferentially with ipsilateral cortical domains in cat areas 17 and 18, and with contralateral domains in the 17/18 transition zone. *J Comp Neurol*, **433**, 441-457.

Olshausen, B.A. & Field, D.J. (2004) Sparse coding of sensory inputs. *Curr Opin Neurobiol*, **14**, 481-487.

Oram, M.W. (2011) Visual Stimulation Decorrelates Neuronal Activity. *Journal of Neurophysiology*, **105**, 942-957.

Orban, G.A., Kennedy, H. & Maes, H. (1980) Functional changes across the 17-18 border in the cat. *Exp Brain Res*, **39**, 177-186.

Otmakhov, N., Shirke, A.M. & Malinow, R. (1993) Measuring the impact of probabilistic transmission on neuronal output. *Neuron*, **10**, 1101-1111.

Otsuka, R. & Hassler, R. (1962) [On the structure and segmentation of the cortical center of vision in the cat]. *Arch Psychiatr Nervenkr Z Gesamte Neurol Psychiatr*, **203**, 212-234.

Pare, D., Shink, E., Gaudreau, H., Destexhe, A. & Lang, E.J. (1998) Impact of spontaneous synaptic activity on the resting properties of cat neocortical pyramidal neurons In vivo. *J Neurophysiol*, **79**, 1450-1460.

Payne, B. & Peters, A. (2002) The cat primary visual cortex. *San Diego, CA: Academic Press*.

Payne, B.R. (1991) Visual-field map in the transcallosal sending zone of area 17 in the cat. *Vis Neurosci*, **7**, 201-219.

Payne, B.R. (1994) Neuronal interactions in cat visual cortex mediated by the corpus callosum. *Behav Brain Res*, **64**, 55-64.

Payne, B.R. & Siwek, D.F. (1990) Receptive fields of neurons at the confluence of cerebral cortical areas 17, 18, 20a, and 20b in the cat. *Vis Neurosci*, **4**, 475-479.

Payne, B.R., Siwek, D.F. & Lomber, S.G. (1991) Complex transcallosal interactions in visual cortex. *Vis Neurosci*, **6**, 283-289.

Peters, A. & Payne, B.R. (1993) Numerical relationships between geniculocortical afferents and pyramidal cell modules in cat primary visual cortex. *Cereb Cortex*, **3**, 69-78.

Porter, J.T., Johnson, C.K. & Agmon, A. (2001) Diverse types of interneurons generate thalamus-evoked feedforward inhibition in the mouse barrel cortex. *J Neurosci*, **21**, 2699-2710.

Ratzlaff, E.H. & Grinvald, A. (1991) A tandem-lens epifluorescence macroscope: hundred-fold brightness advantage for wide-field imaging. *J Neurosci Methods*, **36**, 127-137.

Reich, D.S., Victor, J.D. & Knight, B.W. (1998) The power ratio and the interval map: spiking models and extracellular recordings. *J Neurosci*, **18**, 10090-10104.

Reich, D.S., Victor, J.D., Knight, B.W., Ozaki, T. & Kaplan, E. (1997) Response variability and timing precision of neuronal spike trains in vivo. *J Neurophysiol*, **77**, 2836-2841.

Reynolds, J.H., Pasternak, T. & Desimone, R. (2000) Attention increases sensitivity of V4 neurons. *Neuron*, **26**, 703-714.

Ringach, D.L., Hawken, M.J. & Shapley, R. (1997) Dynamics of orientation tuning in macaque primary visual cortex. *Nature*, **387**, 281-284.

Rochefort, N.L., Buzás, P., Kisvárday, Z.F., Eysel, U.T. & Milleret, C. (2007) Layout of transcallosal activity in cat visual cortex revealed by optical imaging. *NeuroImage*, **36**, 804-821.

Rochefort, N.L., Buzas, P., Quenech'du, N., Koza, A., Eysel, U.T., Milleret, C. & Kisvarday, Z.F. (2009) Functional Selectivity of Interhemispheric Connections in Cat Visual Cortex. *Cerebral Cortex*, **19**, 2451-2465.

Rockland, K.S. & Lund, J.S. (1982) Widespread periodic intrinsic connections in the tree shrew visual cortex. *Science*, **215**, 1532-1534.

Rodriguez, R., Kallenbach, U., Singer, W. & Munk, M.H.J. (2010) Stabilization of visual responses through cholinergic activation. *Neuroscience*, **165**, 944-954.

Roelfsema, P.R. (2006) Cortical algorithms for perceptual grouping. *Annu Rev Neurosci*, **29**, 203-227.

Rose, D. (1979) An analysis of the variability of unit activity in the cat's visual cortex. *Exp Brain Res*, **37**, 595-604.

Salinas, E. & Sejnowski, T.J. (2000) Impact of correlated synaptic input on output firing rate and variability in simple neuronal models. *J Neurosci*, **20**, 6193-6209.

Salsbury, K. & Horel, J.A. (1983) A cryogenic implant for producing reversible functional brain lesions. Behavior Research Methods and Instrumentation. 433-436.

Sanchez-Vives, M.V. & McCormick, D.A. (2000) Cellular and network mechanisms of rhythmic recurrent activity in neocortex. *Nat Neurosci*, **3**, 1027-1034.

Sandell, J.H. & Schiller, P.H. (1982) Effect of cooling area 18 on striate cortex cells in the squirrel monkey. *J Neurophysiol*, **48**, 38-48.

Schmidt, K.E., Kim, D.S., Singer, W., Bonhoeffer, T. & Lowel, S. (1997a) Functional specificity of long-range intrinsic and interhemispheric connections in the visual cortex of strabismic cats. *J Neurosci*, **17**, 5480-5492.

Schmidt, K.E., Goebel, R., Lowel, S. & Singer, W. (1997b) The perceptual grouping criterion of colinearity is reflected by anisotropies of connections in the primary visual cortex. *Eur J Neurosci*, **9**, 1083-1089.

Schmidt, K.E. & Löwel, S. (2002) Long-Range Intrinsic Connections in Cat Primary Visual Cortex. *In: Peters, A. and Payne, B.R. (eds.), The Cat Primary Visual Cortex. Academic Press, San Diego 2002*, 387-426

Schmidt, K.E., Lomber, S.G. & Innocenti, G.M. (2010) Specificity of Neuronal Responses in Primary Visual Cortex Is Modulated by Interhemispheric CorticoCortical Input. *Cerebral Cortex*, **20**, 2776-2786.

Segraves, M.A. & Rosenquist, A.C. (1982) The distribution of the cells of origin of callosal projections in cat visual cortex. *J Neurosci*, **2**, 1079-1089.

Shadlen, M.N. & Newsome, W.T. (1994) Noise, neural codes and cortical organization. *Curr Opin Neurobiol*, **4**, 569-579.

Shadlen, M.N. & Newsome, W.T. (1998) The variable discharge of cortical neurons: implications for connectivity, computation, and information coding. *J Neurosci*, **18**, 3870-3896.

Sherk, H. (1978) Area 18 cell responses in cat during reversible inactivation of area 17. *J Neurophysiol*, **41**, 204-215.

Shoham, S. (2003) Robust, automatic spike sorting using mixtures of multivariate t-distributions. *Journal of Neuroscience Methods*, **127**, 111-122.

Shoumura, K. (1974) An attempt to relate the origin and distribution of commissural fibers to the presence of large and medium pyramids in layer III in the cat's visual cortex. *Brain Res*, **67**, 13-25.

Shu, Y., Hasenstaub, A., Badoual, M., Bal, T. & McCormick, D.A. (2003) Barrages of synaptic activity control the gain and sensitivity of cortical neurons. *J Neurosci*, **23**, 10388-10401.

Siegfried, J., Ervin, F.R., Miyazaki, Y. & Mark, V.H. (1962) Localized cooling of the central nervous system. I. Neurosurg.,. **19**, 840-852.

Sillito, A.M. (1979) Inhibitory mechanisms influencing complex cell orientation selectivity and their modification at high resting discharge levels. *J Physiol*, **289**, 33-53.

Silver, R.A. (2010) Neuronal arithmetic. *Nature Reviews Neuroscience*, **11**, 474-489.

Skottun, B.C., Zhang, J. & Grosof, D.H. (1994) On the directional selectivity of cells in the visual cortex to drifting dot patterns. *Vis Neurosci*, **11**, 885-897.

Softky, W.R. & Koch, C. (1993) The highly irregular firing of cortical cells is inconsistent with temporal integration of random EPSPs. *J Neurosci*, **13**, 334-350.

Somogyi, P., Kisvarday, Z.F., Martin, K.A. & Whitteridge, D. (1983) Synaptic connections of morphologically identified and physiologically characterized large basket cells in the striate cortex of cat. *Neuroscience*, **10**, 261-294.

Spitzer, H., Desimone, R. & Moran, J. (1988) Increased attention enhances both behavioral and neuronal performance. *Science*, **240**, 338-340.

Stepanyants, A., Martinez, L.M., Ferecsko, A.S. & Kisvarday, Z.F. (2009) The fractions of short- and long-range connections in the visual cortex. *Proceedings of the National Academy of Sciences*, **106**, 3555-3560.

Steriade, M. (2001) Impact of network activities on neuronal properties in corticothalamic systems. *J Neurophysiol*, **86**, 1-39.

Stettler, D.D., Das, A., Bennett, J. & Gilbert, C.D. (2002) Lateral connectivity and contextual interactions in macaque primary visual cortex. *Neuron*, **36**, 739-750.

Stevens, C.F. & Wang, Y. (1995) Facilitation and depression at single central synapses. *Neuron*, **14**, 795-802.

Stevens, C.F. & Zador, A.M. (1998) Input synchrony and the irregular firing of cortical neurons. *Nat Neurosci*, **1**, 210-217.

Swindale, N.V. (1998) Orientation tuning curves: empirical description and estimation of parameters. *Biol Cybern*, **78**, 45-56.

Symonds, L.L. & Rosenquist, A.C. (1984) Laminar origins of visual corticocortical connections in the cat. *J Comp Neurol*, **229**, 39-47.

Thiele, A., Pooresmaeili, A., Delicato, L.S., Herrero, J.L. & Roelfsema, P.R. (2009) Additive Effects of Attention and Stimulus Contrast in Primary Visual Cortex. *Cerebral Cortex*, **19**, 2970-2981.

Tolhurst, D.J., Movshon, J.A. & Dean, A.F. (1983) The statistical reliability of signals in single neurons in cat and monkey visual cortex. *Vision Res*, **23**, 775-785.

Tomko, G.J. & Crapper, D.R. (1974) Neuronal variability: non-stationary responses to identical visual stimuli. *Brain Res*, **79**, 405-418.

Trendelenburg, W. (1910) Ausschaltung am Zentralnervensystem. II Zur lehre von den bulbären und spinalen Atmungs und GGefässzentren. *Pflugers Arch.,*, **133**, 469-505.

Treue, S. & Martinez Trujillo, J.C. (1999) Feature-based attention influences motion processing gain in macaque visual cortex. *Nature*, **399**, 575-579.

Ts'o, D.Y., Gilbert, C.D. & Wiesel, T.N. (1986) Relationships between horizontal interactions and functional architecture in cat striate cortex as revealed by cross-correlation analysis. *J Neurosci*, **6**, 1160-1170.

Tusa, R.J., Palmer, L.A. & Rosenquist, A.C. (1978) The retinotopic organization of area 17 (striate cortex) in the cat. *J Comp Neurol*, **177**, 213-235.

Tusa, R.J., Rosenquist, A.C. & Palmer, L.A. (1979) Retinotopic organization of areas 18 and 19 in the cat. *J Comp Neurol*, **185**, 657-678.

Van Hooser, S.D. (2006) Lack of Patchy Horizontal Connectivity in Primary Visual Cortex of a Mammal without Orientation Maps. *Journal of Neuroscience*, **26**, 7680-7692.

Vogels, R., Spileers, W. & Orban, G.A. (1989) The response variability of striate cortical neurons in the behaving monkey. *Exp Brain Res*, **77**, 432-436.

Voigt, T., LeVay, S. & Stamnes, M.A. (1988) Morphological and immunocytochemical observations on the visual callosal projections in the cat. *J Comp Neurol*, **272**, 450-460.

Volgushev, M., Vidyasagar, T.R., Chistiakova, M., Yousef, T. & Eysel, U.T. (2000) Membrane properties and spike generation in rat visual cortical cells during reversible cooling. *J Physiol*, **522 Pt 1**, 59-76.

Wang, C., Waleszczyk, W.J., Burke, W. & Dreher, B. (2000) Modulatory influence of feedback projections from area 21a on neuronal activities in striate cortex of the cat. *Cereb Cortex*, **10**, 1217-1232.

Wang, C., Waleszczyk, W.J., Burke, W. & Dreher, B. (2007) Feedback signals from cat's area 21a enhance orientation selectivity of area 17 neurons. *Exp Brain Res*, **182**, 479-490.

White, J.A., Rubinstein, J.T. & Kay, A.R. (2000) Channel noise in neurons. *Trends Neurosci*, **23**, 131-137.

Williford, T. & Maunsell, J.H. (2006) Effects of Spatial Attention on Contrast Response Functions in Macaque Area V4. *Journal of Neurophysiology*, **96**, 40-54.

Wörgötter, F. & Eysel, U.T. (1989) Axis of preferred motion is a function of bar length in visual cortical receptive fields. *Exp Brain Res*, **76**, 307-314.

Zinke, W., Roberts, M.J., Guo, K., McDonald, J.S., Robertson, R. & Thiele, A. (2006) Cholinergic modulation of response properties and orientation tuning of neurons in primary visual cortex of anaesthetized Marmoset monkeys. *European Journal of Neuroscience*, **24**, 314-328.

8. Acknowledgements

An dieser Stelle möchte ich mich bei einigen Leuten bedanken, die auf die eine oder andere Weise dazu beigetragen haben dass diese Dissertation entstehen konnte. Zunächst möchte ich mich natürlich bei meiner Familie bedanken, die mich in der gesamten Zeit immer unterstützt hat, ohne recht zu wissen was der „Bub“ da eigentlich macht. Vielen Dank! Dann gebührt meiner Betreuerin Kerstin Schmidt natürlich einen besonderen Dank, die mir die Möglichkeit gab meine Dissertation am Max-Planck Institut für Hirnforschung anzufertigen. Vielen Dank für die stete Unterstützung und den faszinierenden Einblick in die Welt der Hirnforschung. In diesem Sinn möchte ich mich auch bei Prof. Ralf Galuske bedanken, ohne den ich wahrscheinlich nie in der Hirnforschung gelandet wäre.

Bedanken möchte ich mich auch bei den anderen Mitgliedern meiner Arbeitsgruppe, die über all die Jahre tapfer meine Launen ertragen haben. Ganz besonders bei David Eriksson, der mir oft genug versucht hat die Geheimnisse der Mathematik näher zu bringen. Einen wichtigen Teil meiner Zeit in Frankfurt hat sicherlich auch das „Team Schwanheim“ beigetragen. Boris Ebisch, Sascha Gotthardt und Tobias Reiff, sowie meine WG Genossen David Fernengel und Benjamin Dann/Wellner haben erfolgreich für ein Leben außerhalb des Labors gesorgt. Auch das „Team Darmstadt“ sein an dieser Stelle erwähnt.

Dann möchte ich mich noch bei einer Reihe von Leuten bedanken, deren Hilfe zum Entstehen dieser Arbeit beigetragen habe. Sergio Neuenschwander, Bruss Lima und William Barnes für ihre Hilfe bei den Experimenten. Ebenso der Mechanikwerkstatt, EDV und Haustechnik für die kompetente Versorgung mit jeglichen Bauteilen sowie den Angestellten vom Tierhaus.

9. Lebenslauf

Name:	Thomas Wunderle
Geburtsdatum- und Ort:	15.04.1981, Seeheim-Jugenheim
Staatsbürgerschaft:	deutsch
Familienstand:	ledig
Anschrift:	Ingelheimer Str. 24, 60529 Frankfurt

Schulbildung

08/1987 bis 07/1991	Grundschule Gernsheim
08/1991 bis 06/2000	Gymnasium Gernsheim

Zivildienst

08/2000 bis 06/2001	Kindergarten der evangelischen Kirchengemeinde Pfungstadt

Studium

10/2001 bis 01/2007	Technische Universität Darmstadt mit dem Abschluss Diplom Biologe

Promotion

04/2007 bis 04/2011	Max-Planck-Institut für Hirnforschung Frankfurt/a.M. in der Selbstständigen Nachwuchsgruppe „Kortikale Funktion und Dynamik“

10. Eidesstattliche Erklärung

Ich erkläre hiermit an Eides statt, dass ich die vorliegende Dissertation selbständig und nur mit den angegebenen Hilfsmitteln angefertigt habe.

…… …….....

Datum Unterschrift